NASA Contractor Report 177615

Survey of Lift-Fan Aerodynamic Technology

David H. Hickey and Jerry V. Kirk

CONTRACT A25364D
September 1993

National Aeronautics and Space Administration

NASA Contractor Report 177615

Survey of Lift-Fan Aerodynamic Technology

David H. Hickey, Retired
NASA Ames Researcher
Sunnyvale, California

Jerry V. Kirk
Ames Research Center
Moffett Field, California

Prepared for
Ames Research Center
CONTRACT A25364D
September 1993

National Aeronautics and
Space Administration

Ames Research Center
Moffett Field, California 94035-1000

Notation

a	distance form fan axis to center of pressure, ft
A	area, sq ft
AR	aspect ratio, b^2/S or D/c
b	span, ft
BLC	boundary layer control
c	wing chord, ft
c_l	two-dimensional lift coefficient
C_L	lift coefficient, L/(qS) or $L_D/(qcD_F)$
$C_{L_{\delta_1}}$	rate of change of lift coefficient with full span flap deflection, per radian
C_{μ_f}	BLC blowing momentum coefficient, BLC nozzle thrust/$\left(2A_F q_{F_{BLC\ OFF}}\right)$
d	suction plate diameter
D	diameter, ft
f	acoustic frequency
F	force, pounds
F_G	gross thrust, $\rho A V_j^2$, pounds
F_2	force on vane in exhaust, pounds
H	serration chord and height above ground, ft
K	relationship between induced lift and momentum coefficient
L	lift, pounds
M	pitching moment, foot-pounds
PNL	perceived noise level, PNdb
P_o	ambient static pressure, pounds per square foot
P_t	total pressure, pounds per square foot
PWL	sound power level, db
q	dynamic pressure $1/2\rho V^2$, pounds per square foot
q_1	average fan exhaust dynamic pressure in the streamwise direction, pounds per square foot
q_2	average fan exhaust dynamic pressure in the spanwise direction, pounds per square foot
R	Reynolds number, dimensionless, or fan radius, ft
S	area, sq ft, or serration spacing, ft
T	thrust, pounds
T_c	thrust coefficient, To/qS
V	free stream airspeed,
x	distance in a streamwise direction or from fan axis to center of pressure, ft
y	distance in a spanwise direction, ft
z	distance in a vertical directon, ft
α	angle of attack, degrees
β	exit louver angle from the fan axis, degrees
δ	flap deflection or jet exhaust deflection, degrees
Δ	increment in a value, downstream minus upstream, or outboard minus inboard
ρ	air density, slugs/(cu ft)

Subscripts

o	$\alpha = 0, \delta = 0$
1	surface upstream from fan
2	fan area or fan exhaust
2d	two-dimensional chord through fan axis
3	surface aft of the fan
D	duct
e	effective diameter
F	fan or flap
i	incidence or induced
j	jet
n	nozzle
s	static
t	total
x	along the flight path or distance from the nozzle

Introduction

Representatives of NASA Ames Research Center asked that a summary of technology appropriate for lift fan powered short takeoff/vertical landing (STOVL) aircraft be prepared so that new programs could more easily benefit from past research efforts. This paper represents one of six prepared for that purpose. The authors have conducted or supervised the conduct of research on lift fan powered STOVL designs and some of their important components for decades.

This paper will first address aerodynamic modeling requirements for experimental programs to assure realistic, trustworthy results. It will next summarize the results of efforts to develop satisfactory specialized STOVL components such as inlets and flow deflectors. It will also discuss problems with operation near the ground, aerodynamics while under lift fan power, and aerodynamic prediction techniques. Finally, results of studies to reduce lift fan noise will be presented. The paper will emphasize results from large scale experiments, where available, for reasons that will be brought out in the discussion. Some work with lift engine powered STOVL aircraft is also applicable to lift fan technology, and will be presented herein. Small-scale data will be used where necessary to fill gaps.

Experimental Modeling

When planning aerodynamic modeling for conventional aircraft studies, both viscous effects (Reynolds number effect) and scale effects must be considered. The term "scale effect" is meant as the likelihood that structural details of small scale models will probably be different than the details of aircraft construction, and in sensitive aerodynamic areas can influence the results. For STOVL aircraft, where the propulsion flow has a major influence on the aircraft flow environment, the situation is further complicated by the necessity to model the propulsion and free stream flow mixing and entrainment. The requirement has a significant impact on selection of powerplant simulators.

Transition Flight

Figures 1 and 2 from references 1 and 2 contain data showing viscous effects on the angle-of-attack for tilting duct lip flow separation on several tilting ducts and the performance of a cascade of turning vanes behind lift fans. Although the small scale X-22 duct was a reasonable size (about 17 inches diameter), the upstream inlet flow separation at a given velocity ratio occurred about 35 degrees before the full scale duct flow separation. On the downstream lip, the separation occurred about 50 degrees before full scale. In order to obtain meaningful overall performance results, it is necessary to enlarge the small scale inlet radius in the sensitive areas to avoid this premature flow separation. The data in figure 2 shows that the 1/6 scale cascade had a major loss in turning efficiency compared to a full scale cascade. The chord of the small scale cascade was only 1 1/4 inches, so the performance detriment may have partially been caused by manufacturing anomalies as well as viscous effects. In addition, the poor vectoring performance accelerated the back pressuring of the fan, further reducing performance. It would be very difficult to make a cascade this size comparable in efficiency to a large scale cascade.

In 1960, in cooperation with the Army and the General Electric Co., NASA Ames studied the first large scale model with a lift fan mounted in the fuselage (5.2 foot diameter GE X-353). The model is shown in figure 3, from reference 3. A 1/9 model of the Ames model was later fabricated by NASA Langley. The test setup for the small scale model duplicated as closely as possible the Ames 40 x 80 test section and mounting struts. Figure 4 from reference 4 shows the setup. A cross section of the propulsion systems for the two models is shown in figure 5. The two models had scaled inlet radii and inlet vanes. The fans, however, were very different. The fan in the large scale model was a typical axial flow fan with a 36 bladed rotor and a stator. The fan was powered by a J-85 engine and had an augmentation ratio of 2.8. The small scale fan had 4 blades, no stator, with the exception of vanes designed to turn the flow for thrust, and was powered by shop air through nozzles on the fan blades. The augmentation ratio of the fan is believed to be in the neighborhood of 1.5, with an exit velocity distribution that peaks at the tip due to the pervasiveness of the drive jets. In addition, the velocity distribution had a large flow deficit in the center. The lift to static thrust ratio as a function of airspeed for the two models is presented in figure 6. The upper curve is for the large scale model (the two symbols are with and without wall corrections) and the lower curve is for the small scale model. The results indicate that the wall corrections were small, but more importantly, that there was a major problem with the small model simulation. After considerable analysis, reference 4 attributed most of the lower lift of the small scale model to more negative pressures on the bottom of the fuselage. The difference is contrary to expectations from Reynolds number differences. Reference 5 argues that the decay rate of a jet must be modeled for a correct aerodynamic simulation. The swirl in the small scale exhaust and the different exhaust profiles probably resulted in different mixing and entrainment rates thus decay rates for the two models,

and produced the discrepancy in lower surface pressures and lift.

The results of the work described above stimulated additional work to help define modeling requirements for VTOL propulsion. Reference 2 presents results from another investigation using the Ames 40 × 80 foot wind tunnel. Two 3 foot diameter fans were independently installed in a large scale semi-span wing. One fan was designed to be a 1.3 pressure ratio lift fan. The other was a 0.6 scale version of the 1.1 pressure ratio GE X-353 fan. While the diameters of the fans were the same, the internal flow paths were quite different. Figure 7 shows that the thrust variation with forward speed was similar on a non-dimensional basis, however, figure 8 shows that the lift induced by the propulsive flow was not only different, but the shape of the lift variation with forward speed was different. As show in figure 9, the pitching moment due to the propulsive flow also varied for the two fans. In this case, the physical fan exhausts are different. The turbine of the 1.3 pressure ratio fan completely surrounds the exhaust periphery, while the 1.1 pressure ratio fan exhaust covers 180 degrees. This difference, along with the different internal flow paths may have caused different entrainment rates and the discrepancy shown. This work indicates that it may not be enough to model a good axial flow fan with another good axial flow fan; exhaust characteristics must be appropriately modeled as well. Other results from reference 2 are shown in figure 10. The thrust variation with forward speed of the 3 foot diameter 1.1 pressure ratio fan, presented in figure 7, is compared with results from a 15 inch diameter fan powered by a coaxial hub turbine, mounted in a thick wing. Internal design of the two fans is quite different; the larger fan had high aspect ratio blading while the smaller fan had low aspect ratio blading. Thrust variation with forward speed is similar for the two fans, but as just observed, this doesn't mean that induced lift and moment would be similar. Finally, the thrust variation with forward speed for a 3 foot diameter, 1.1 pressure ratio fan is compared with that of a tip turbine driven 8 inch fan. Both were installed in similar wings. For this comparison, in figure 11 from reference 2, the variation of thrust with forward speed was substantially different.

Hover

Classical fundamental studies done at Langley Research Center, reference 6, showed the importance of exhaust decay on the induced hover lift loss. These results are reproduced in figure 12. The exhaust decay is a function of the entrainment of outside air by the jet, which depends on such things as scale and frequency of the jet turbulence, and the physical environment at the jet exhaust.

To examine some of these factors at full scale, Ames performed a fundamental ground-effect test using a J-97 jet engine and a TF-34 turbofan engine. The results are compared with one prediction equation derived from small scale data in figure 13, from reference 7. Out of ground effect, the equation under predicts the lift loss somewhat, indicating that the decay rate of the small scale data used to derive the equation was slower than for the large scale data. In ground effect, at heights less than 5 exhaust diameters, the full scale engines had as much as double the lift loss, indicating a major difference in the jet impingement and ground-jet small and large scale flows. More recent studies (SAE Paper 901060, by Corsiglia, Wardell, and Kuhn) have not been able to reproduce the small scale results in figure 13. Indeed, few fundamental ground effect experiments are above reproach for reasons such as test room size, ground plane size, jet flow quality (turbulence content and flow profile), ground plane surface texture, etc. Even the large scale results can be questioned because the engine was horizontal so that one side of the ground plane could be influenced by real ground proximity.

If the fundamental studies are suspect, what results can be trusted? Removing the questionable factors mentioned above is done by testing outside, using the ground for the ground plane, and having full scale modeling and propulsion very similar to the planned propulsion. Figure 14, from reference 8 shows the hover lift increment due to ground effect for the VAK 191B lift engine STOVL aircraft and a 10% scale model of the aircraft. The aircraft suckdown is approximately twice that of the model. A comparison of ground effect between a large scale model (fig. 15) using 3 three foot diameter fans and a small scale model using 2 inch air jets to stimulate fans is shown in the other part of figure 14. Again the large scale model had more sever adverse ground effect. Another size effects comparison is available from the Grumman 698 configuration (fig. 16). Figure 16 shows a full scale model using TF-34 engines for propulsion. Figure 17, from reference 9 shows a ground effect test set up with a detailed 11% scale model using two sophisticated 5 inch diameter turbofan simulators. In this case, adverse ground effect (if any with the large scale model was less than with the small scale model (fig. 18) and the fountain effect at large scale was more pronounced.

Figure 19 shows one more reason for realistic simulation of VTOL propulsion when hover testing in ground effect. The ground proximity can back-pressure the fan and reduce the fan thrust. Ground effect data from the models reported in references 3 and 10 is shown. The fan thrust was reduced about the same amount for both models, but the fan-in-fuselage model had a further lift reduction due to negative induced lift. The fan-in-wing model had

fountain flow that offset the fan thrust loss and gave neutral ground effect. Without true propulsion system characteristics, the ground effect results would be in error by as much as 15%. It should be noted that the fan in wing data from figure 19 were from an approximate full scale GE XV-5 model with full scale GE XV-5 propulsion, and the flight and ground test results were the same, verifying the earlier hypothesis that the way to test for ground effects with confidence is by full scale modeling.

Shaft and gear or pneumatic drive (that is by engine exhaust or engine exhaust driven compressor) may be feasible for a lift fan powered aircraft. For hub driven fans of any type, blade pitch may be a suitable option for rapid response control, whereas tip driven fans can probably not use this control method. On a variable pitch fan, flow mixing and entrainment will vary as a function of blade pitch because the exhaust turbulence and profile will vary with blade angle at a fixed rpm. This means that with variable pitch fans, induced effects from flow entrainment may vary as much as the discrepancies noted in figures 6, 13, 14, and 18. With fixed pitch fans such as the GE tip driven fans, internal aerodynamics may be unchanged to the first order when thrust is changed, so that the flow environment of the aircraft is unchanged as long as the flight velocity ratio, V/V_j, is constant.

It is apparent from the results presented here, that if ground-based facilities are to provide accurate results in the hover and transition flight regimes of STOVL aircraft, appropriate simulation of the flow from full scale powerplants must be simulated, and performance of inlets and vectoring components must be comparable with real hardware. The flow simulation requirement is further complicated because the properties to be simulated have not been fully defined. Even when the modeling requirements are known, it may not be acceptable to perform experiments at small scale because of viscous and scale detail effects. Therefore, experimental work should be at the largest practical scale, with real engines as near to the planned full scale engines as possible. When compared to the cost of a precision small scale model with simulators, as discussed in reference 11, the cost of large scale hardware can be competitive; especially when confidence in the results is factored into the evaluation.

Components For Lift Fan Installations

The components considered here are inlet arrangements to take flow to lifting powerplants and the exhaust deflecting devices to provide lift or drag in transition flight.

Inlets

Inlets for STOVL aircraft can range from the very shallow inlets of a fan-in-wing design to the much deeper inlets that are compatible with fuselage installations, therefore this discussion will include the considerable amount of work done on lift engine inlets.

Fan-in-wing inlets– In 1956, Ames conducted its first wind tunnel test of a fan-in-wing model using a propeller in a semispan wing (ref. 12). Results from this study were limited because the propeller failed after a half hour of wind-on time. This enhanced our fears about cyclic loads of a fan located in the modified rotary wing environment. In 1958, we continued our research with a stronger 20 inch diameter propeller in a semispan wing (fig. 20). Upon learning of our enterprise, the General Electric Co. joined us and provided the inlet and exhaust cascades and professional assistance. This investigation was more successful and provided much useful information for the Army sponsored Ryan/GE XV-5 design. Figure 21, from reference 13, shows that flow distortion through the fan in the streamwise and spanwise directions. Figure 22 from reference 14 shows the distortion more clearly. The measured total pressure ratio around the fan midpassage circumference is shown at several forward speeds along with the theoretical blade angle of incidence. In figure 21, distortion in the streamwise direction was small below a V/V_j of 0.6 and in the spanwise direction the distortion was small below a V/V_j of 0.4 for some inlet vane configurations, including no inlet vanes. In the range of velocity ratios where fan blade are highly stressed (below $V/V_j = 0.3$), the distortion is low, thus the need for inlet vanes can be questioned. With the extremely short inlet for wing mounted lift fans, the fan seems to act as an inlet flow control to minimize the effects of inlet flow separation.

Full scale GE X-353 (5.2 foot diameter, 1.1 pressure ratio, tip turbine driven) fans were exposed to the short duct, wing environment in a joint Army, NASA, GE program in the 40 × 80 foot wind tunnel in 1961. The complete model is shown in figure 23, from reference 15, and figure 24 shows the inlets tested. The more complicated articulated inlet did reduce flow distortion through the fan but reduced lift at low speed unless the vane angles were programmed with airspeed, and it provided less net transition thrust than the fixed vanes. Consequently, the fixed vane arrangement was chosen for the GE XV-5A airplane.

The GE X-353 fan is a conventional rotor-stator turbomachinery design which permits installation in relatively thick wings designed for subsonic flight. Design of thin, statorless fans for thinner wings is discussed in reference 16. To provide a thin fan for wind tunnel models with thin wings, the stator was removed from the GE X-353 and the outboard 180 degrees of inlet was replaced by a blowing boundary layer control (BLC) inlet which much

reduced the radius and hence height. Except for the hub, this modified fan could fit in a 60 degrees swept back triangular wing 5% thick. Figure 25, from reference 17, is a photograph of the fan mounted in the wing, with the conventional inlet on the inboard side of the fan, and the BLC inlet on the outboard side of the fan. Figure 26 shows cross sections of the conventional and modified fan, and figure 27 shows details of the BLC inlet. Figure 28 presents the static performance of the statorless fan and the conventional fan. Surprisingly, the performance is about the same, probably because the thrust from the BLC inlet was about 2.4% of the fan thrust and the exhaust deflection vanes partially fulfilled the mission of the removed stator. Forward speed performance of the statorless fan, figure 29, is slightly better than for a conventional fan. Figure 30 gives an indication of BLC requirements. If the thrust of the BLC jet is 3% of the fan thrust without BLC, the thrust of the fan is increased 30%. Figure 31 presents an attempt to find a dimensionless parameter to describe the overall lift increase with the application of BLC. The parameter shown collapsed the effect of airspeed and fan rpm to ±6%.

Study of the thin fan designs in reference 16 and the modified thin fan can lead one to question that a thin fan in a supersonic wing can be driven by a shaft because of the depth of a right angle gear drive, or that it could have variable pitch because of the depth needed for the change mechanism. Reference 16 studied fans with inlet guide vanes rather than outlet guide vanes as well as the statorless fans for thin applications.

Deep fan mounting– Figure 3 from reference 3 shows the mounting of the GE X-353 fan in a fuselage. The fan is mounted one diameter deep, the upstream side of the inlet has a large radius and is protected by a long chord vane (fig. 32). Figure 32 also shows the ram pressure recovery of the inlet. The vane nearly doubles the velocity over which good ram recovery is obtained. Work done on lift engine inlets can be applicable to deep mounted lift fans installations. Reference 18 contains a body of results on inlet pressure recovery and distortion for five inline J-85 engines canted forward 10 degrees, and with a forward inlet radius of 0.56 diameters. Figure 33 shows the layout of the model and figure 34 presents total pressure recovery and distortion for the plain inlet. Up to a V/Vj of 3, the distortion stayed within the 0.1 limit at 0 degrees angle of attack. The upstream engine had relatively high distortion because it didn't have the benefit of an engine in front drawing in air, thus inducing a flow toward the inlet. The effect of angle of attack on recovery and distortion is shown in figure 35. At a $V/V_j = 0.45$, the distortion stayed within limits, but the inlet on engine 2 was influenced by the proximity of the wing leading edge so that inflow became distorted as angle of attack was increased. Reference 18 considers the effect of scoop and folding door inlet covers on distortion as well. If the reader wishes, he can peruse reference 18 for additional information, however, the data show that the best recovery and distortion results were obtained with the clean, no doors configuration.

Results from another lift engine study featuring a more realistic model, although still using J-85 engines for lift engine simulators, are presented in reference 19. Here, three lift engines are mounted vertically inside of a highly swept glove, as shown in figure 36. Figure 37 is a detail of the engine inlet. The inlet radius-to-diameter ratio is 0.19, which is the most severe at the upstream station of any inlet shown here. An inlet vane scaled from the lift fan deep inlet was available to help flow around the upstream radius. Figure 38 presents pressure recovery and distortion with this inlet at 0 degrees angle of attack, with and without the inlet vane. The vane was beneficial, especially at high velocity ratios. Figure 39 shows the variation of distortion and pressure recovery with angle of attack. Unlike the other example, flow to all three engines was insensitive to angle of attack.

Consideration of data from the fan-in-wing arrangements as well as from the deep inlets indicates that the fan is an excellent boundary layer control device when placed near the inlet radius. Placing the fan well downstream from the inlet (ref. 3) allows a significant portion of the fan to operate in turbulent flow when the inlet flow is separated. Data from all three models with deep inlets discussed here, are in figure 40. Comparison of the results indicates that a small amount of tilt and taking advantage of that to increase the upstream radius is a powerful tool to improve recovery and minimize distortion.

Exhaust Deflectors

Lift fan or cruise fan exhaust deflectors to provide horizontal force or lift in transition flight range from cascades of vanes to multi-segmented hoods to rotating tail pipes.

Figure 41 from references 20 and 2 show the effectiveness of a cascade of vanes in this capacity. The results are shown as lift as a function of thrust so that the effective exhaust angle and the reduction in fan thrust can be seen. The 7 inch chord GE XV-5 cascade is shown for reference. A swept or chevron planform intended to reduce backpressure at the hub improved performance at high deflections slightly. Doubling the chord to increase Reynolds number also improved performance over the baseline slightly. The flapped cascade was the best, but not markedly so, however, it did increase effectiveness at negative vectoring thus providing the possibility of even

more extreme descent performance. Finally, a swiveling cascade canted 45 degrees provided superior performance, but probably at a weight and volume penalty.

A vane arrangement for modest amounts of thrust deflection is pictured in figure 42, as developed by Grumman with NASA's help, for the Grumman 698 design (ref. 21). As shown in figure 43, from reference 22, a single vane mounted in the exhaust provides 35% thrust deflection. With the vane out of the hot exhaust core, but in the fan flow, the vane still provided a 30% side force.

The performance of exhaust deflectors, as would be used to lift/cruise applications is summarized in figure 44, from reference 21. Both the "D-shaped" hood (ref. 23) and canted variable camber vanes approach a lift-thrust ratio of 0.94 at 90 degrees, which, though remarkably good, would probably sill make a significant reduction in VTOL payload. Perhaps an even larger concern is the weight and size these structures can assume. For lift/cruise applications, designers may wish to also consider tilting engines.

STOVL Aerodynamics

This section of the paper discusses ground effects and aerodynamics when in the powered lift flight range.

Ground Effects

Ground effects during hover have been treated by many authors (for example, refs. 24–26). The existence of fountains in multijet cases and of the wall jet type of flow on the ground is well known and understood in a general way. Effects of variables such as nozzle arrangement, wing height, lower surface contour, and special fountain containment devices on ground effects have been studied exhaustively at small scale and to a much lesser degree at large scale. This data base has spawned ground effect prediction techniques that are still being verified. However, the failure of large and small scale ground effect results to agree in the simplest of cases, as discussed earlier, indicates a need for further knowledge of flow details and makes the many small scale contributions to the data base for empirical ground effect prediction techniques suspect. Unfortunately, the lack of large and small scale correlation also casts a shadow on predictions using these results. A program to examine ground effect sensitivity to exhaust flow parameters could yield valuable results. The explanation of the phenomena of ground effect has been addressed well and often, so will not be covered herein.

The flows that make ground effect forces are sometimes hot, depending on the engine type and the mixing along the flow path length. While modest temperature rises in the aircraft, environment reduce lift-off capability, the catastrophic problem of engine stalls from the ingestion of cells of hot air can be much more serious. This difficulty was recognized early and was the driving reason for the shape and arrangement of the GE XV-5. The engine inlets were placed above the fuselage and over the wing to provide direct intervention to ingestion of exhaust gases on a short path. This effort was largely successful for the GE XV-5, but it was necessary to derate the engine to avoid stall. Inspite of a bypass ratio of 8, derating the engine, and interventional design, engine stalls did occur (rarely) when hovering near the ground. Because of the GE XV-5 two-engine, balanced design, engine stall was not catastrophic. New designs will probably have higher temperature engines and the problem could be more severe. In evaluating the ingestion problems with a configuration, it is suggested that methods as used in reference 19 be used. That is, engine and fan inlets be equipped with rapid-response thermocouples and time histories of inlet temperature be obtained both in static free air conditions and near the ground in a wind tunnel at forward speed. Figures 45 and 46 are photographs of a lift engine fighter model in the 40 × 80 wind tunnel and a static test stand. Figure 47 shows an example of temperature time histories in engine inlets when an engine stalled.

Ground effects at forward speed can be measured in wind tunnel even though the wind tunnel may not be specially equipped with devices to eliminate the wind tunnel boundary layer. Reference 11 shows reingestion at forward speed for the GE XV-5. The temperature rise shown predicted the rise in flight and the onset of turbulence from the ground vortex. Sometimes investigators, in quest of free air data accuracy, artificially limit their testing because of so called wind tunnel flow breakdown and do not avail themselves of the opportunity to acquire valuable ground effect data. Tests should go to the low speed at which exhaust flow reflected from the wind tunnel walls impinge on the model and interfere with the ground effect simulation. Model mounted dynamic pressure measuring equipment to augment the usual wind tunnel static pressure rings will help determine true speed when the ground vortex is present.

Aerodynamics in Transition

Operation of lift fans and engines to provide lift during transition flight can induce major forces and moments over and above those from direct thrust. Research in this area has consisted of fundamental studies of jet exhaust

physics, such as that described in reference 5, and small and large scale studies of complete configurations as in figure 48.

A jet oriented to issue into a crossflow will bend back and roll up into contrarotating vortices (fig. 49). Immediately at the jet exhaust surface, flow separation occurs, then as the vortices form downstream from the jet exit, the jet entrains a great deal of air form the surrounding environment as shown in figure 50 from reference 27. Figure 50 shows the result of flow streamline tracing with a three-dimensional laser velocimeter. Streamlines far from the jet are drawn down into the center of the rolling-up vortices showing the powerful entrainment by a jet-in-crossflow. If the jet is surrounded by a large surface, especially behind the jet, the jet flow field will induce negative lift on the surface and adjacent wing and tail surfaces. This has been demonstrated in many small scale experiments (ref. 5). If a fan is surrounded by a large area, this lift loss in transition should be estimated.

Most small scale experiments did not include the effects of inlet flow. In early post World War II experiments, it was shown that sucking air in the upper surface of a wing at or near the trailing edge, provided "Circulation Control," that is, increased lift. Inflow to a fan or engine when in the proper location with respect to the airframe can be expected to contribute to the induced effects. When quantifying induced effects, care should be taken to account for the inlet flow as well as the exhaust flow. Negative induced lift has been noted on full scale test rigs, and is graphically shown in figure 51 from reference 10. Here, the GE XV-5 nose fan was operated over an airspeed range and the thrust variation and model lift variation are shown. Negative pressure behind the fan and downflow on the wing from the jet entrainment produced negative lift. This is not a representative of GE XV-5 operation, however, because the airplane used a thrust reverser in the pitch fan flow for a pitch control device.

In the 1960s and 1970s, a number of large scale models of varying configurations were tested in the Ames 40- by 80-Foot Wind Tunnel. Figure 52, from reference 28, tabulates the major parameters of thirteen configurations varying from fuselage mounted fans to wing mounted fans to pod mounted fans. The fans used in these models were either the 5.2 foot diameter GE X-353 or the 3 foot diameter X-376 tip turbine driven fans. Figure 53 shows the variation of induced lift with airspeed for several lift fan arrangements. Induced lift is defined as total lift measured on the wind tunnel scales minus aerodynamic lift due to angle of attack or lifting surface camber minus fan thrust. A fan mounted near the wing trailing edge produces positive induced lift while a fan near the wing leading edge produces negative induced lift. Data in figure 54 indicate that to maximize induced lift, the fan should be inboard at the wing trailing edge. These results are consistent with conventional flap loading theory and tend to support the view of a lift fan flow field as being similar to that of a thick, low aspect ratio jet flap. Induced lift from forward mounted lift fans, figure 55, shows that if a fan is to be mounted forward of the wing, it should be mounted outboard, if possible.

Induced lift also induces pitching moments. Non-dimensionalized pitching moment is shown as a function of airspeed in figure 56. Data for the fan-in-wing configuration shows a large positive change in pitching moment. This characteristic is typical of fan-in-wing configuration. While a trailing edge flap can eventually reverse the direction of moment change, that tends to introduce a control reversal with airspeed that would be looked on unfavorably by a pilot. The moment variation with airspeed for podded configurations, shown in figure 56, is much less and would be much easier to handle. The variation of pitching moment with airspeed is sensitive to the vertical as well as the horizontal location of the center of gravity. With a deep duct, deflection of the fan exhaust for thrust in transition can be a major contributor to pitching moments.

Lift fan powered aircraft could have retractable or folding lift fans distributed around the airframe, as well as lift/cruise in front of a wing, in figure 57 from reference 29, shows that the fan flow significantly reduces wing lift. At low speed, the fan in all three locations would reduce wing lift an amount equal to an average of 8 degrees angle of attack at velocity ratios of about 0.1. When possible, it would be desirable to mount the fan well below the wing chord plane. Lift induced by a jet only, without an inlet, is shown for various locations around a wing in figure 58 from reference 30. These results compliment those from the lift fans in that a jet located in front of the wing induced negative lift and a jet, located at the trailing edge produced positive induced lift. Finally, results (fig. 59) from the large scale lift engine test rig of reference 18 show that the lift engines induced lift. As might be anticipated from the previous discussion, the upstream engine induced negative lift while the downstream engine induced positive lift.

The location of fans and engines can be important in terms of lifting capacity at low speeds, because of induced lift. A STOVL aircraft, being designed for short, high load takeoffs should take advantage of theses induced lift capabilities if at all possible. The induced lift data is nearly all from fans within the same configurational family so that jet turbulence and entrainment should be similar and the data should define trends accurately. With variable pitch or fans with other

geometry, the trends should remain the same, but the quantitative results will probably differ.

Prediction Methods

Sophisticated prediction techniques using paneling techniques and complex models of the jet in crossflow have been developed (refs. 31 and 32). These methods are valuable for final prediction of aerodynamic characteristics where they can be merged with semi-empirical means of account for the effects of flow separation on the airframe caused by propulsion flows. Development of complicated aircraft geometry for paneling approaches can be difficult and time consuming for some applications. Relatively, simple semiempirical prediction techniques are useful for preliminary study of transition flight and for simulation. These methods can also be used to separate good from bad when examining preliminary design options. The methods that will be described can easily be combined and incorporated in the spread sheet of a personal computer.

Ground Effects

Empirical methods to estimated ground effects, including fountain flow, have been developed from generalized small scale data. References 25, 26, and 33 are examples of this effort. The upper set of data in figure 60 shows that excellent agreement between the estimate and experiment is possible. However, the lower set of results probably shows the danger of making estimates outside the parameters used in the method development. As discussed in the modeling section of this paper, some of the results of fundamental studies are being questioned, so care must be exercised in interpreting the results of predictions based on small scale data.

Jet-in-Crossflow

If it is desired to locate a fan or engine in a surface with a considerable amount of surface behind the jet, suckdown in transition should be calculated using the relationships developed from small scale data such as those in reference 32. Good agreement with small scale experiments is possible. However, these results are susceptible to the same modeling problems as previously discussed, and care must be taken with their interpretation.

Fan-in-Wing

For prediction purposes, a fan-in-wing arrangement can be presented by a mid-chord jet flap. The jet flap can be at any spanwise or chordwise location as long as it is bounded by the wing. As shown in figure 61, from reference 28, a two dimensional lift coefficient is developed for the wing section through the fan. Two-dimensional jet flap theory (ref. 34) was used to calculate the lift on the wing section upstream of the fan. The aft section of the wing behind the fan has separated flow on the under surface. A lift coefficient of $-V/V_j^{3/2}$ was found to give reasonable agreement with experiment and has been used for computational purposes. The front and rear section lift coefficient are joined to give one complete two-dimensional lift coefficient inside the brackets. One term outside the brackets, from reference 35, converts from two dimensions to three dimensions, and the rest of the terms convert from lift coefficient to lift ratio. The results from this equation are compared with experiment in figure 62 for some of the models listed in figure 52. For the four velocity ratios shown, and for a vertical jet, the equation generally gives the correct trend with configuration variables and, in many cases, reasonable agreement. Figures 63 and 64 show the variation of lift ratio with flight velocity ratio for models 2 (ref. 15) and 3 (ref. 10) with the exit louvers deflected to give thrust. The lift calculated for model 2 does not agree well with the test results with the louvers deflected 20 and 35 degrees. It would appear that the down load behind the fan at lower velocity ratios is substantially more than calculated. The calculated lift is the difference between large loads upstream and downstream from the fan, so that small errors in either value can yield large percentage changes in the final calculated induced lift. Model 3, in figure 64, has a smaller area behind the fan and agreement at low velocity ratios is much better for all vane settings, but deviation is growing at the highest velocity ratio used in the comparison. A more sophisticated representation of the lift aft of the fan could probably improve agreement.

If lift on the wing is known, moment can be calculated assuming that the center of pressure for a jet flap is at midchord. The slope of non-dimensional moment variation with flight-velocity ratio was calculated for models one through six and is compared with experiment in figure 65. Since moment would be expected to be a sensitive indicator of the accuracy of a method, the agreement shown tends to give confidence in the calculation method, at least for a vertical vane setting.

Drag and thrust from deflecting the lift fan exhaust can be calculated but must include the ram drag, the force realized from turning the free stream airflow into the fan. Ram drag can be expressed as $D/T_S = (T/T_S)\,(V/V_j)$. As shown in figure 66, the variation of ram drag with velocity ratio, as calculated from data in reference 10, was actually 1.1 $(T/T_S)(V/V_j)$. This relationship held well to a velocity ratio of 0.4. Next, the equation for the total horizontal force, F_X/T_S was derived.

$$\frac{F_x}{T_s} = \frac{T}{T_s}\left[1.1\frac{V}{V_j}\cos\beta - \sin\beta\left(1-\frac{V}{V_j}\right)\right]$$

The equation is ram drag, assumed to vary by the reduction in flow area by deflecting the turning vanes, minus the thrust force reduced by the residual momentum of the air turned into the fan. Figure 67 shows the variation of horizontal force ratio with flight velocity ratio for the data in reference 10. The data from the reference should be nearly a straight line, and can be extended to zero airspeed to determine the actual flow angle. The calculations on the figure use the actual flow angle. The experiment and calculation agree quite well for zero and 35 1/2 degrees flow turning, but do not agree well with the intermediate flow turning angle. A similar comparison is shown with data from reference 17 in figure 68. This data is for a statorless fan with a boundary layer control inlet. This agreement was good through a flow turning angle of 25 degrees. The above equation seems to give results that can only be made more accurate by test of actual hardware. If thought to be appropriate, the airplane drag can be included in the calculation.

Tilting Lift/Cruise Fans

This component produces lift and thrust be rotating the fan from horizontal to vertical. Since it is used for cruise propulsion, the inlet and nacelle must be compatible with that requirement. The basic equation for net thrust is

$$T = \rho A\left[V_j^2 - VV_j\right]$$

As a thrust coefficient, T_c, the equation becomes

$$T_c = \left(\frac{Fx_D}{qS_D}\right)_{\alpha=0} = 2\frac{A_F}{S}\frac{V_j}{V}\left(\frac{V_j}{V}-1\right)$$

This equation is compared with data from reference 36 in figure 69. The results agree very well inspite of ignoring the duct drag. T_c is the thrust coefficient at zero degrees angle of attack. The horizontal force coefficient, Fx/qS, is the same as T_c at zero degrees, but reflects the effect of angle of attack as shown below

$$\frac{Fx_D}{qS_D} = 2\frac{A_F}{S_D}\frac{V_j}{V}\left[\sin^2\alpha_D - \left(\frac{V_j}{V}-1\right)\cos(\alpha_D+\delta)\right]$$

The $\sin^2\alpha_D$ term empirically compensates for increased duct drag. As shown in figure 70, results from the equation and reference 36 agree quite well.

An expression for F_x/T_s can be derived if constant power is assumed. This means that $V_j = V + V_{js}$. At constant power, V_j increases as airspeed increases because of the ram effect. Either fan blade pitch or fan rpm varies to keep power absorption constant. The resulting equation is

$$\frac{Fx_D}{T_s} = \frac{V}{V_{j_s}}\left(\frac{V}{V_{j_s}}+1\right)\sin^2\alpha_D - \left(\frac{V}{V_{j_s}}+1\right)\cos\alpha_D$$

Expressions for duct lift have also been derived. The equation is of the form

$$C_{LD} = \frac{Fx_D}{qS_D}\sin\alpha_D + C_{L\alpha_D}\alpha D + K\left(\frac{Fx_D}{qS_D}\right)^{1/2}$$

where the first expression is the lift of a jet at some angle to the flight path, the second is the power off lift of the duct and the third represents lift induced on the duct by the jet exhaust. The empirical relationships were derived from data in references 36–38. The equation for duct lift coefficient is, with apologies for length

$$C_{LD} = \frac{Fx_D}{qS_D}\sin(\alpha_D+\delta) + (0.005+0.048AR_D)\alpha_D + \left[(0.011+0.00716AR_D)(\alpha_D+\delta) - (0.00011+0.0000121AR_D)(\alpha_D+\delta)^2\right]\left(\frac{Fx_D}{qS_D}\right)^{1/2}$$

Results from reference 36, for thrust coefficients other than used in the empirical derivations are shown with calculations from the equation in figure 71. Except at the smallest thrust coefficient (highest speed) the agreement was good. Figure 72 contains a comparison with a duct of similar geometry from reference 37. Except for a mid range thrust coefficient, agreement was good. Figure 73 shows similar results from reference 38. This comparison, for an engine of normal turbofan dimensions, showed good agreement to maximum lift which was over predicted by as much as 10%, but the angle for maximum lift agreed well. Finally, in figure 74, data from refer-

not used in the derivation of the equation, and falls somewhat out of the geometric range (smaller aspect ratio) of those powerplants. Agreement is adequate for preliminary design purposes. More precise definition of parameters such as aspect ratio might yield a more accurate equation.

The results for duct lift coefficient may be easily converted to L_D/T_s with the following equation

$$\frac{L_D}{T_s} = \frac{1}{2} C_{L_D} \frac{S_D}{A_F} \frac{V^2}{V_{j_s}^2}$$

Acoustics

Airplane design studies conducted in the 1960s indicated than fan pressure ratio should be much higher than the 1.1 pressure ratio fans provided for the GE XV-5 and used in the models that provided most of the wind tunnel data herein. NASA Ames contracted with GE for the fan whose cross section is shown in figure 75. This fan, designated the LF336, was 36 inches in diameter, had a design pressure ratio of 1.3, and was powered by a J-85 engine. The fan met design specifications but was noisy because it used conventional 1970 design techniques. The fan had 42 blades and 45 stator vanes with 0.15 fan blade chord spacing between. One design goal of most lift fans is to keep them thin, especially for wing-mounted installations. However, this goal is at odds with producing a "quiet" fan. To establish practical quieting techniques, the LF336 was used as a test vehicle to examine the effectiveness of several techniques as applied with lift fan constraints. Reference 40 presents the results of this program.

The noise of a lift fan consists of the so called machinery noise and the noise due to exhaust jet mixing. Machinery noise occurs at blade passing frequency and its harmonics, and is caused by the potential field interaction between the rotor and stator, the fluctuation loading of the stator caused by the wakes from the rotor, inflow distortion, and inflow distortion caused by quasi-steady distortion from atmospheric turbulence. Machinery noise can be reduced by spacing between the rotor and stator (or eliminating the stator), reducing rotor tip speed, controlling propagation with vane-blade ratio and vane lean, careful design of hub support struts, and use of acoustically absorbent material in the flow path.

The test set up for noise measurements is shown in figure 76. Several stator designs are shown in figure 77. In addition, spacing could be changed to one or two chord lengths by inserting plain or acoustically treated spacers between the rotor and the stator. Results of these studies are summarized in figures 78–80. Figure 78, with one chord spacing, shows the effect of increasing stator blade number. While the 90 vane stator reduced the peak perceived noise level only 2 PNdb, over a range from 30 to 100 degrees, noise was reduced 4-5 PNdb. Figure 79, at 80% rpm, shows that the stator with 90 leaned vanes reduced peak noise about 8 PNdb. This was done with no increase in fan thickness. Two chords spacing with acoustic treatment further reduced peak noise 4 PNdb, while acoustically treated louvers reduced the noise peak another 2 PNdb. Similar results at 95% fan rpm are shown in figure 80. The total noise reduction, without acoustic louvers, was 10 PNdb compared with 12 PNdb at the lower power setting.

In the early 1970s, a single stage fan designed to function without a stator did not exist, but was thought to offer the best chance for a quiet thin fan for a thin wing. Therefore, under contract to NASA, GE designed and fabricated a statorless fan to fit the LF336 frame. Figure 81 is a cross section of this fan. While the fan turbomachinery worked to specification, as discussed in reference 41, the hub base pressure was much more negative then expected, so that total thrust was less than expected. Peak PNL is compared with a fan with stator from reference 40. Figure 82 shows the statorless fan noise was about the same level as the conventional rotor-stator fan with two chords.

Another research topic was included in this program. Reference 42 described noise reductions from a serrated edge on a low speed rotor. This idea was studied at turbomachinery Mach numbers and Reynolds numbers in a two dimensional cascade (ref. 43). Figure 83 shows the serration configurations studied. All serration configurations reduced noise and improved aerodynamic performance. Configuration SR6 was chosen for study on the statorless fan. Data in figure 84 show that the serrations reduced PNL for the three fan speeds. Although not shown by PNL comparisons, the serrations reduced broad band noise substantially in the forward arc. Perhaps more interesting are the gains in performance due to the serrations shown in figure 85. Both the flow deviation angle and the total pressure loss coefficient were reduced by serrations, and flow noise from the cascade, shown in figure 86, also was reduced by serrations.

Fan noise variation with flight speed received limited study. Figure 87 shows on installation in the 40 × 80 foot wind tunnel. The semispan model had the LF336 fan mounted in a wing. Acoustic treatment was put on the floor of the tunnel and the J-85 drive engine inlet was heavily muffled. Figure 88 shows another model powered with X-376 fans that was used in the study. The data in figure 89, from reference 44, show the variation of blade

passing frequency sound power level with airspeed. Two of the data curves are from the models just described, and one is from the GE XV-5B in flight. While the shapes of the curves vary, the noise increases with airspeed. It was stated at the beginning of this section that blade passing frequency noise is caused by distorted inlet flow, so it is not surprising that noise increased as flight speed and hence distortion increased. Broad band jet mixing noise is presented as a function of Strouhal number for several airspeeds in figure 90, from reference 45. The jet noise increased with flight speed, illustrating the highly turbulent nature of a jet in cross flow. These effects of forward speed on noise should be included in STOVL lift fan noise estimates.

Noise of a lift fan can be reduced by appropriate noise control design techniques, with little, if any performance or weight penalty. Noise can be further reduced by lining the flow path with noise attentuating material.

Concluding Remarks

The salient points made in the above text are summarized here.

Experimental experience indicates that, if ground based facilities are to provide accurate results in the hover and transition flight regimes of lift fan aircraft, the propulsion systems, jet turbulence, and flow entrainment must be accurately simulated. Large or full scale powerplants, as similar as possible to those planned for the aircraft, are most likely to provide an adequate simulation.

For lift fans in any installation, minimum inlet hardware is best to minimize flow anomalies that are induced into the inlet. Placing the fan rotor very near the inlet radius, even in a deep installation, forces the fan to act as an inlet flow control device. Small angularity in deep ducts can dramatically improve performance.

An inlet boundary layer control system was shown to be effective in a very short inlet. This is a method that can reduce fan thickness in installations where that is important.

For a 1.3 pressure ratio fan, a flow deflection of 90 degrees is possible with only 6% losses. This could, however, be a major portion of the payload on a VTOL mission. Weight and complexity of a flow turning device may make tilting powerplants, as in the VJ-101, attractive.

Flows from lift fans and engines induce sizable forces and moments on the airframe. These induced effects may be favorable or unfavorable in hover and transition flight, depending on fan location. Careful utilization of these effects can augment STOVL performance.

Unsophisticated semiempirical prediction techniques were presented for some forces and moments on wings and tilt duct nacelles. These methods can be incorporated in the spread sheet of personal computers for preliminary design purposes. Where necessary, configuration specific equations can be developed for the same use.

A number of ways to minimize lift fan noise will not compromise performance or increase volume, and should be included in any design. An increase in fan depth and adding acoustic treatment can further reduce noise with some penalty. A statorless fan can provide a relatively thin installation with noise levels comparable to the best conventional fan.

Forward speed increases lift fan noise in two ways. The inlet flow distortion increases the noise at blades passing frequency and its harmonics, and the jet mixing noise in increased by the jet-in-crossflow environment.

References

1. Mort, Kenneth.: Summary of Large-Scale Tests of Ducted Fans. NASA SP 116, Paper 8, April, 1966.

2. Hickey, David H.; and Cook, Woodrow L.: Aerodynamics of V/STOL Aircraft Powered by Lift Fans. AGARD CP 22, September 11–13, 1967.

3. Aoyagi, Kiyoshi; Hickey, David H.; and deSavigny, Richard A.: Aerodynamic Characteristics of a Large-Scale Model with a High Disk-Loading Fan Mounted in the Fuselage, NASA TN D-775, October, 1961.

4. Davenport, Edwin E.; and Kuhn, Richard E.: Wind Tunnel-Wall Effects and Scale Effects on a VTOL Configuration With a Fan Mounted in a Fuselage. NASA TN D-2560, January, 1965.

5. Margason, Richard: Propulsion-Induced Effects Caused by Out-of-Ground Effects. Proceedings of the International Powered Lift Conference, December 7–10, 1987, pp. 31–57.

6. Gentry, G. L.; and Margason, R. J.: Jet-Induced Lift Losses on VTOL Configurations Hovering In and Out of Ground Effect. NASA TN D-3166, February, 1966.

7. Kuhn, Richard E.: Hover Suckdown and Fountain Effects. Proceedings of the International Powered Lift Conference, December 7–10, 1987, pp. 1–18.

8. Christiansen, R. S.: A Large Scale Investigation of VSTOL Ground Effects. AIAA Paper 84-0336, presented at the 22nd Aerospace Sciences Meeting, January 9–12, 1984.

9. Schmidt, Susan B.: Hover Test Results of a Small-Scale Twin-Tilt Nacelle Model. NASA TM-86665, March 1984.

10. Kirk, Jerry V.; Hickey, David H; and Hall, Leo P.: Aerodynamics of a Full-Scale Fan-In-Wing Model Including Results in Ground Effect With Nose-Fan Pitch Control. NASA TN-2368, July 1964.

11. Koenig, D. G.: Wind Tunnel Testing, Special Course on V/STOL Aerodynamics. AGARD Report 710, June 1984, pp. 9–1 to 9–71.

12. Hickey, David H.: Preliminary Investigation of the Characteristics of a Two-Dimensional Wing and Propeller with the Propeller Plane of Rotation in the Wing-Chord Plane. NACA RM A57F03, 1957.

13. Hickey, David H.; and Ellis, David R.: Wind-Tunnel of a Semispan Wing with a Fan Rotating in the Plane of the Wing. NASA TN D-88, 1959.

14. Diedrich, J. H.: Summary of Model VTOL Lift Fan Tests Conducted at NASA Lewis Research Center, Proceedings of NASC Workshop on Prediction Methods for Jet V/STOL Propulsion Aerodynamics, July 28–31, 1975.

15. Hickey, David H.; and Hall, Leo P.: Aerodynamic Characteristics of a Large-Scale Model with Two High-Disk-Loading Fans Mounted in the Wing. NASA TN-1650, February 1963.

16. Przedpelski, Zygmunt J.: Lift Fan Technology Studies. NASA CR-761, April, 1967.

17. Hodder, Brent K.; Kirk, Jerry V.; and Hall, Leo P.: Aerodynamic Characteristics of a Large-Scale Model with a Lift Fan Mounted in a 5-Percent-Thick Triangular Wing, Including the Effects of BLC on the Lift-Fan Inlet. NASA TN D-7031.

18. Tolhurst, William H., Jr.; and Kelly, Mark W.: Characteristics of Two Large-Scale Jet-Lift Propulsion Systems. NASA SP-116, Paper 15, April 4–5, 1966.

19. Kirk, Jerry V.; and Barrack, Jerry P.: Reingestion Characteristics and Inlet Flow Distortion of V/STOL Lift-Engine Fighter Configurations. NASA TN D-7014, December, 1970.

20. Hodder, Brent K.; and Kirk, Jerry V.: Large-Scale Studies of Propulsion-Flow Turning Devices for Pan-Powered V/STOL Aircraft, Proceedings of NASC Workshop on Prediction Methods for Jet V/STOL Propulsion Aerodynamics. Vol 1, July 28–31, 1975.

21. Anonymous: Full-Scale Tests of Grumman Design 698-411 Tilt-Nacelle V/STOL Model at the NASA Ames Research Center. Grumman Aerospace Corp., December, 1981.

22. Anonymous: Large-Scale Tests of a Tilt-Nacelle V/STOL Propulsion/Attitude Control System. NASA CR-152181, 1978.

23. Esker, D. W.: Ground Tests of the "D" Shaped Vented Thrust Vectoring Nozzle. NASA CR-137959, October, 1976.

24. Kuhn, R. E.: An Empirical Method for Estimating Jet Induced Lift Losses of V/STOL Aircraft. NADC Proceedings of a Workshop on V/STOL Aerodynamics, May 1979.

25. Foley, W. H.: Development of an Experimental Basis for a Handbook-Method to Predict Ground-Induced Forces on a Hovering V/STOL Aircraft. NADC Proceedings of a Workshop on V/STOL Aerodynamics, May 1979.

26. Kotansky, D. R.; and Glaze, L. W.: Development of an Empirical Data Base and Analytical Modeling of Multi-Jet V/STOL Flow Fields in Ground Effect. NADC proceedings of a Workshop on V/STOL Aerodynamics, May 1979.

27. Orloff, Kenneth L.; Snyder, Philip K.; and Reinath, Michael S.: Laser Velocimetry in the Low Speed Wind Tunnels at Ames Research Center. NASA TM-85885, January, 1984.

28. Hickey, David H.; and Kirk, J. V.: Studies of Forces Induced on V/STOL Aircraft by Propulsion Flows. Proceeding of NASC Workshop on Prediction Methods for Jet V/STOL Propulsion Aerodynamics, July 28–31, 1975.

29. Hickey, David H.; Kirk, Jerry V.; and Hall, Leo P.: Aerodynamic Characteristics of a V/STOL Transport Model with Lift and Lift-Cruise Fan Power Plants. NASA SP-116, Paper 7, April 4–5, 1966.

30. Winston, M. M.: Propulsion Induced Aerodynamic Interference Effects on Jet-Lift Aircraft. Proceedings of NASC Workshop on Prediction Methods for Jet V/STOL Propulsion Aerodynamics, July 28–31, 1975.

31. Beatty, T. D.: A Prediction Methodology for Propulsive Induced Forces and Moments in Transition and STOL Flight. Proceedings of a NADC Workshop on V/STOL Aerodynamics, May 16–18, 1979.

32. Margason, Richard; and Kuhn, Richard: Application of Empirical and Linear Methods to V/STOL Powered-Lift Aerodynamics, Proceedings of the International Powered Lift Conference, December 10, 1987.

33. Spong, David E.; Kamman, J. H.; and Flood, J. D.: V/STOL Jet-Induced Interactions. Proceeding of a NADC Workshop on V/STOL Aerodynamics, May 16–18, 1979.

34. Malavard, Lucien C.: Recent Developments in the Method of Rheo-Electric Analogy Applied to Aerodynamics. Journal of Aerospace Science, vol. 24, no. 5, May 1957, pp. 321–331,

35. De Young, John: Theoretical Symmetric Span Loading Due to Flap Deflection for Wings of Arbitrary Planform at Subsonic Speeds. NACA TR-1071, 1952.

36. Mort, Kenneth W.; and Gamse, Berl: A Wind Tunnel Investigation of a 7-Foot-Diameter Ducted Propeller. NASA TN-4142.

37. Mort, Kenneth W.; and Yaggy, Paul F.: Aerodynamic characteristics of a 4-Foot-Diameter Ducted Fan Mounted on the Tip of a Semispan Wing. NASA TN D-1301, April, 1962.

38. Betzina, Mark D.; and Kita, Richard: Aerodynamic Effects of an Attitude Control vane on a Tilt-Nacelle V/STOL Propulsion System.

39. Giulianetti, Demo J.; Biggers, James C.; and Corsiglia, Victor R.: Wind-Tunnel Test of a Full-Scale, 1.1 Pressure Ratio, Ducted Lift-Cruise Fan. NASA TN D-2498, November, 1964.

40. Kazin, S. B.; and Volk, L. J.: LF336 Lift Fan and Acoustic Test Program. NASA CR-1934, December, 1971.

41. Smith, E. G.; Stempert, D. L.; and Uhl, W. R.: Design, Fabrication and Acoustic Tests of a 36 inch (.914 meter) Statorless Turbotip Fan. NASA CR-2597, September, 1975.

42. Soderman, Paul T.: Leading Edge Serrations Which Reduce the Noise of Low-Speed Rotors. NASA TN D-7371, 1973.

43. Smith E. G.; and Sowers, H. D.: Cascade Tests of Serrated Leading Edge Blading at High Subsonic Speeds. NASA CR-2472, December, 1974.

44. Stimpert, D. L.: Effect of Crossflow Velocity on VTOL Lift Fan Blade Passing Frequency Noise Generation. NASA CR-114566, February, 1973.

45. Stimpert, D. L.; and Fogg, R. G.: Effect of Crossflow Velocity of the Generation of Lift Fan Jet Noise in VTOL Aircraft. NASA CR-114571, February, 1973.

PAGE 12 INTENTIONALLY BLANK

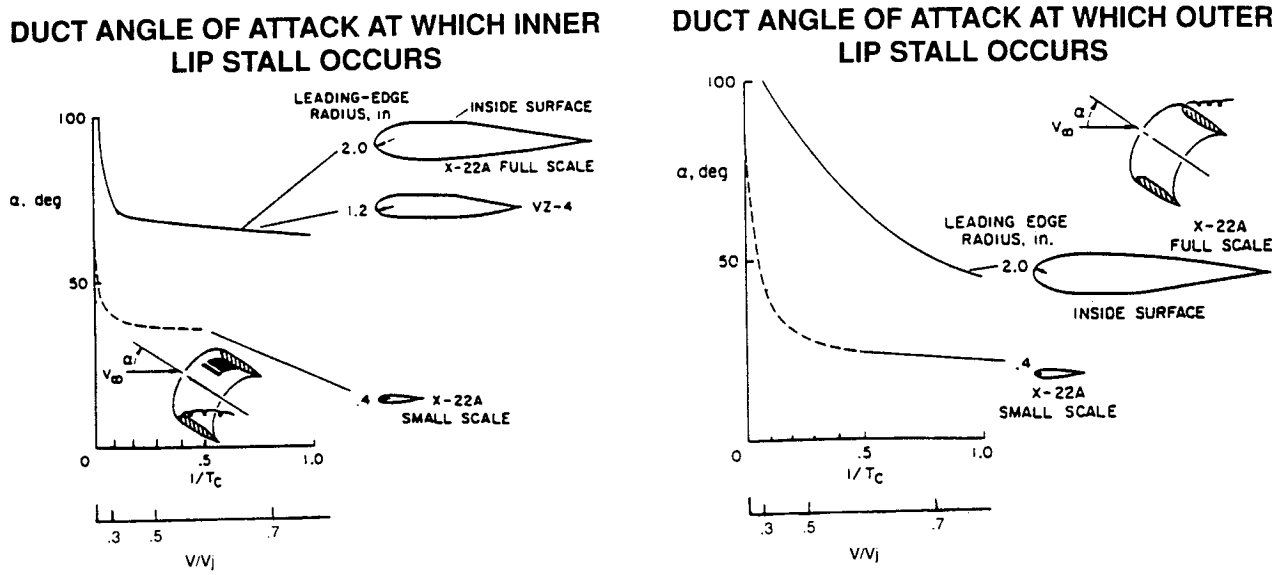

Figure 1. Effect of Reynolds number on duct inlet flow separation

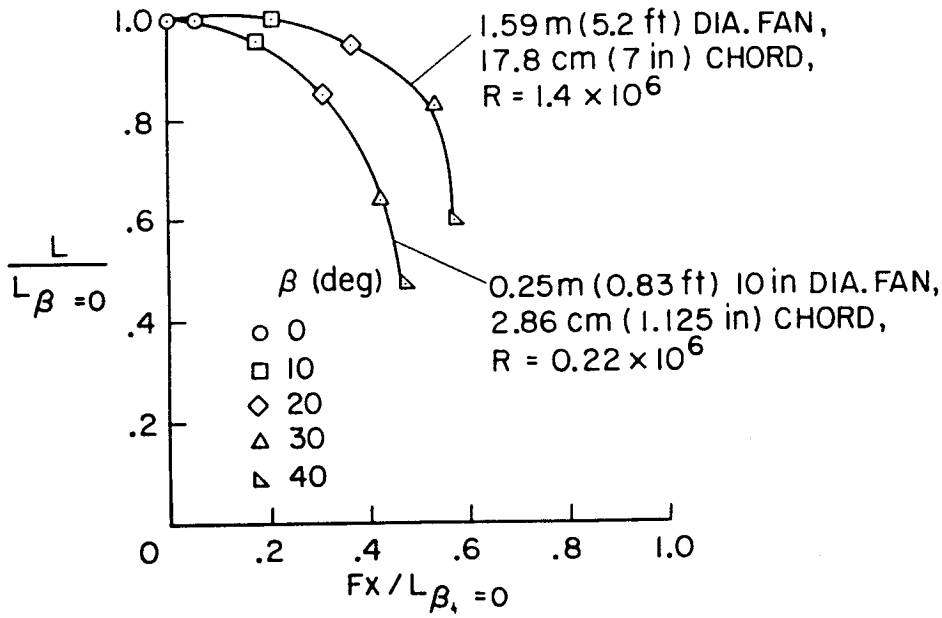

Figure 2. Effect of Reynolds number on vane cascade turning efficiency

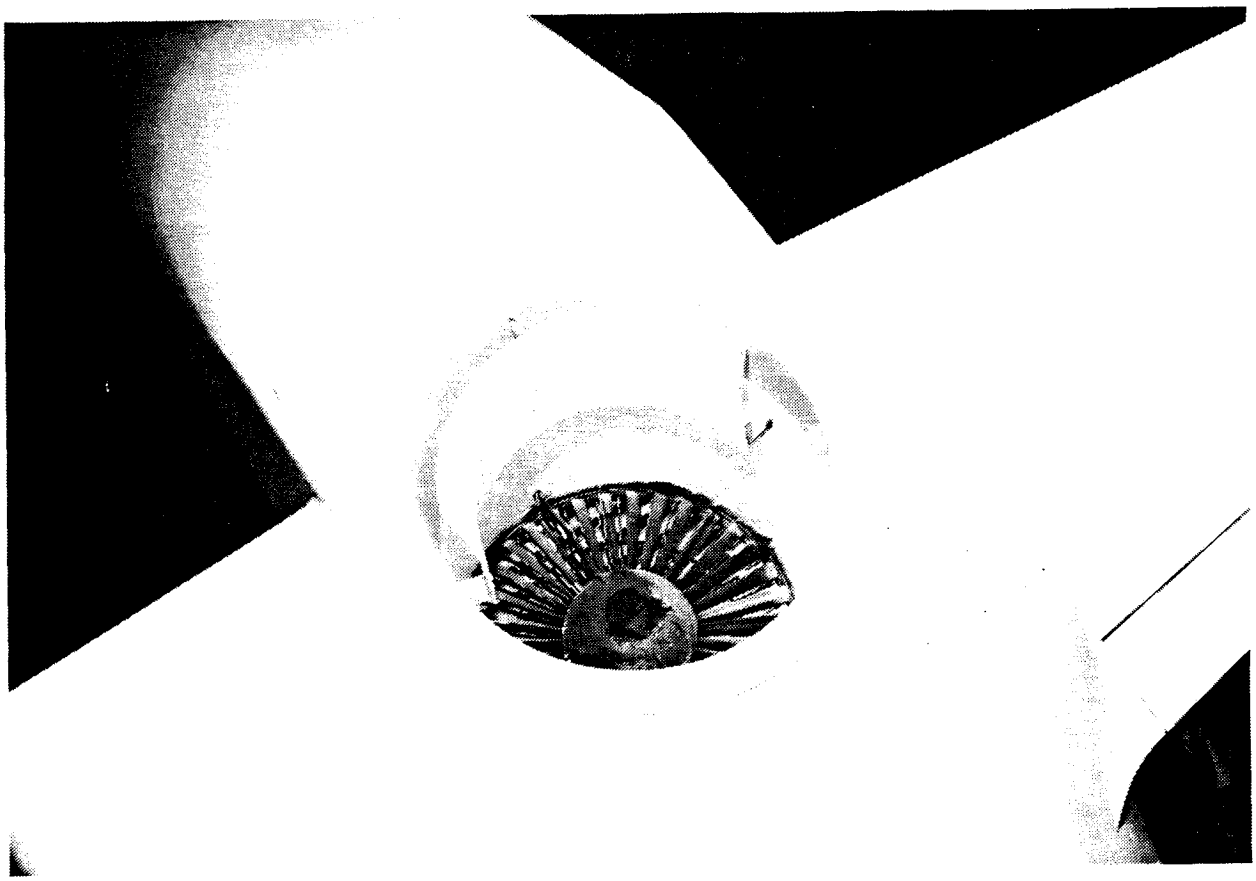

Figure 3. View of full-scale fan-in-fuselage model mounted in the 40x80- foot wind tunnel

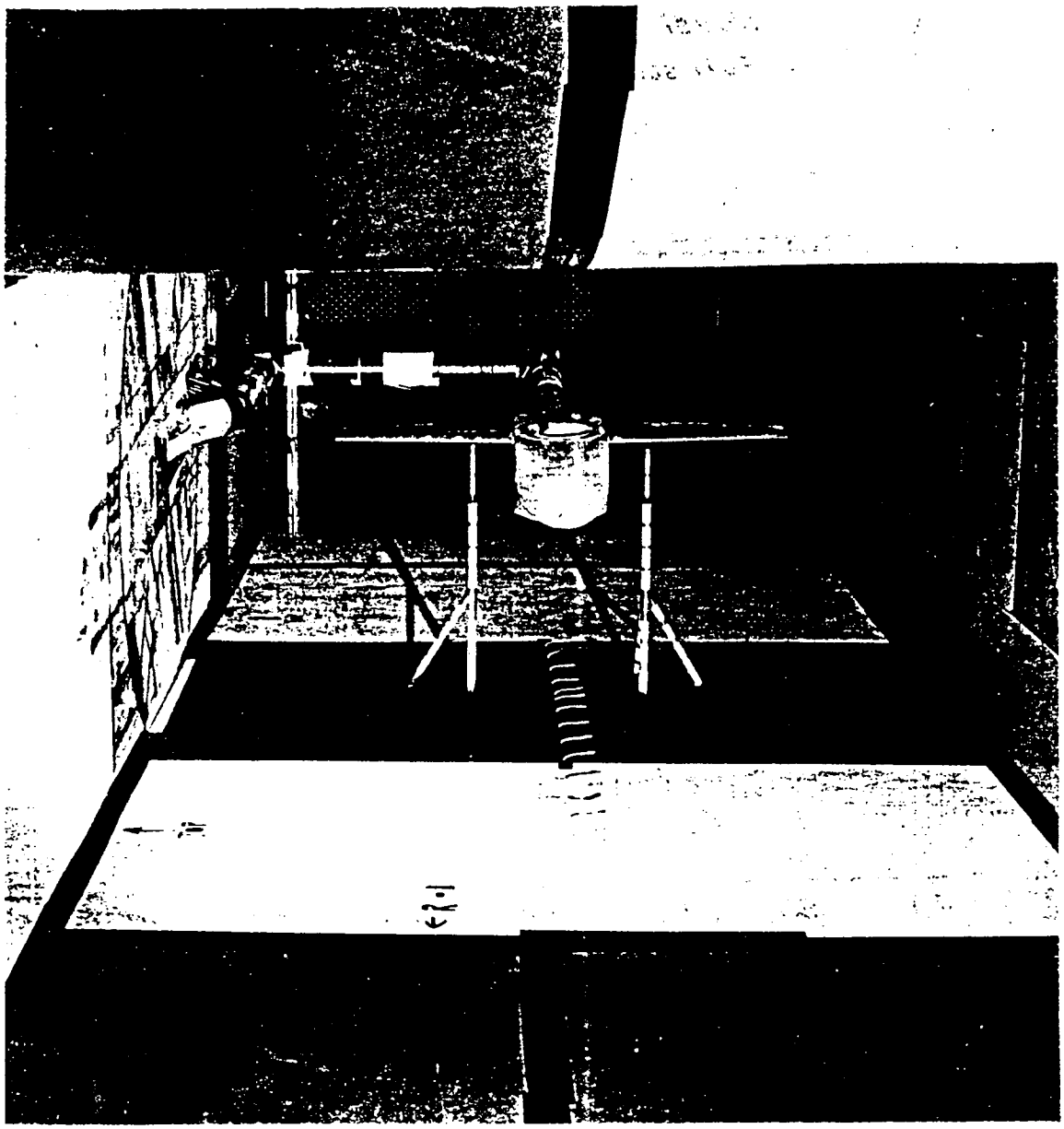

Figure 4. Test setup for the 1/9 scale fan-in-fuselage model in the Langley Research Center's 7x10- foot wind tunnel

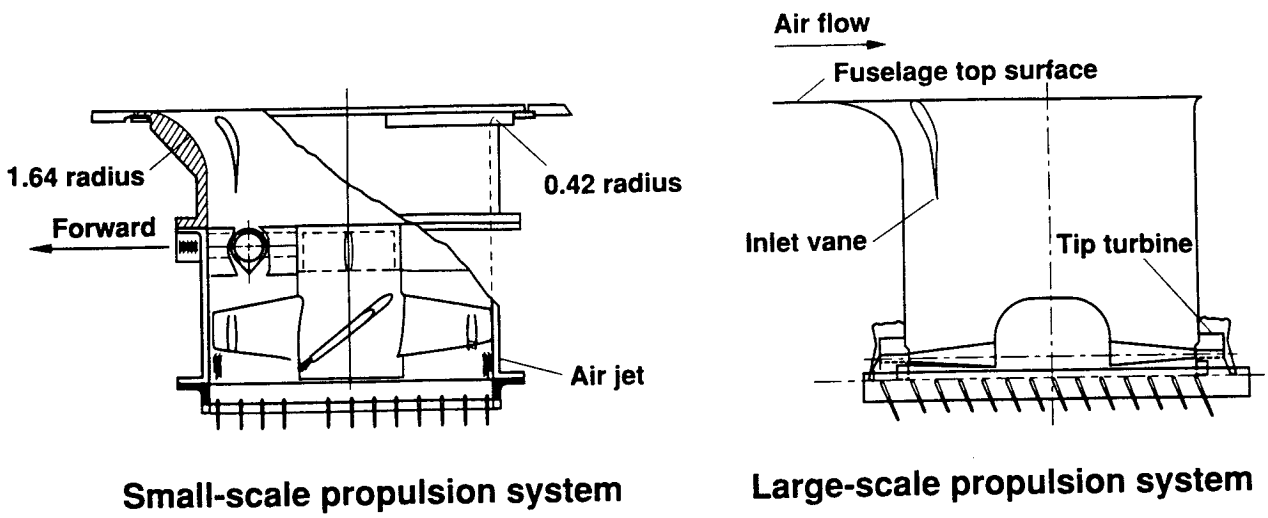

Figure 5. Powerplant cross sections for the full- and small-scale fan-in-fuselage models

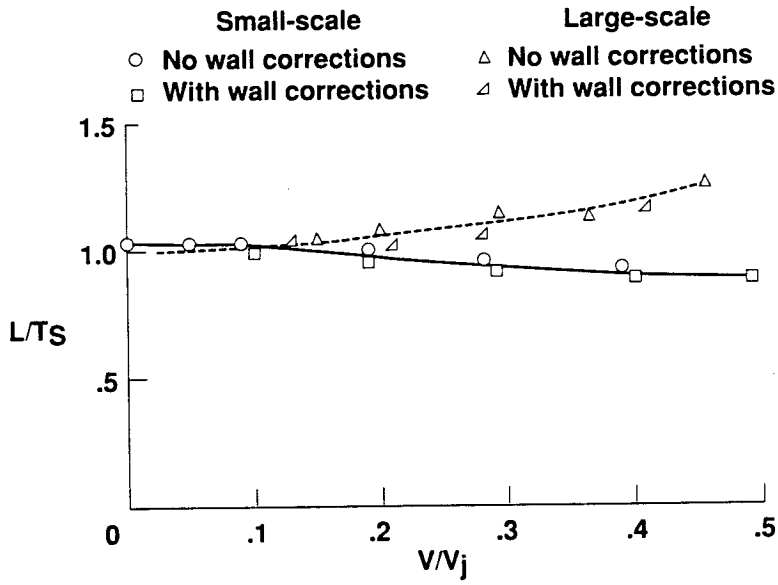

Figure 6. Comparison of small- and large-scale model lift variation with forward speed

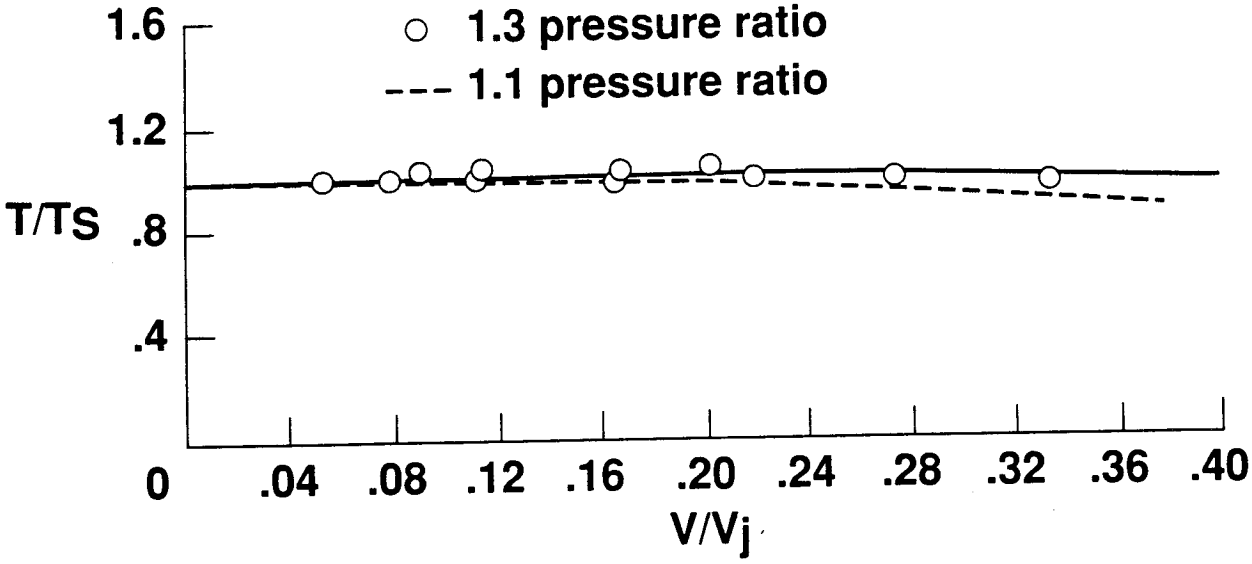

Figure 7. Variation of thrust with airspeed for two full-scale lift fans

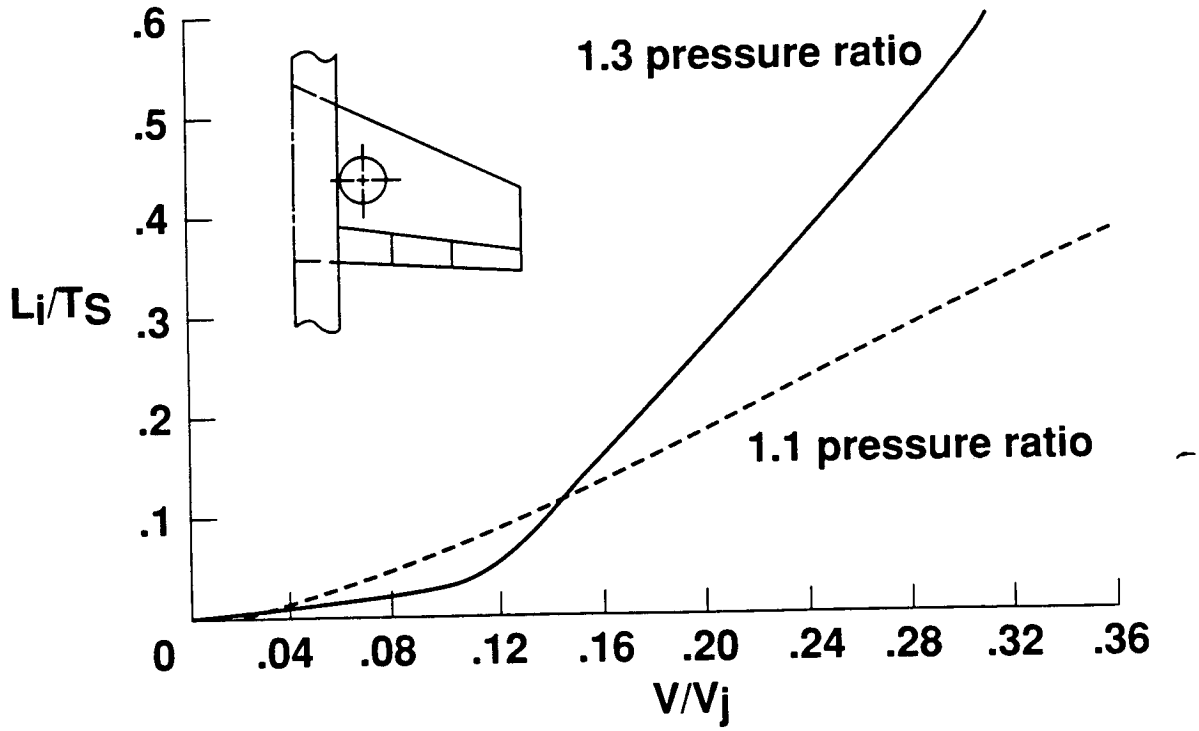

Figure 8. Variation of induced lift with airspeed for two different full-scale fans mounted in the same wing

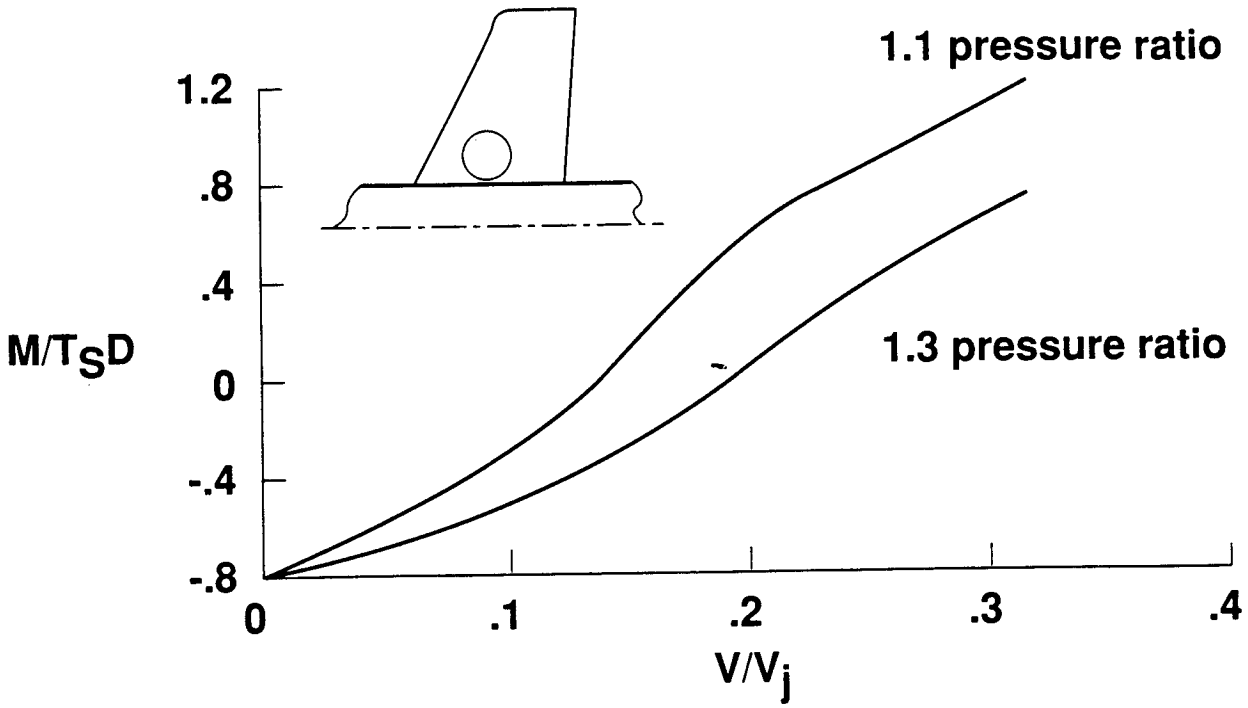

Figure 9. Variation of pitching moment with airspeed for a small- and full-scale fan

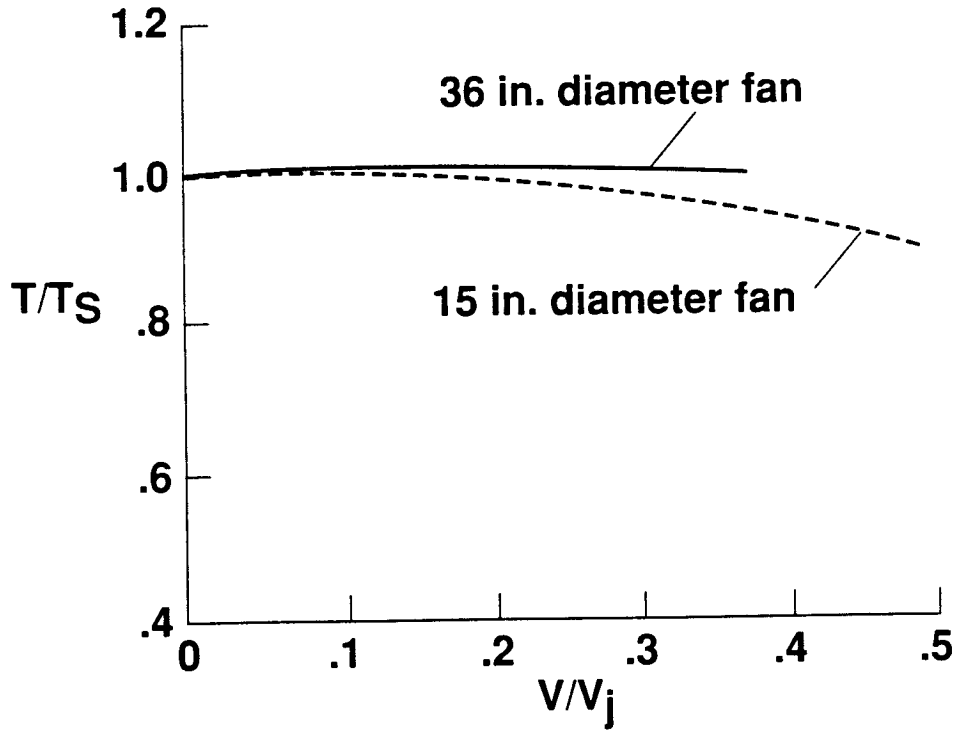

Figure 10. Variation of thrust with airspeed for a small- and full-scale fan

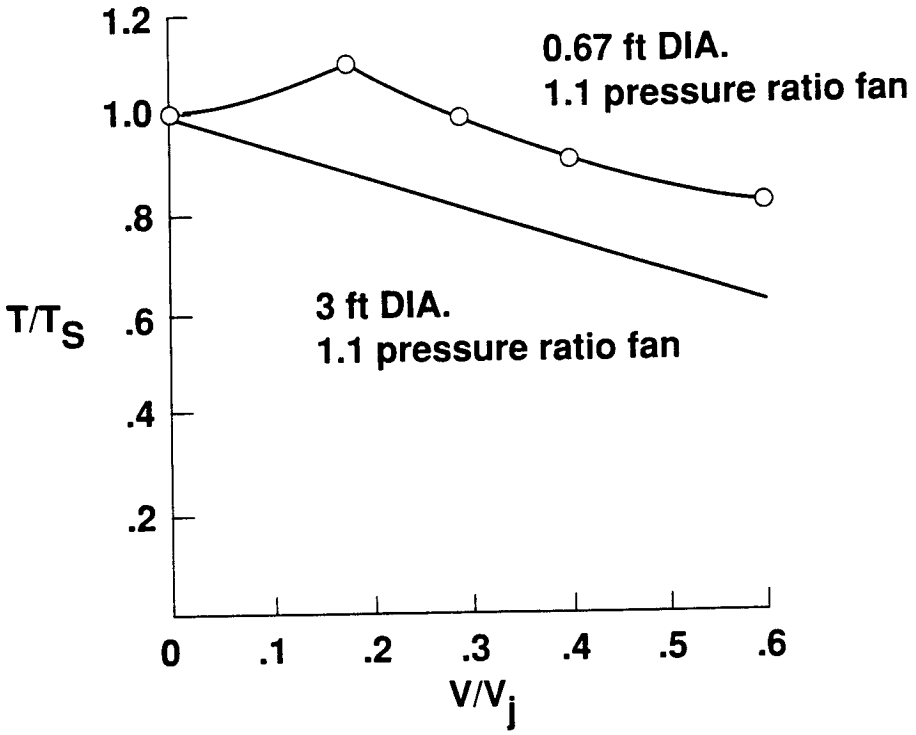

Figure 11. Variation of thrust with airspeed for a small- and full-scale fan

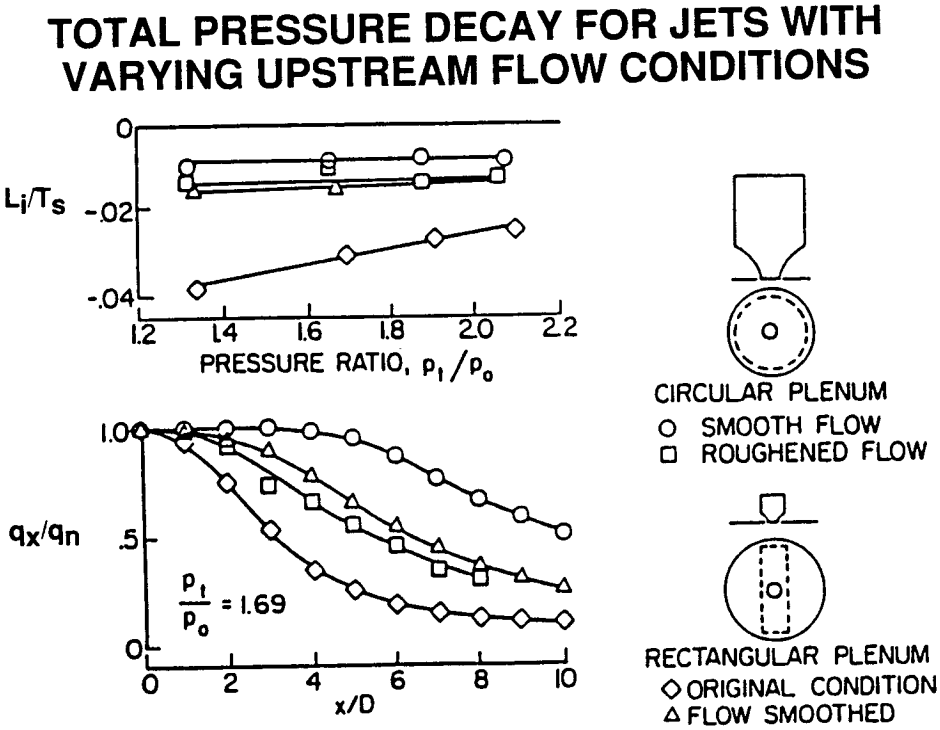

Figure 12. Total pressure decay for jets with varying upstream flow conditions

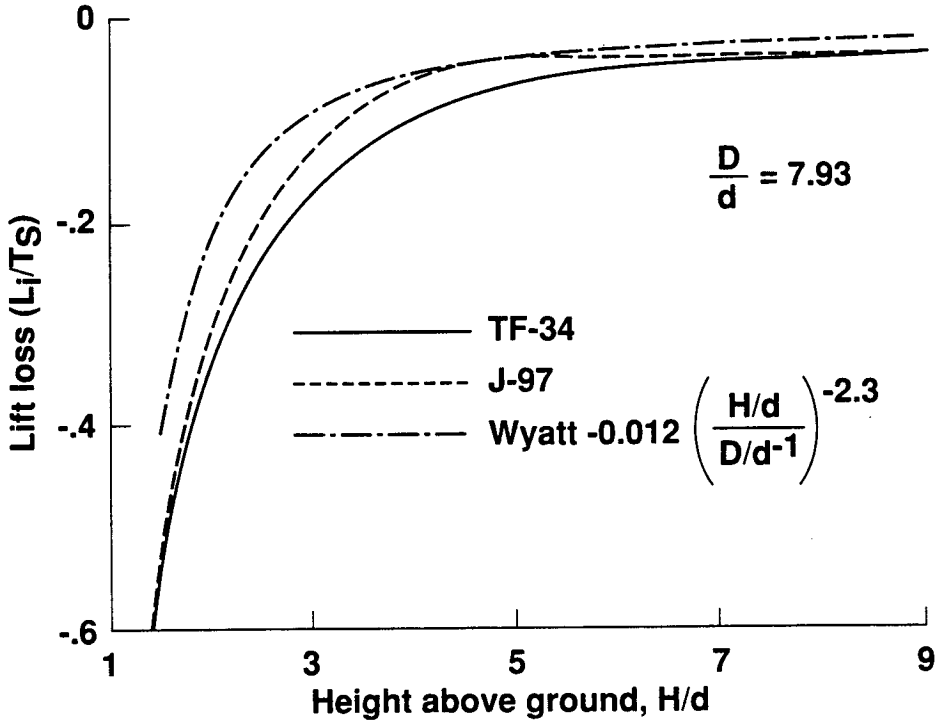

Figure 13. Hover induced lift in ground effect for two full-scale engines and an empirical result from small-scale experiments

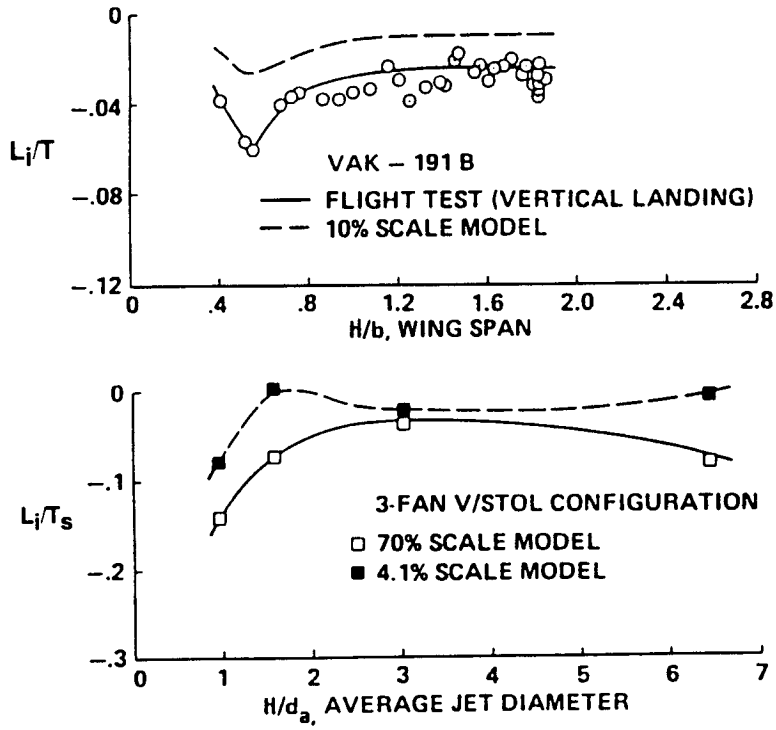

Figure 14. Small- and large-scale comparisons of ground effect for complete aircraft configurations

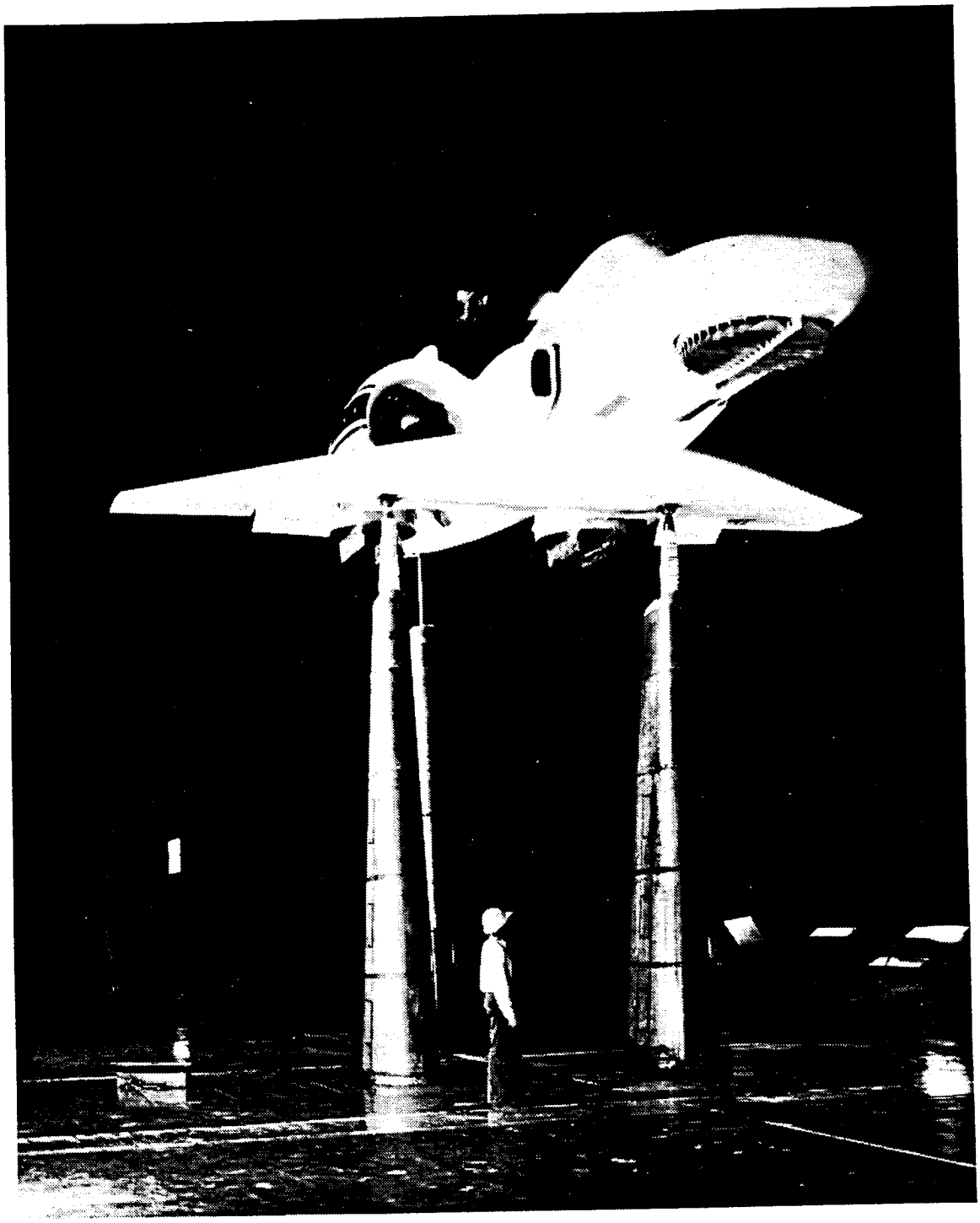

Figure 15. The McDonnel Douglas model 260 in the 40x80-foot wind tunnel

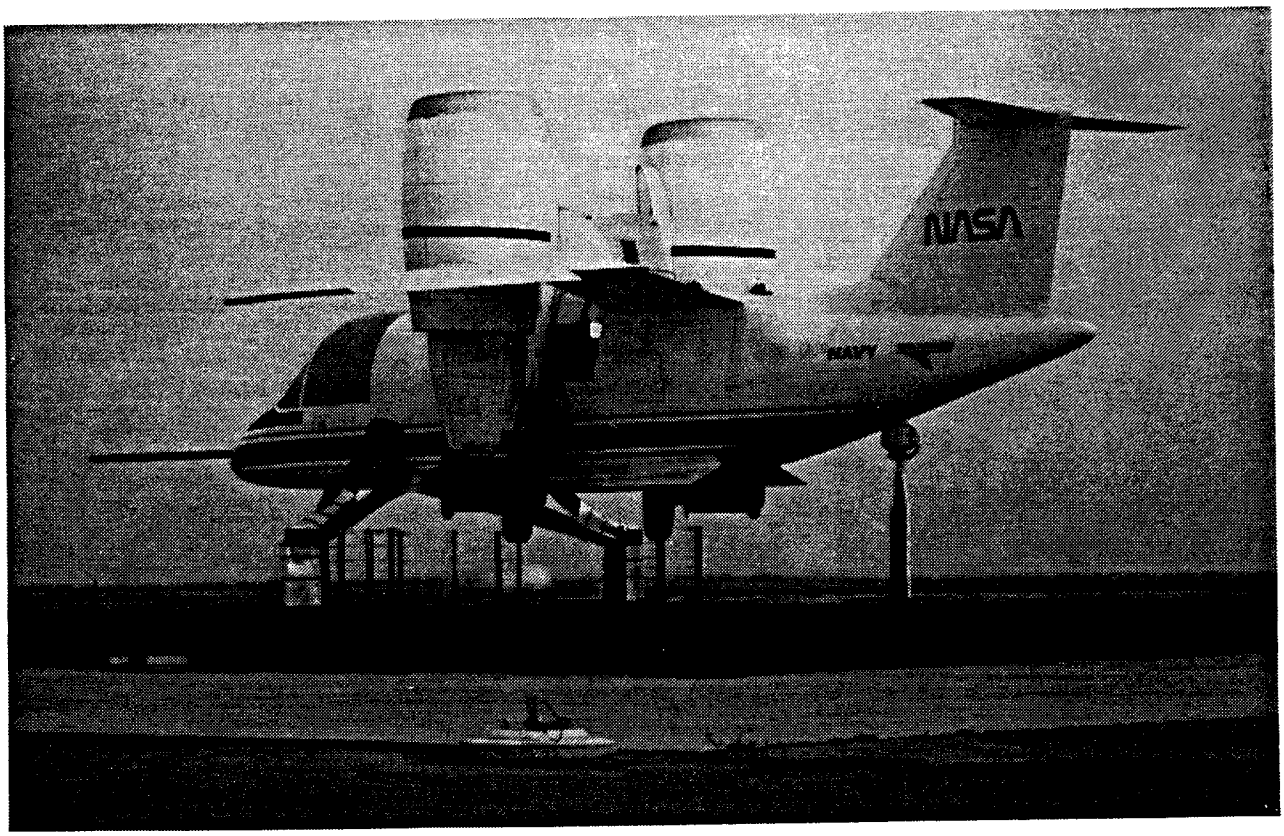

Figure 16. Full-scale Grumman model 698 on the Ames Outside Aerodynamic Research Facility

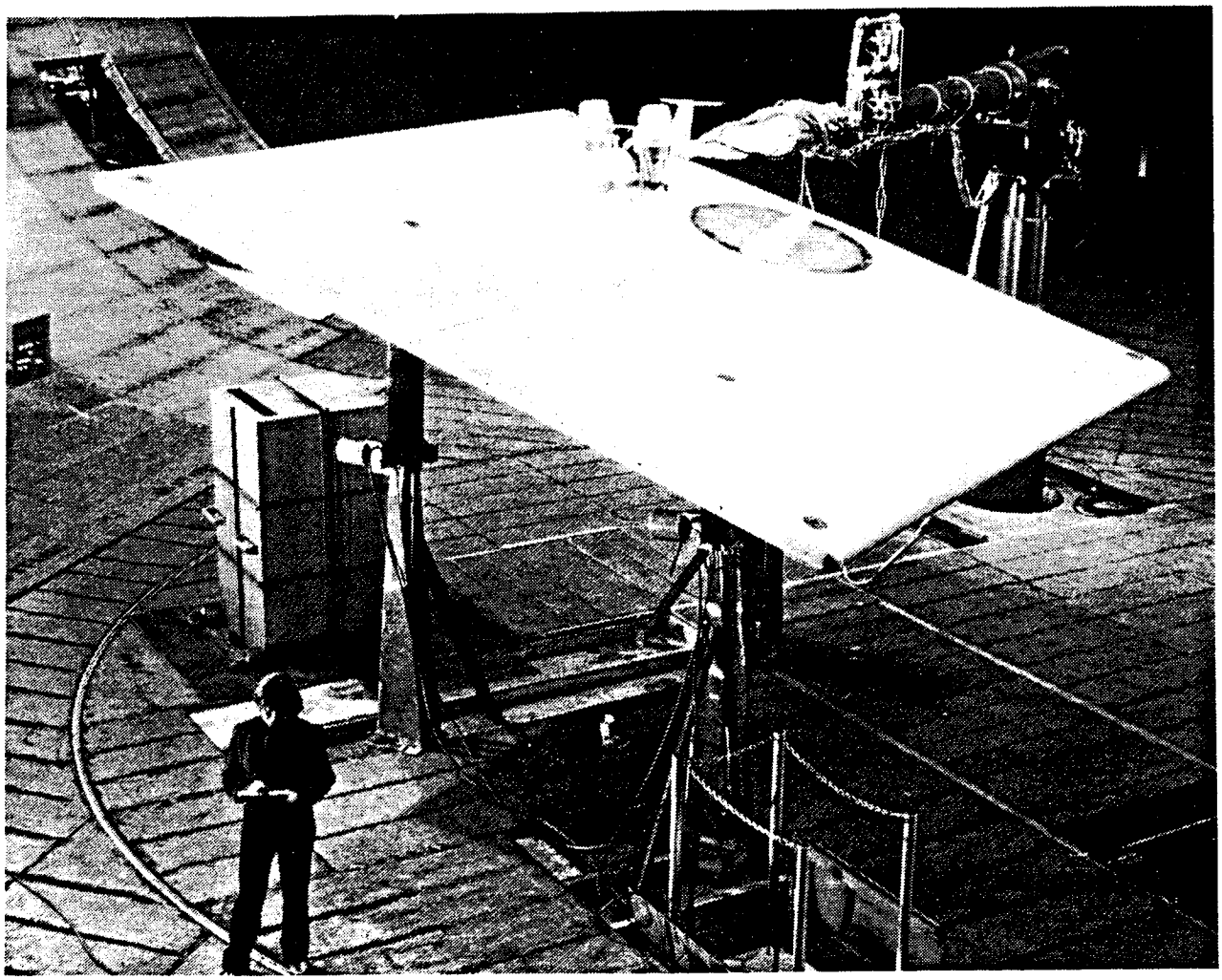

Figure 17. Set up for small-scale ground effect tests of the Grumman model 698

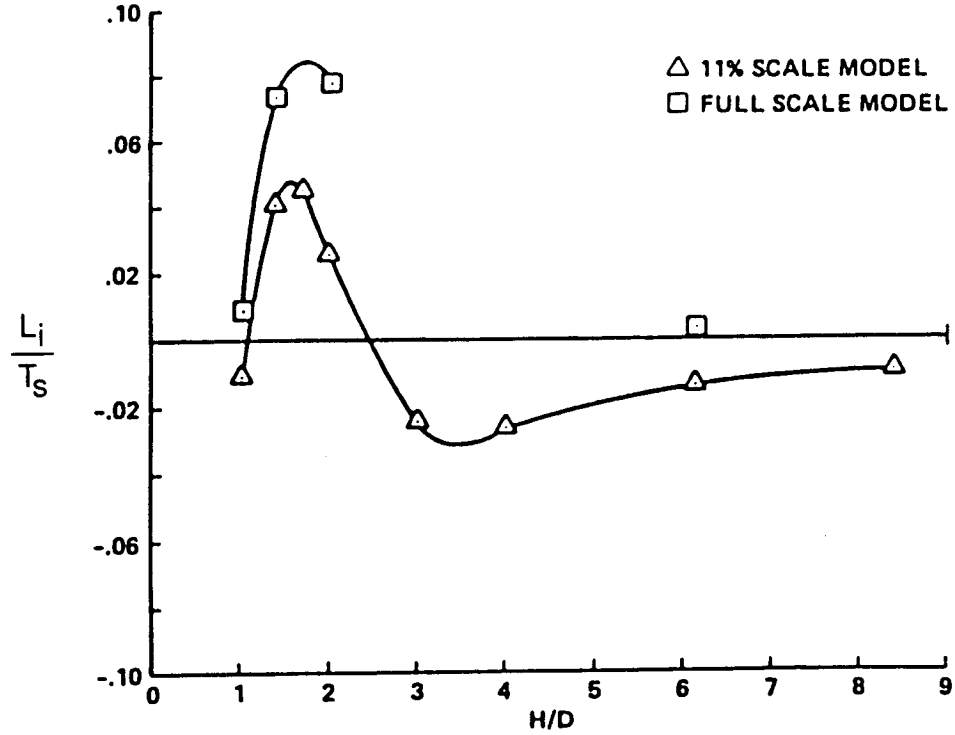

Figure 18. Ground effects for the small- and large-scale Grumman model 698

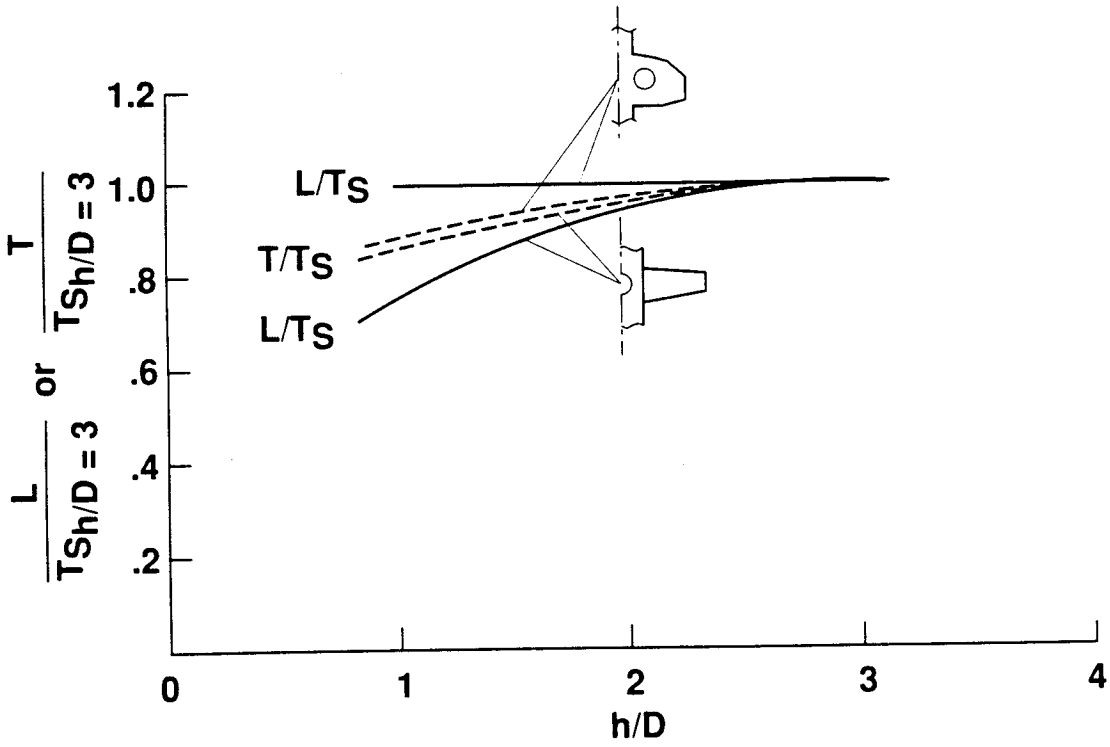

Figure 19. Ground effect for two full-scale models

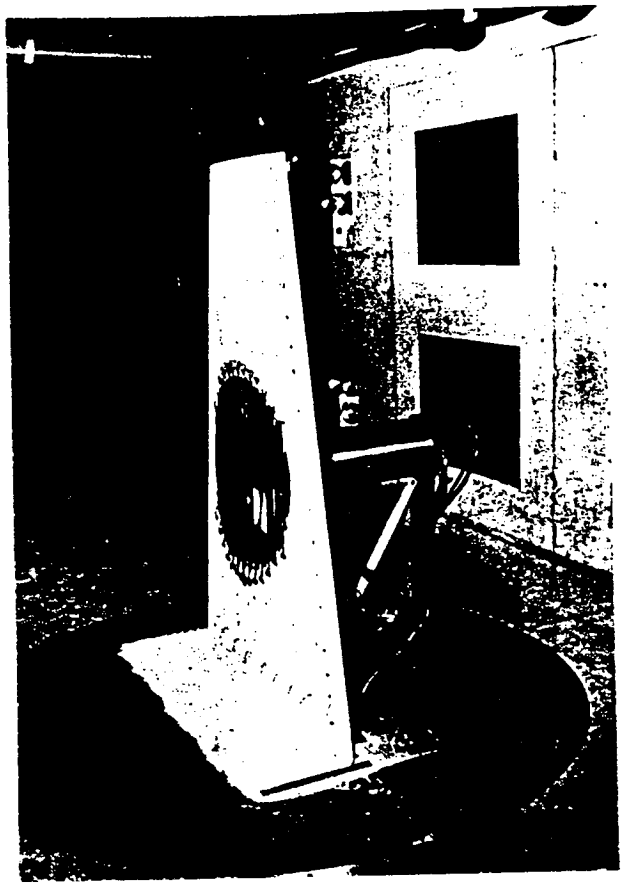

With inlet vanes.

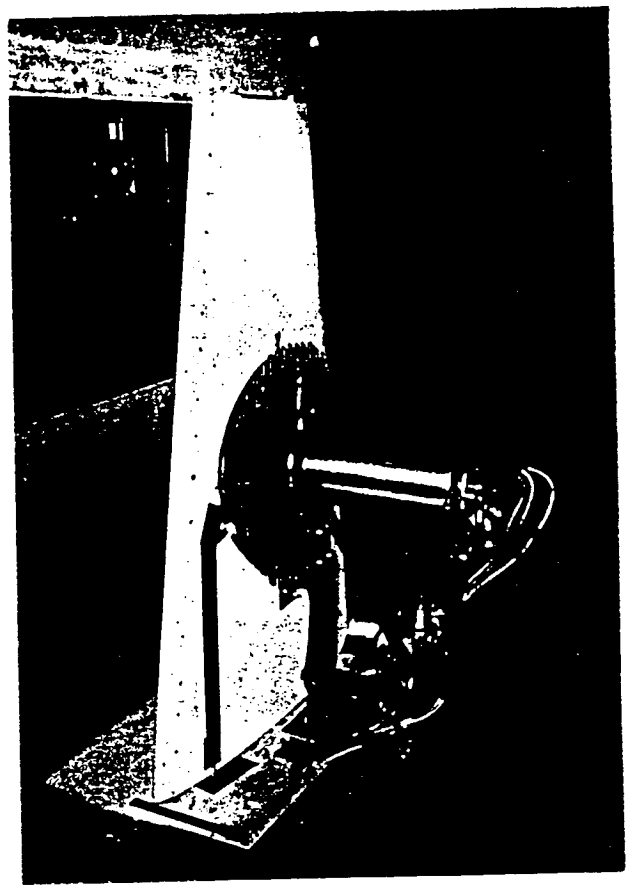

With exit vanes.

Figure 20. 1958 arrangement for semispan fan-in-wing model in the Ames 7x10 foot wind tunnel

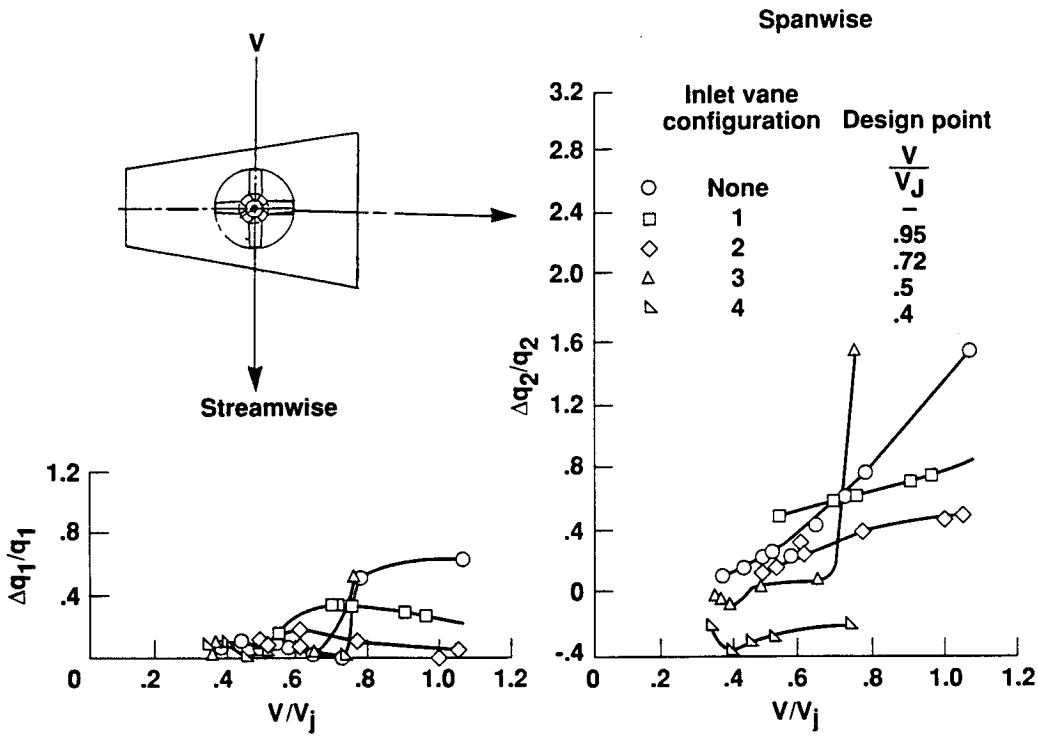

Figure 21. Distortion of fan flow

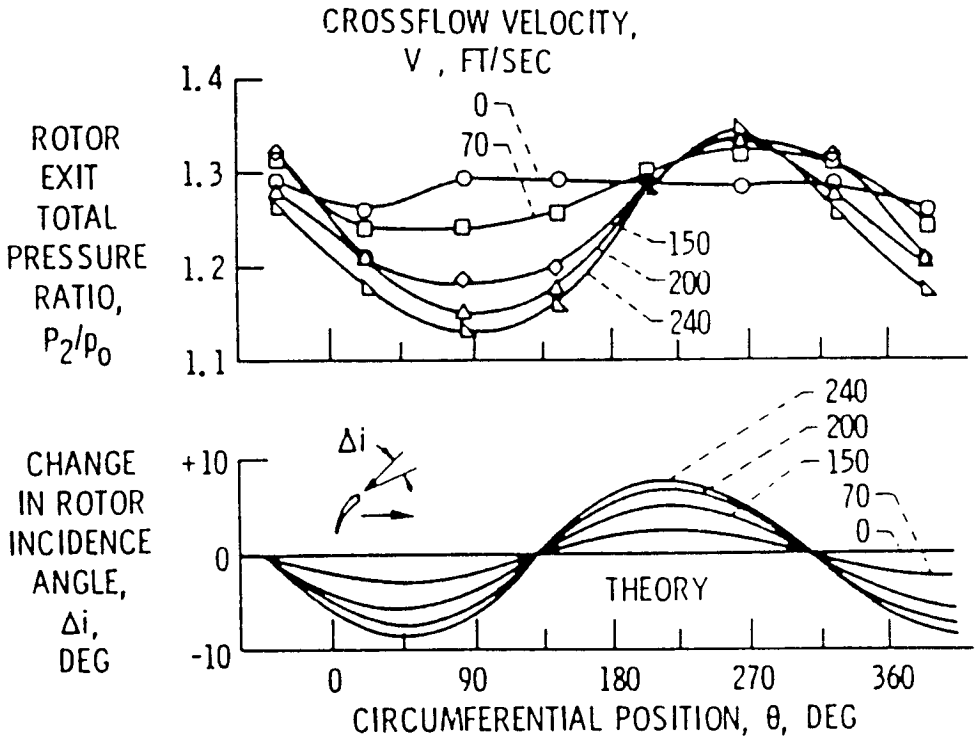

Figure 22. Fan-in-wing internal aerodynamics at forward speed

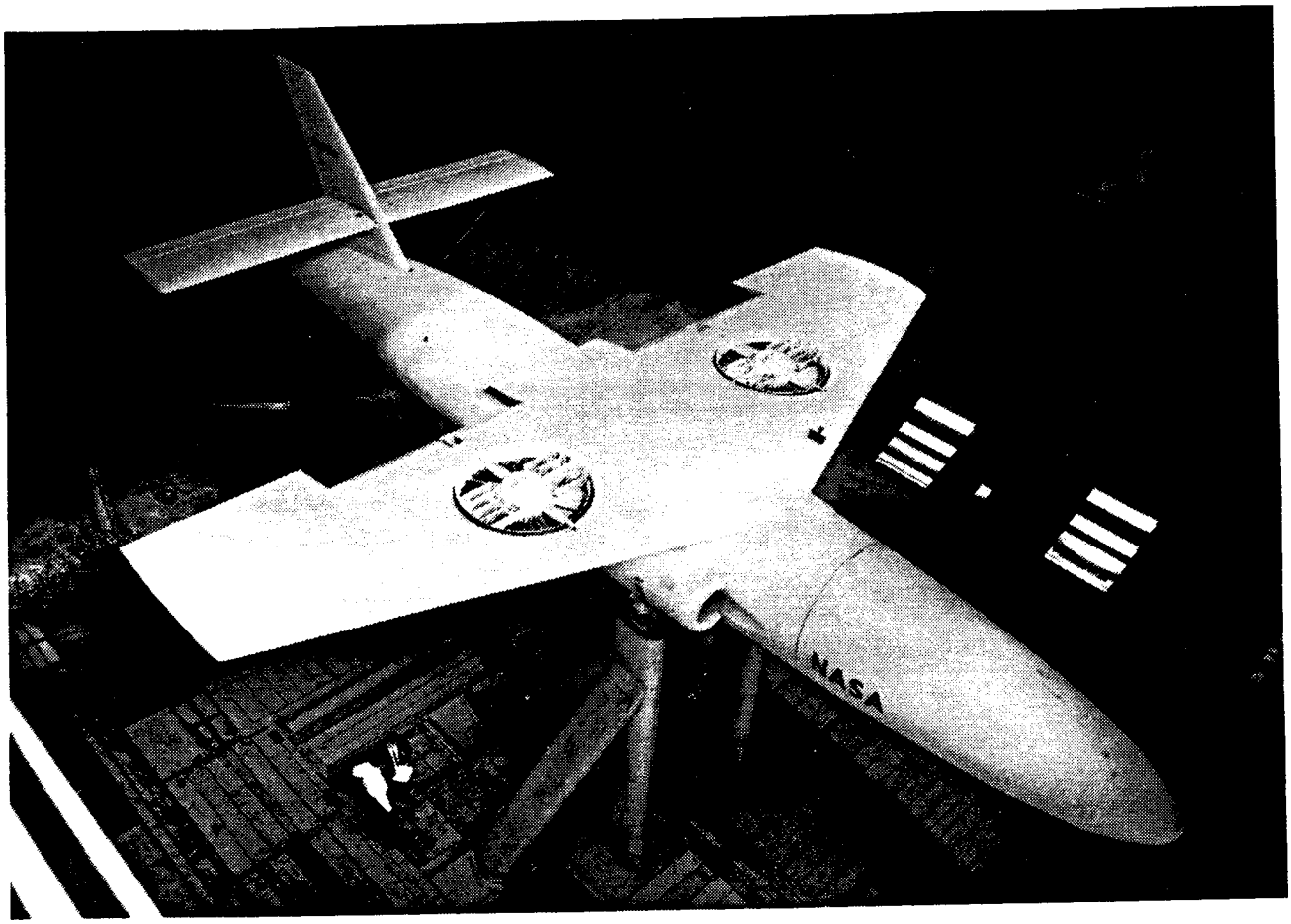

Figure 23. Full-scale fan-in-wing model in the Ames 40x80-foot wind tunnel

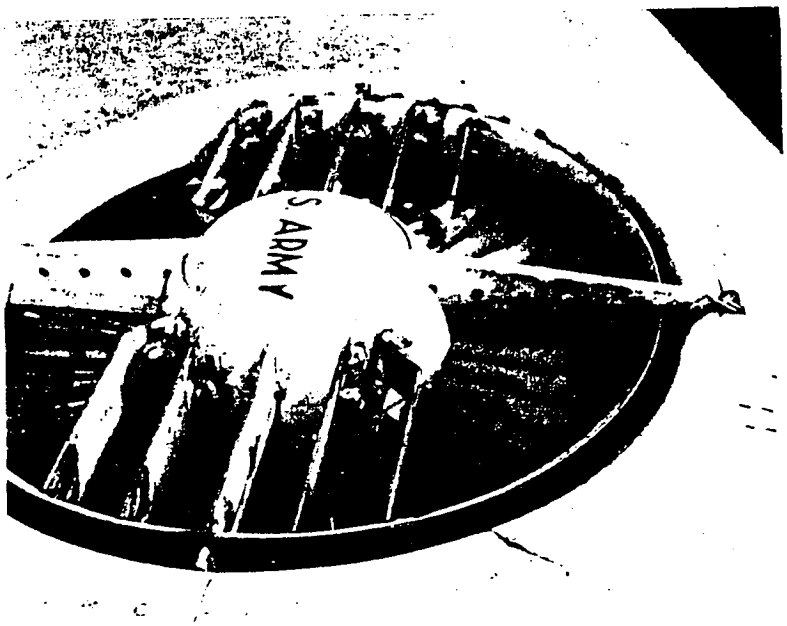

Inlet number 2
Fixed inlet vanes

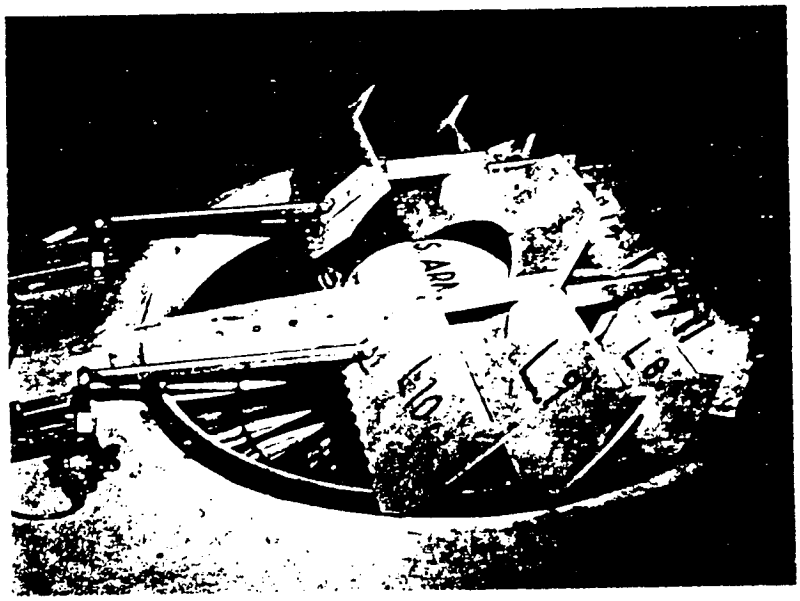

Inlet number 3
Articulated inlet vanes

Figure 24. Full-scale fan-in-wing inlets

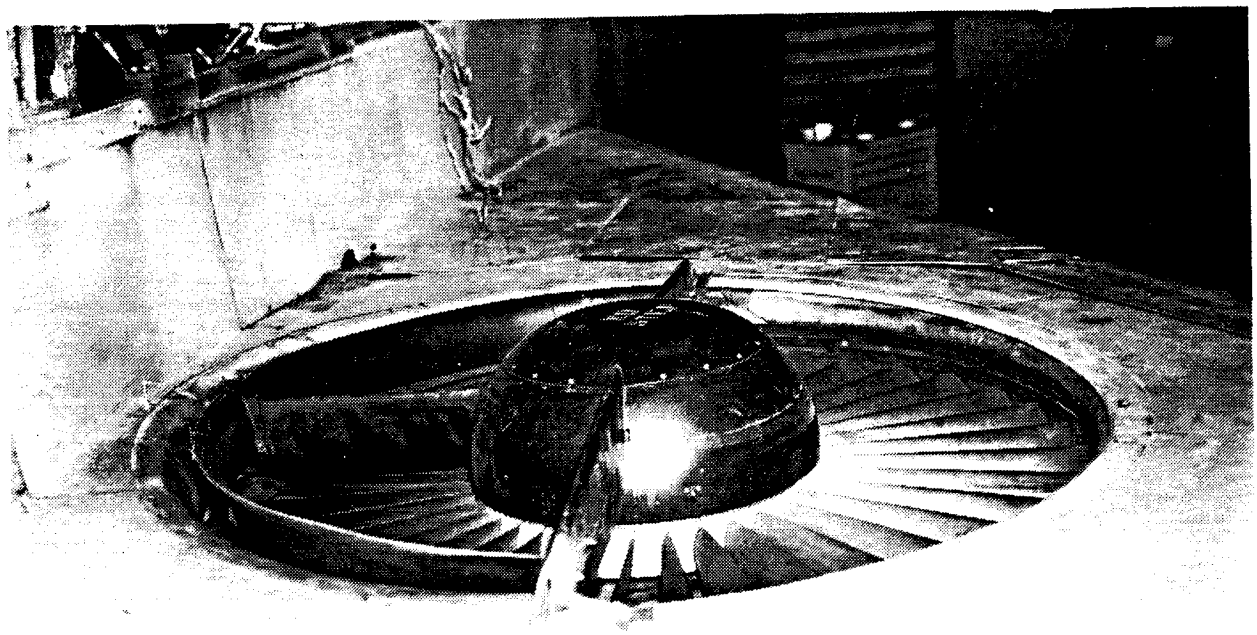

Figure 25. Full-scale modified statorless fan with a BLC inlet

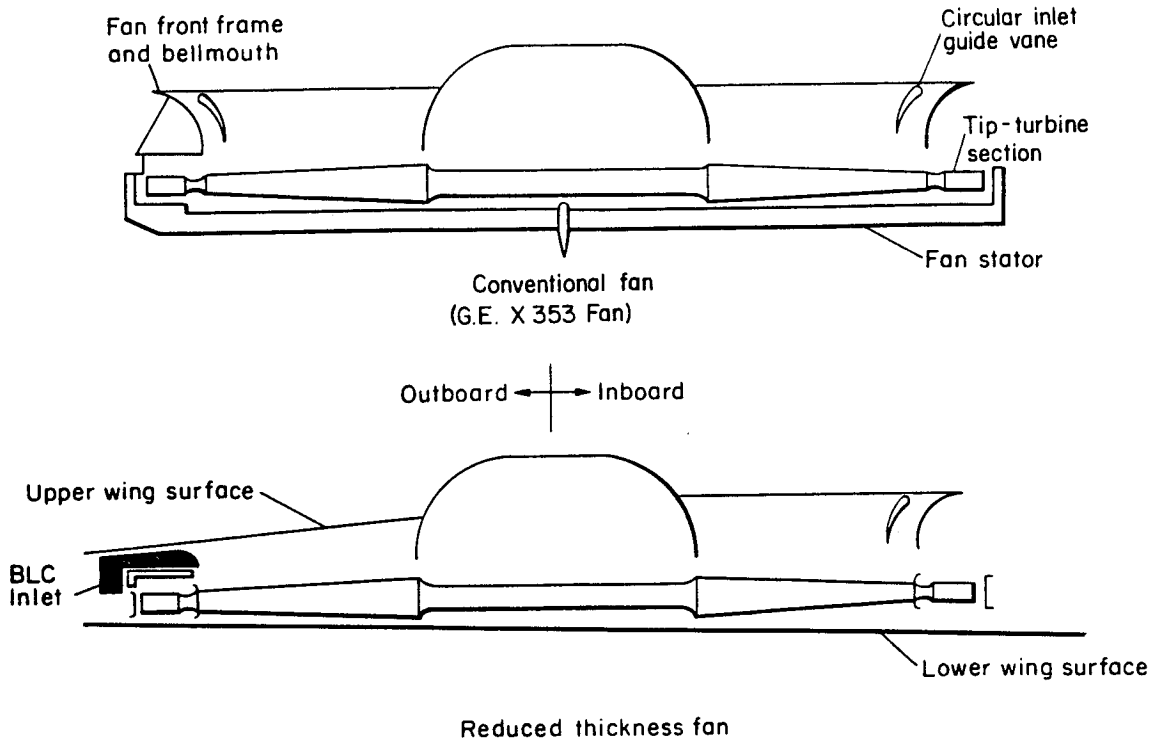

Figure 26. Cross sections of the conventional and modified statorless fan

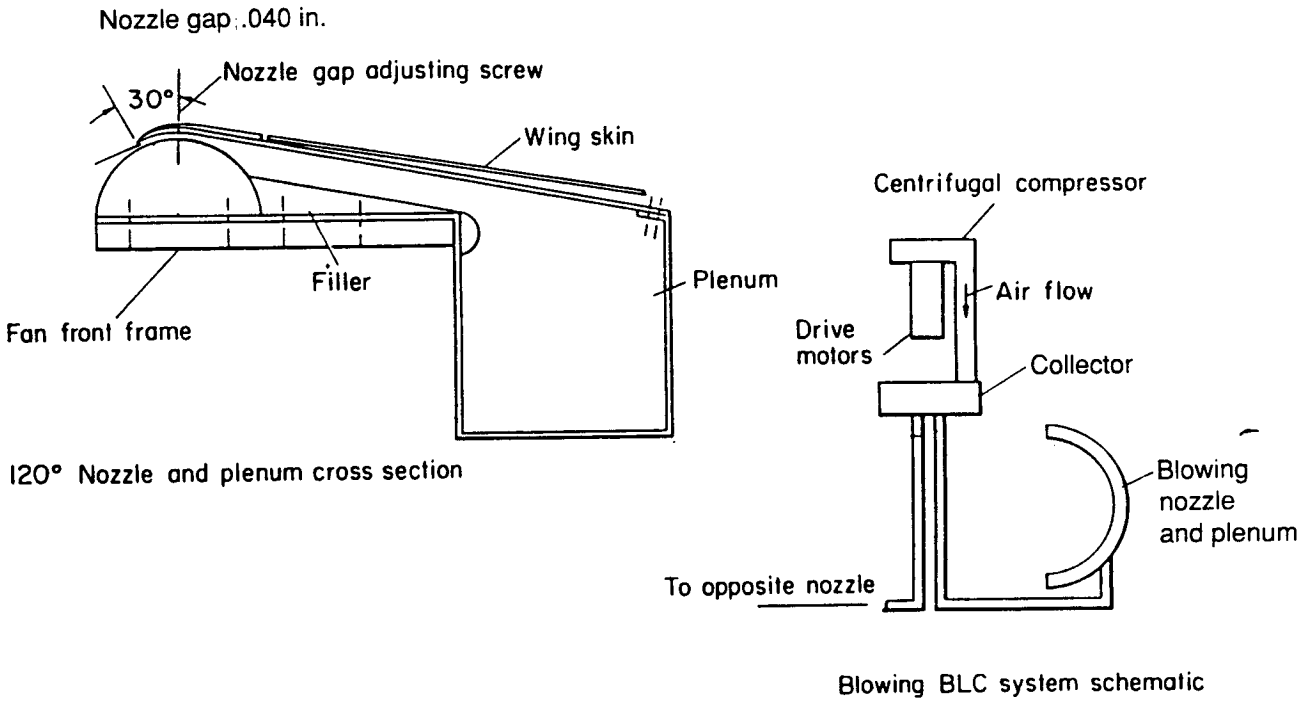

Figure 27. Detail of modified statorless fan BLC

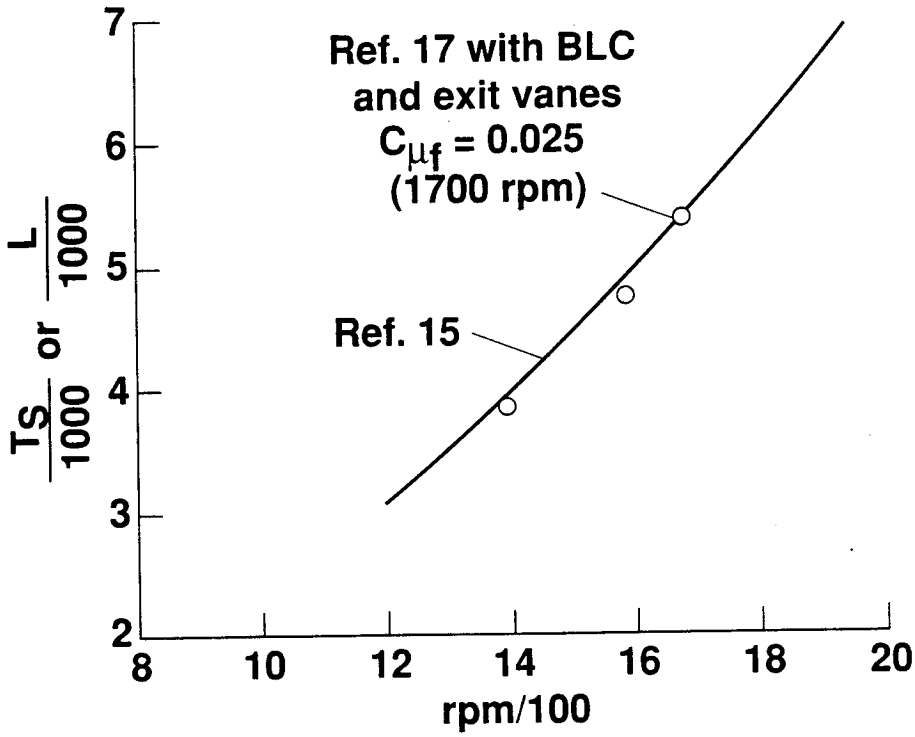

Figure 28. Static thrust of the modified statorless fan

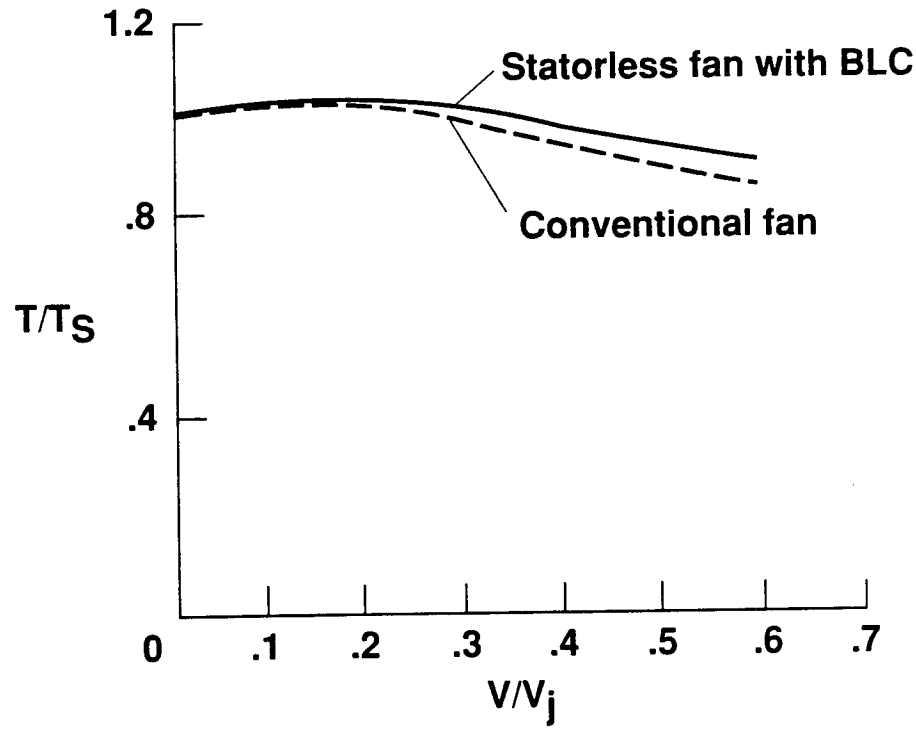

Figure 29. Variation of modified statorless fan thrust with forward speed

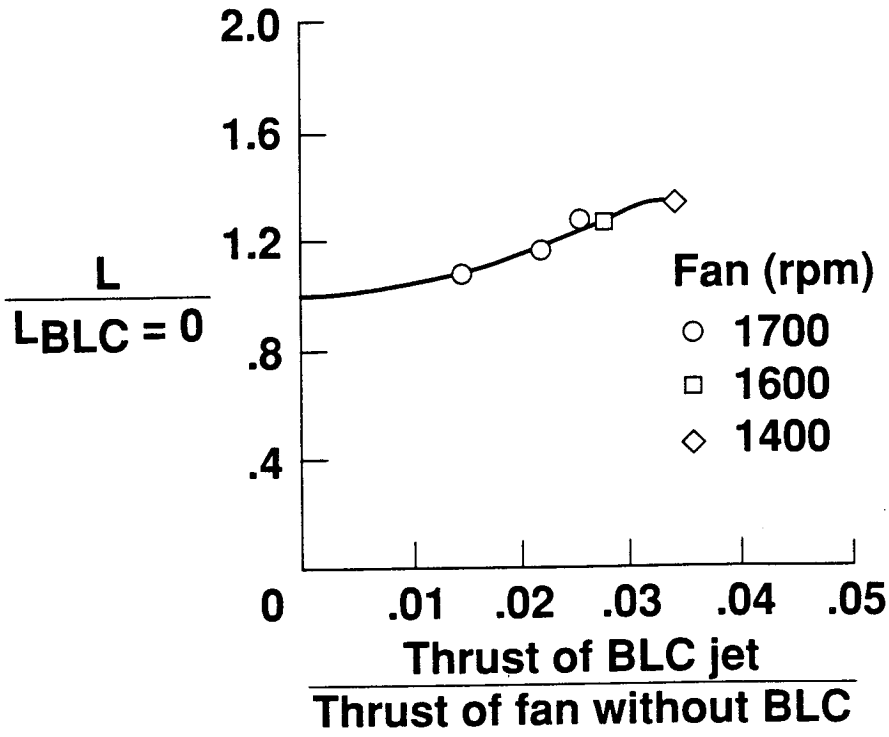

Figure 30. Modified fan lift improvement with BLC

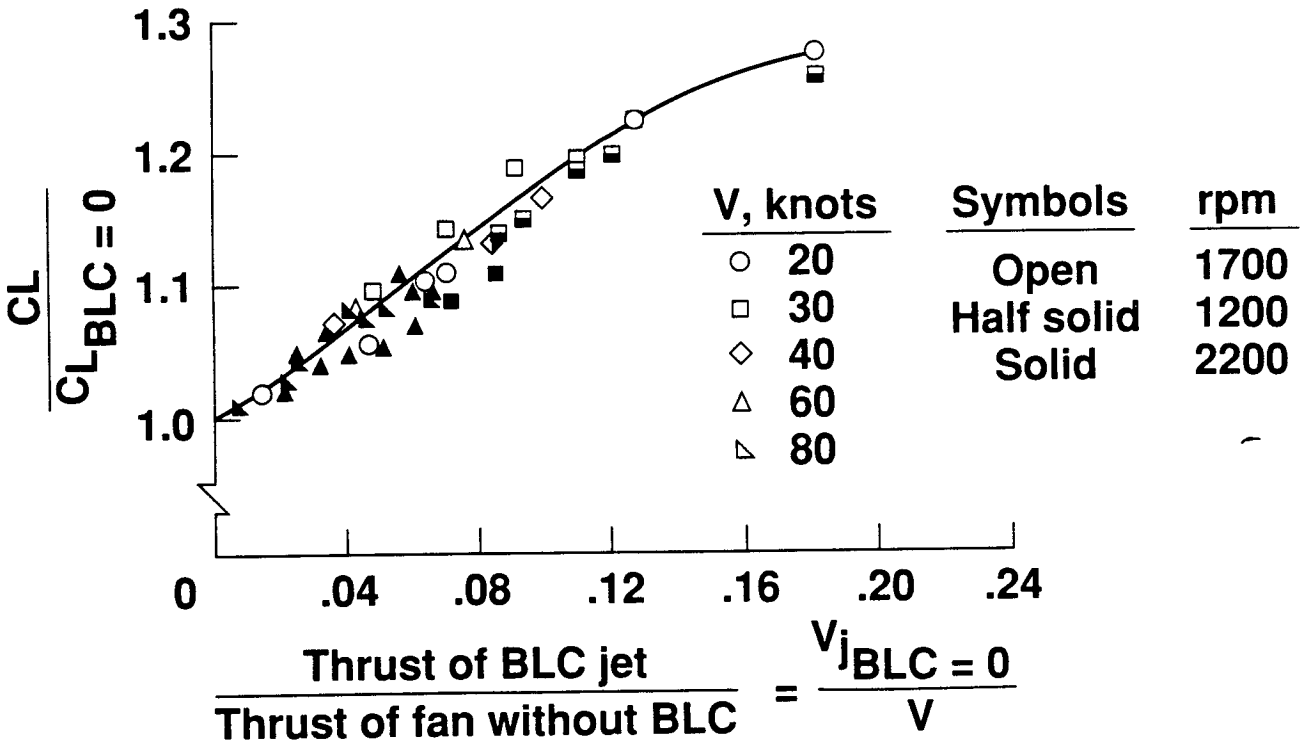

Figure 31. BLC flow parameter for modified fan

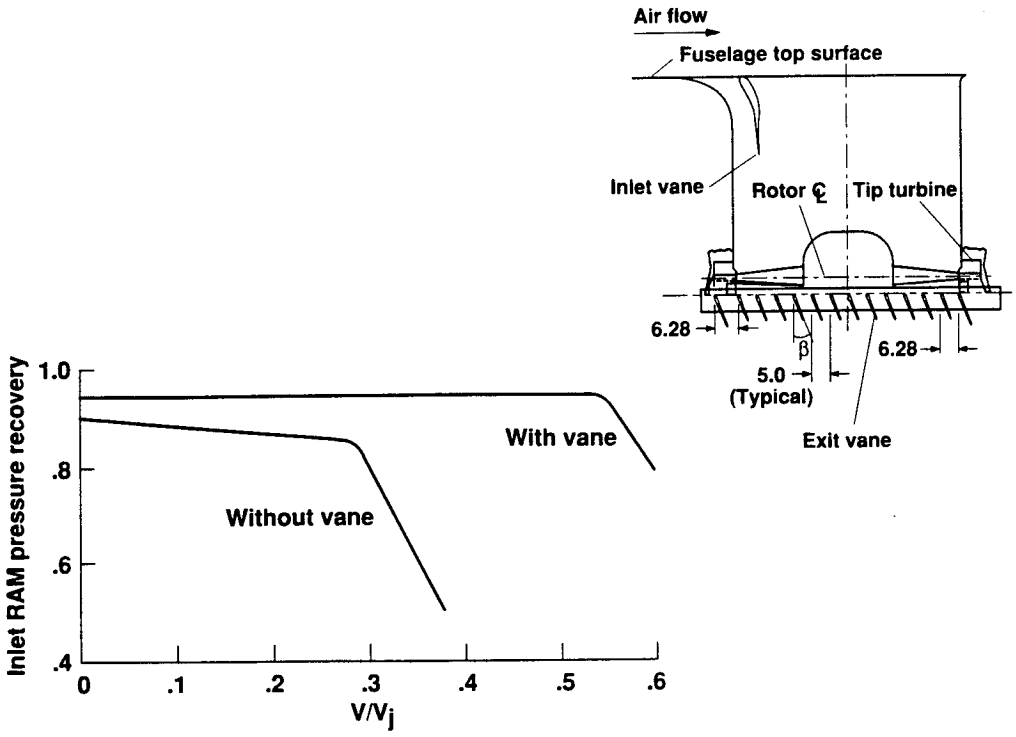

Figure 32. Fan-in-fuselage inlet performance

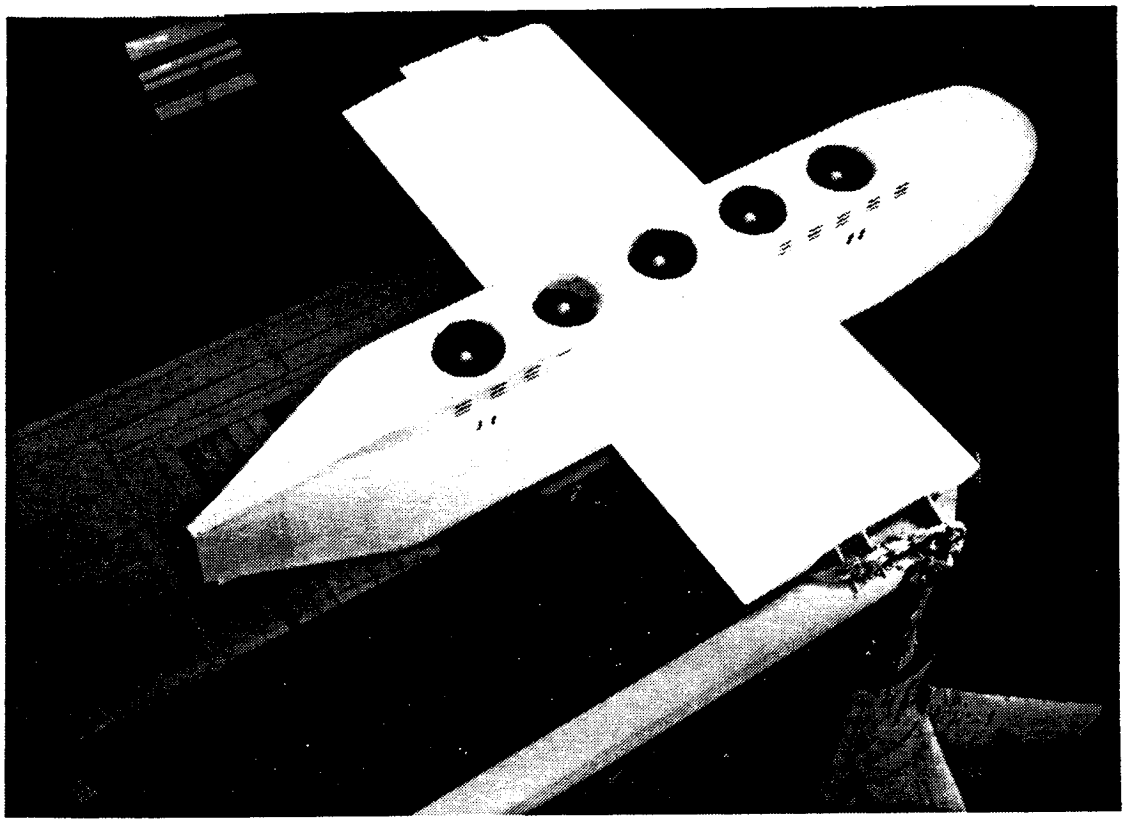

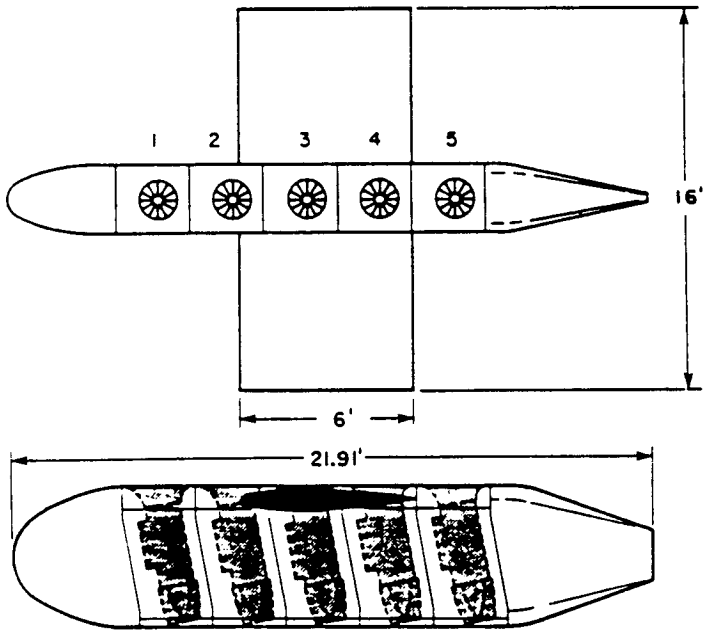

Figure 33. Lift engine research test bed in the Ames 40x80-foot wind tunnel

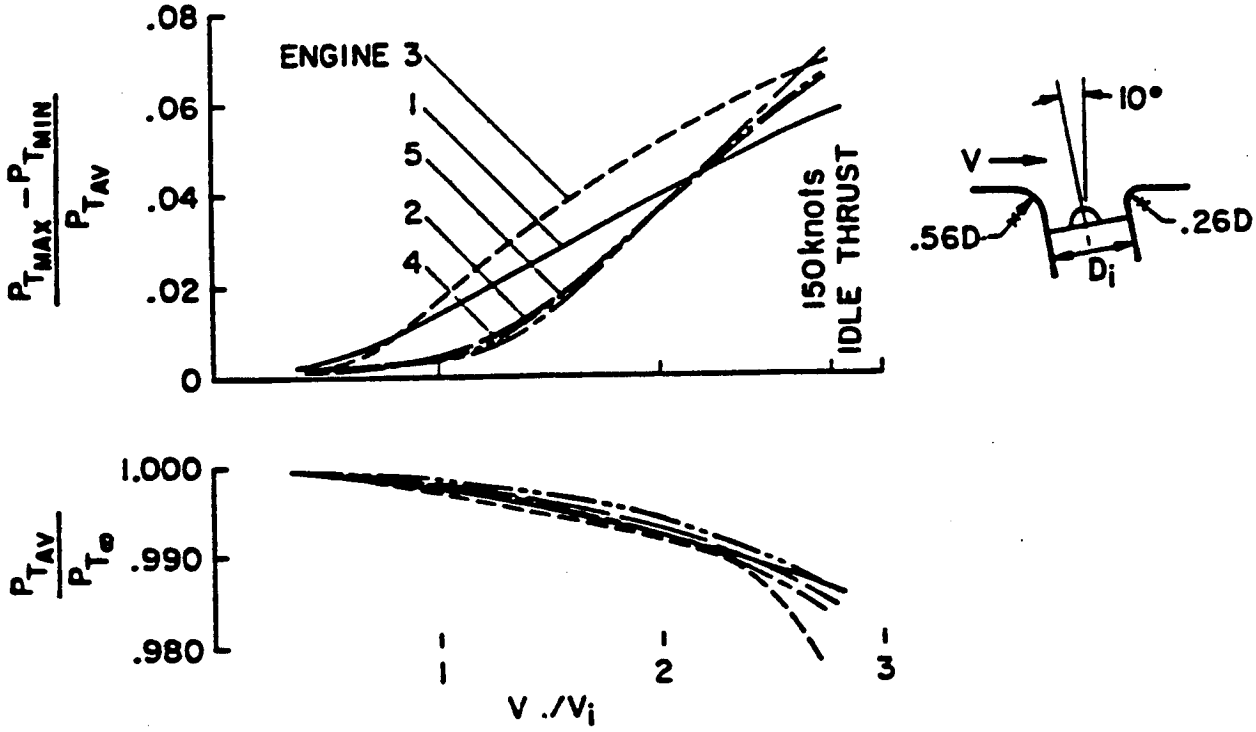

Figure 34. Flow distortion in the lift engine inlets as a function of airspeed

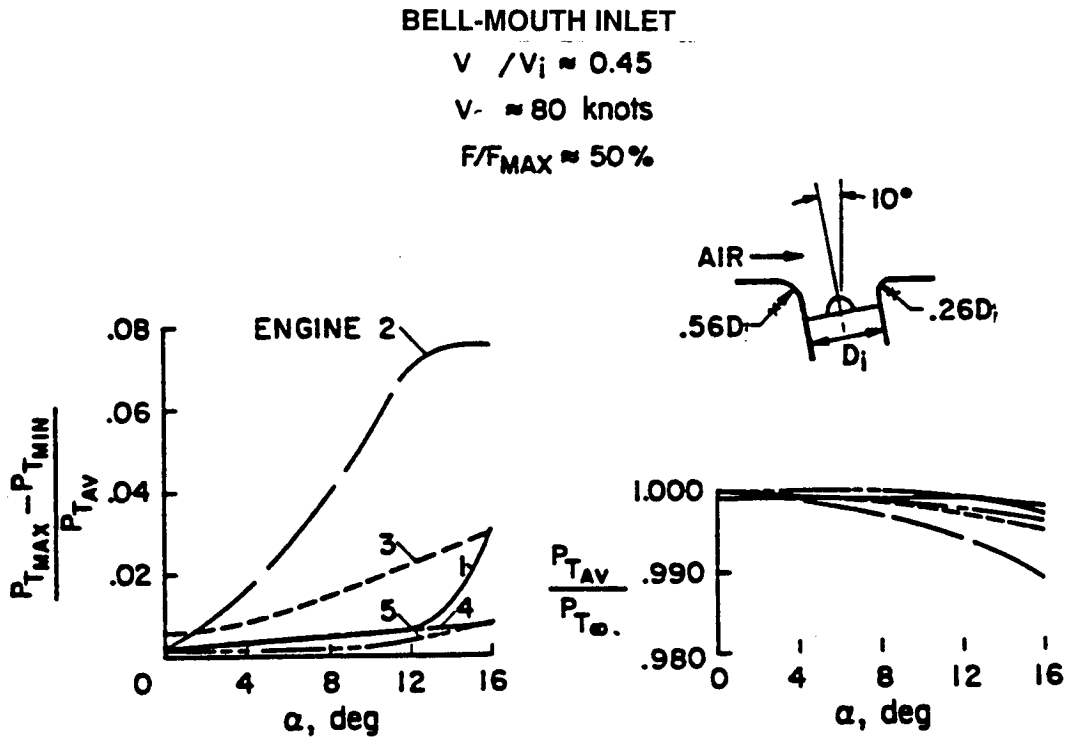

Figure 35. Variation of lift engine inlet flow distortion with angle of attack

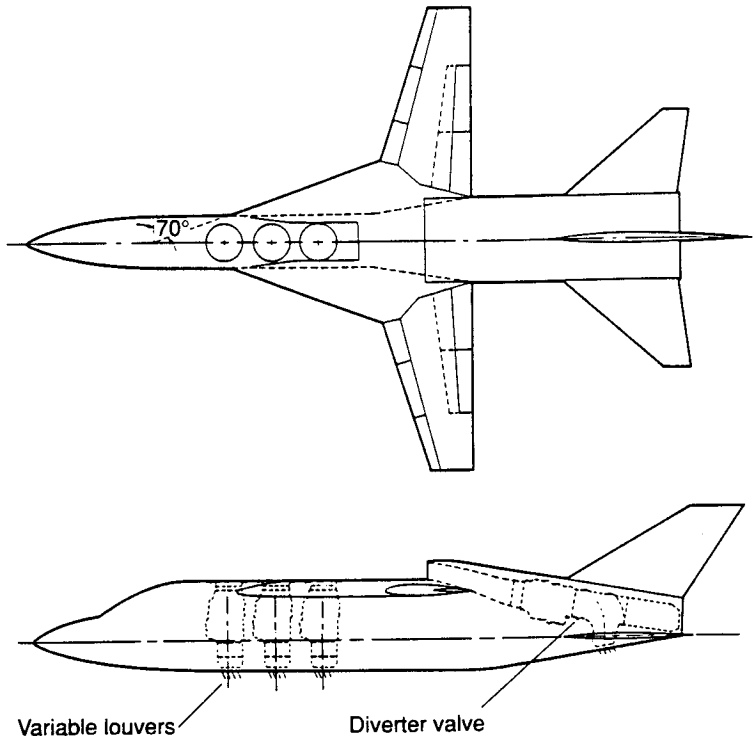

Figure 36. Large-scale lift/lift-cruise model

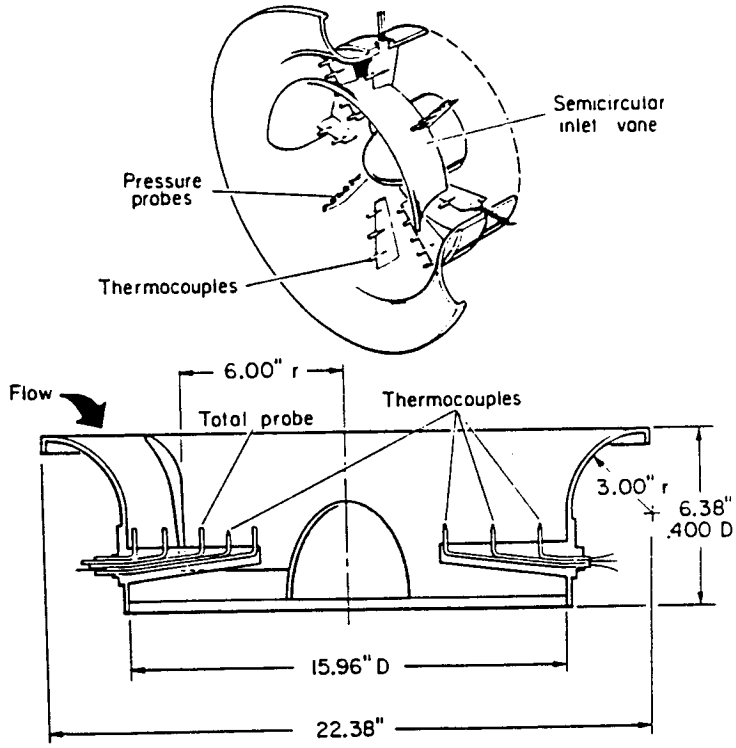

Figure 37. Lift engine inlets for J-85 engines

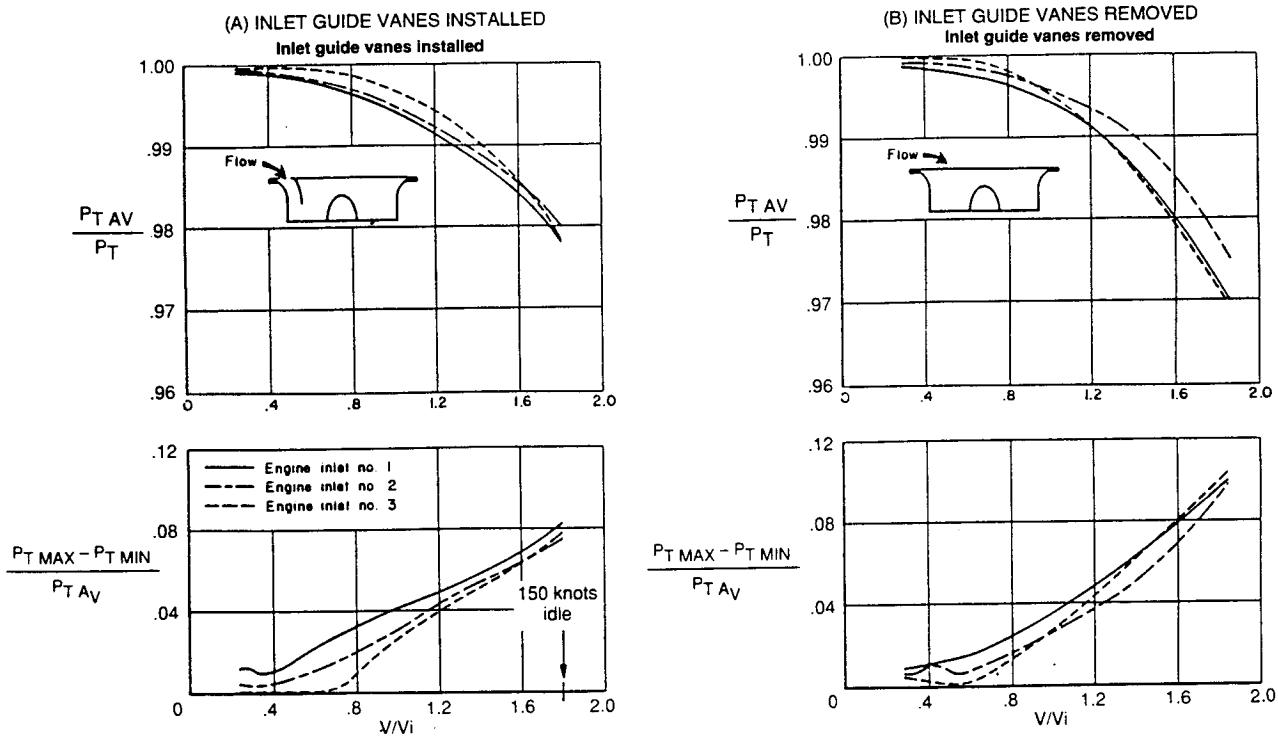

Figure 38. Performance of lift engine inlets with and without inlet vane

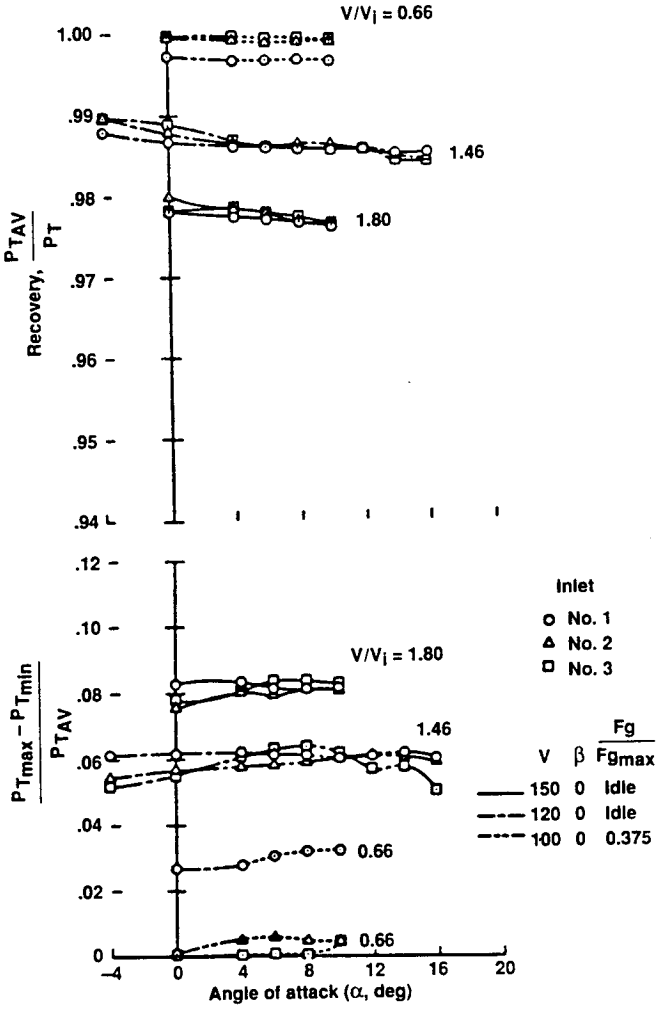

Figure 39. Effect of angle of attack on lift engine inlet performance

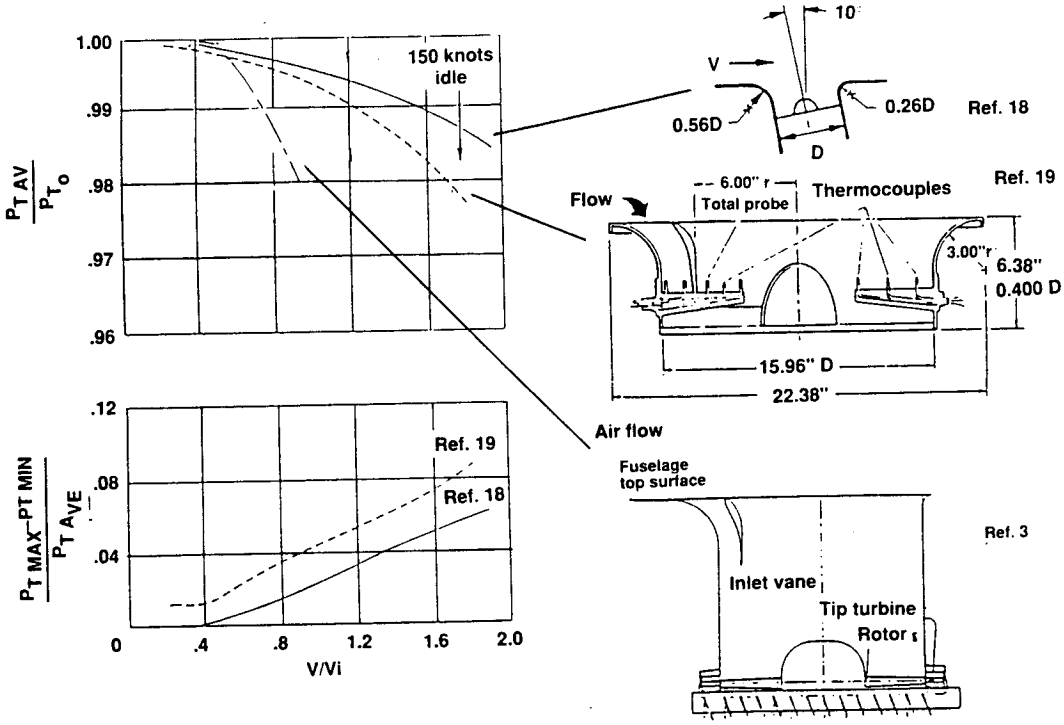

Figure 40. Comparison of performance of 3 lift engine inlets

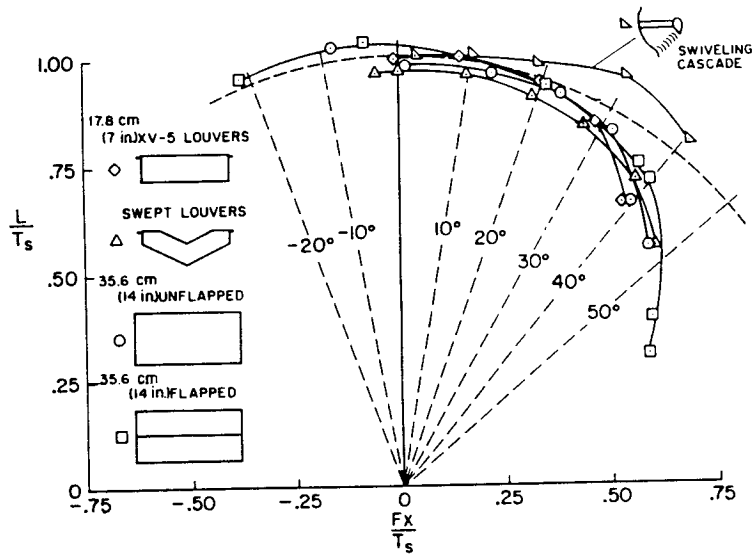

Figure 41. Flow turning effectiveness of several fan louver systems

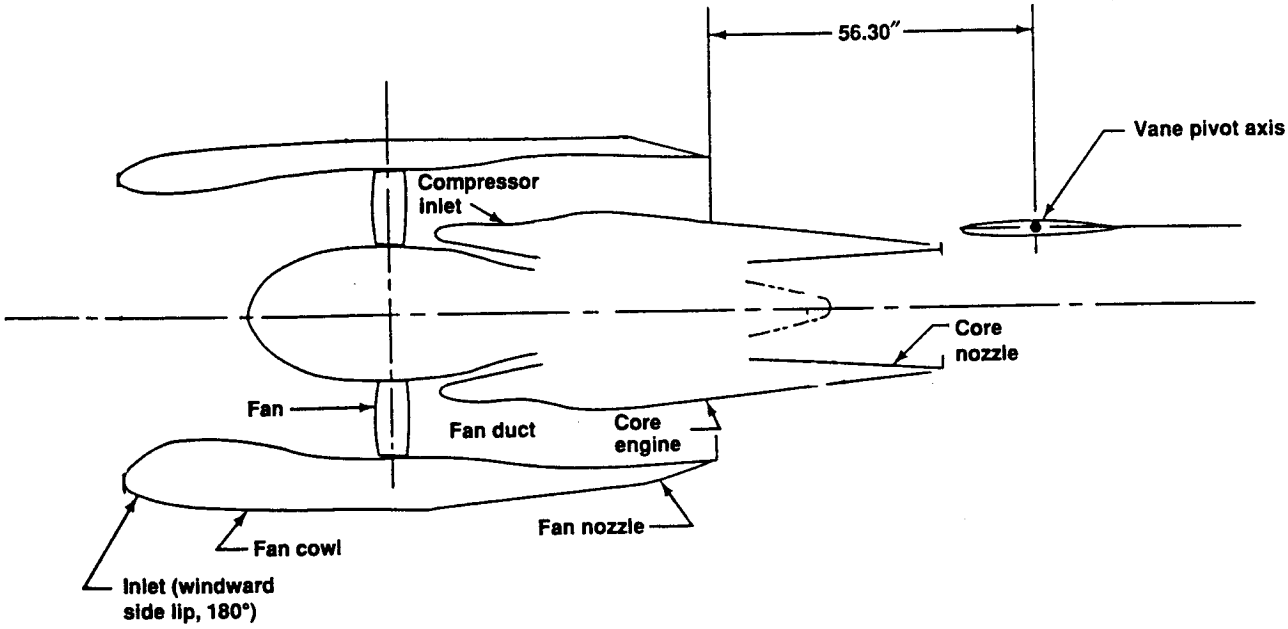

Figure 42. Q-fan engine with exhaust vane for control

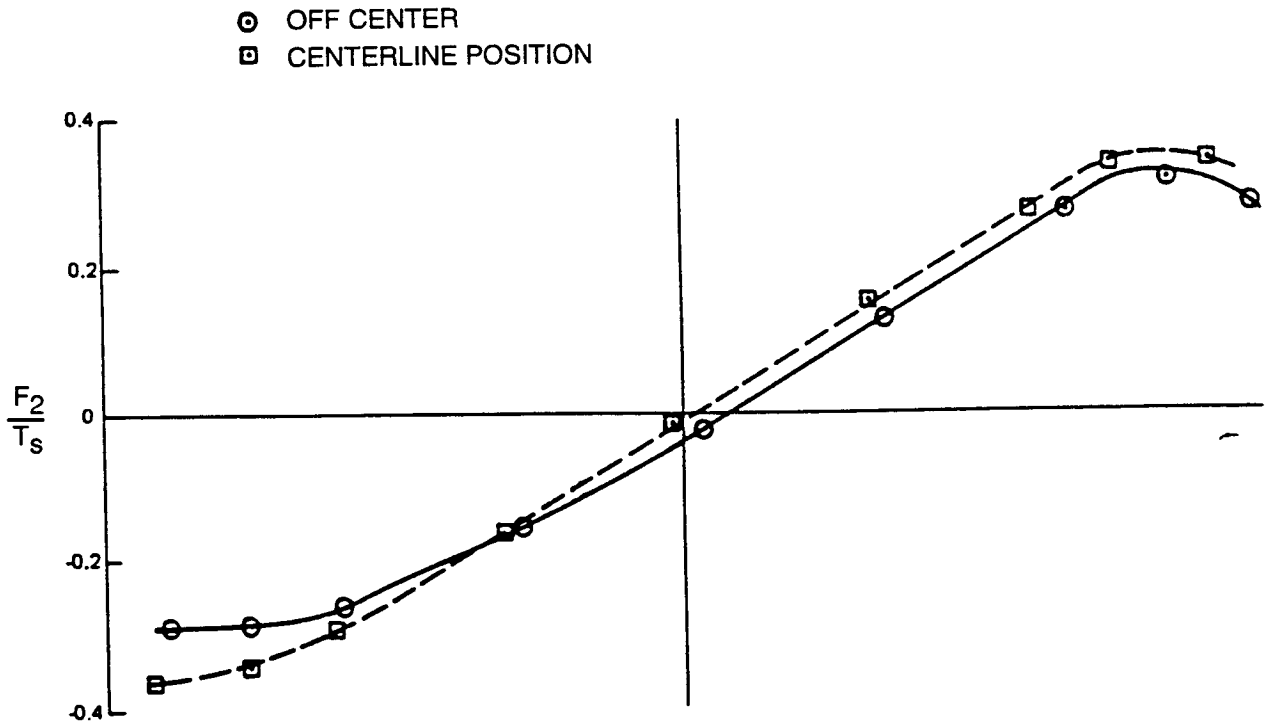

Figure 43. Force generating capability of a single vane in the exhaust

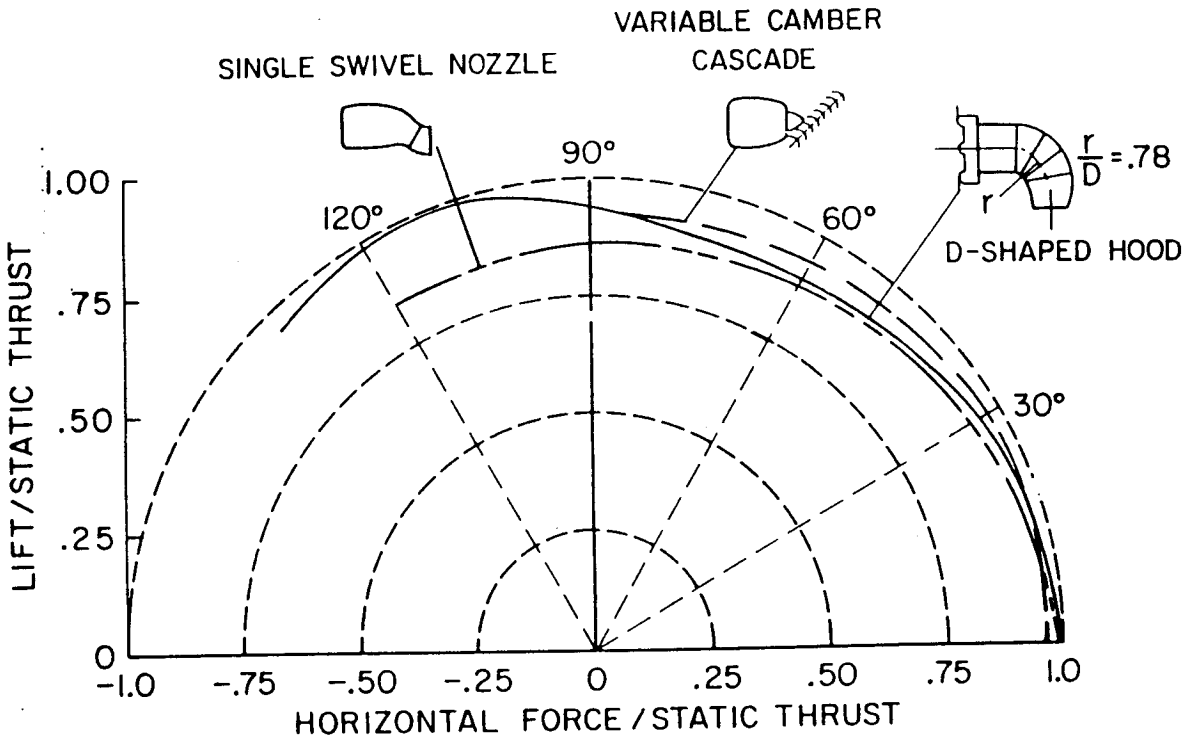

Figure 44. Flow turning performance of several exhaust hood deflectors

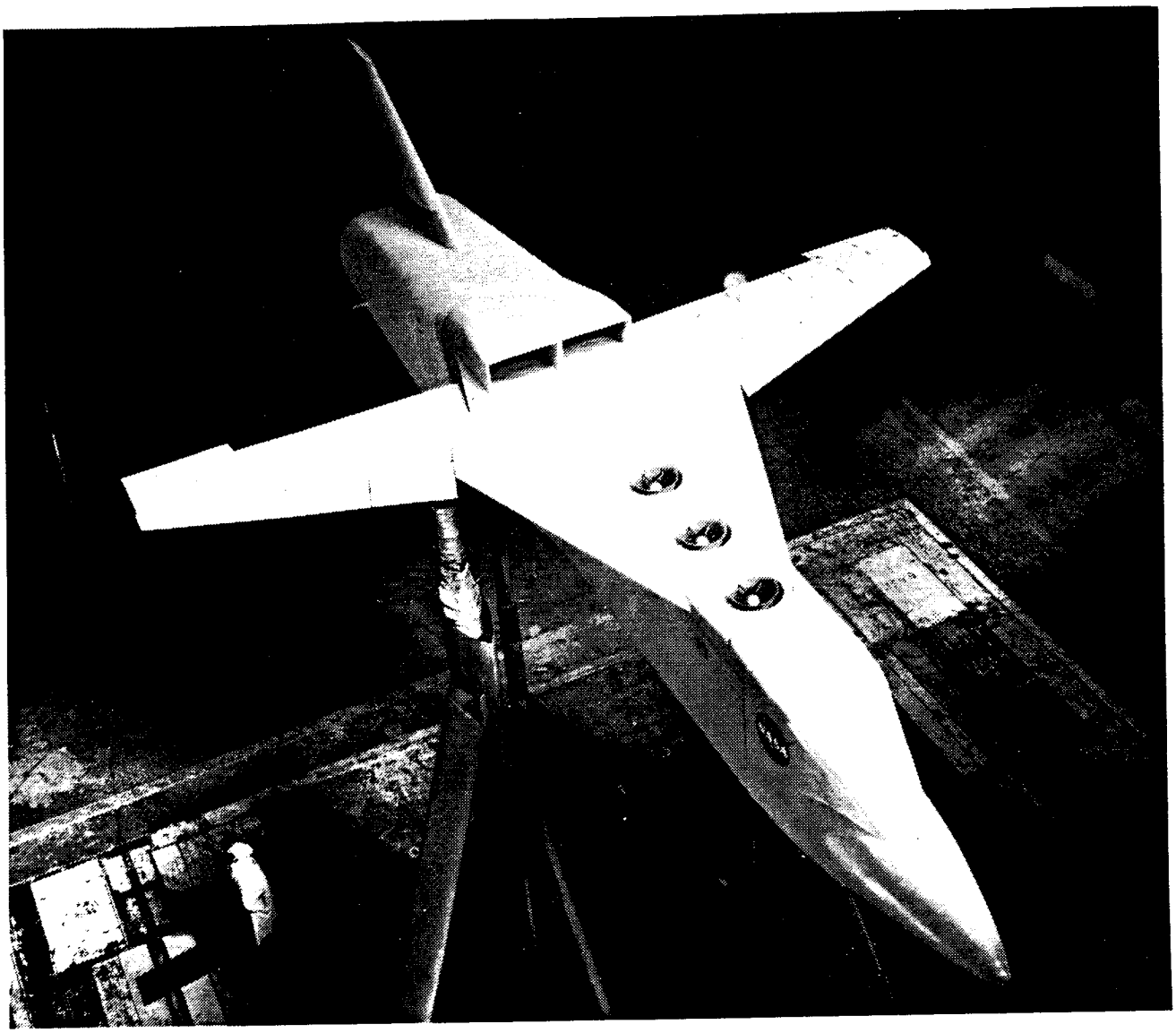

Figure 45. Lift/lift-cruise fighter model in 40x80-foot wind tunnel

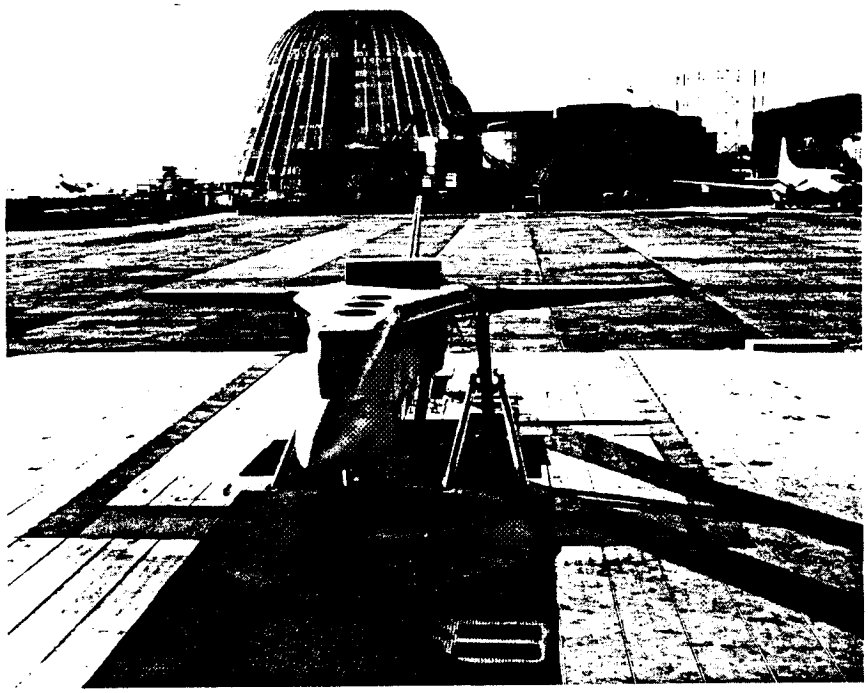

Figure 46. Lift/lift-cruise fighter model on static test facility

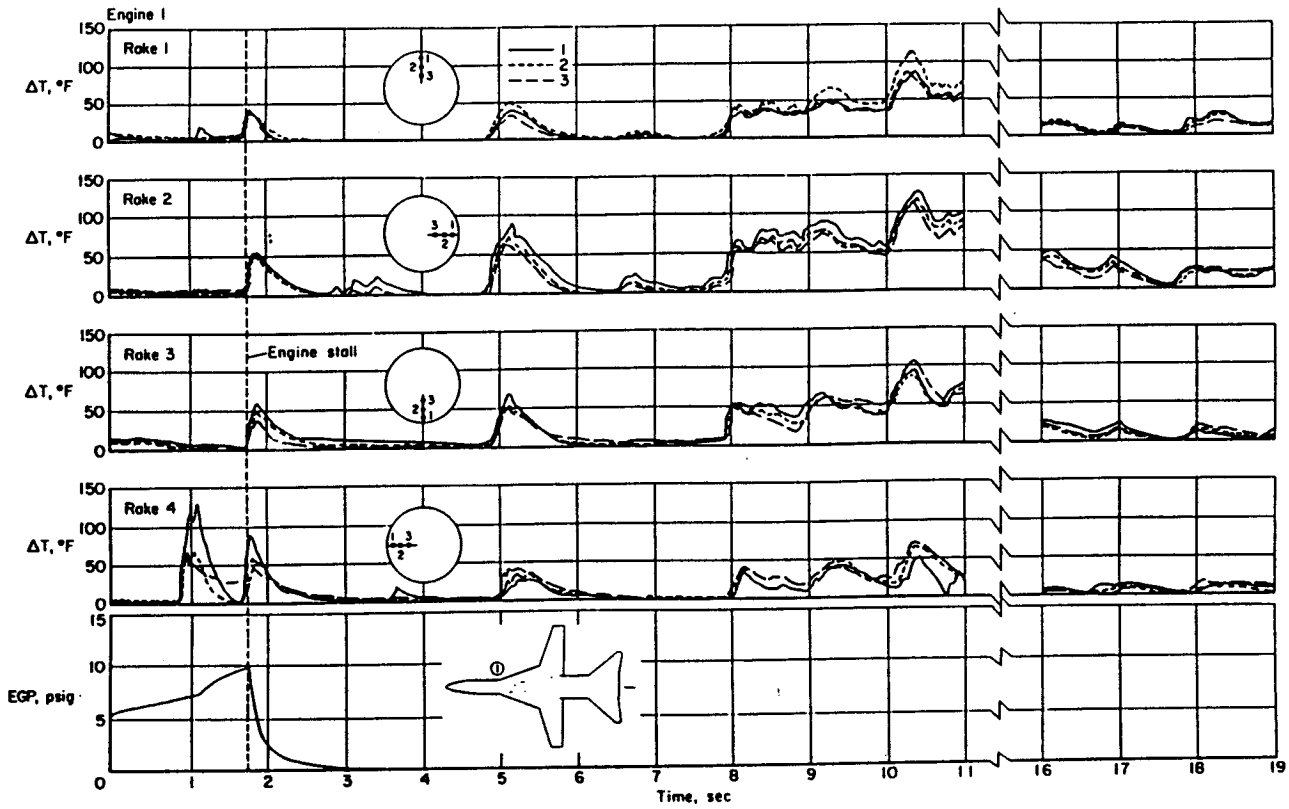

Figure 47. Exhaust gas reingestion in the forward inlet on the lift/lift-cruise model

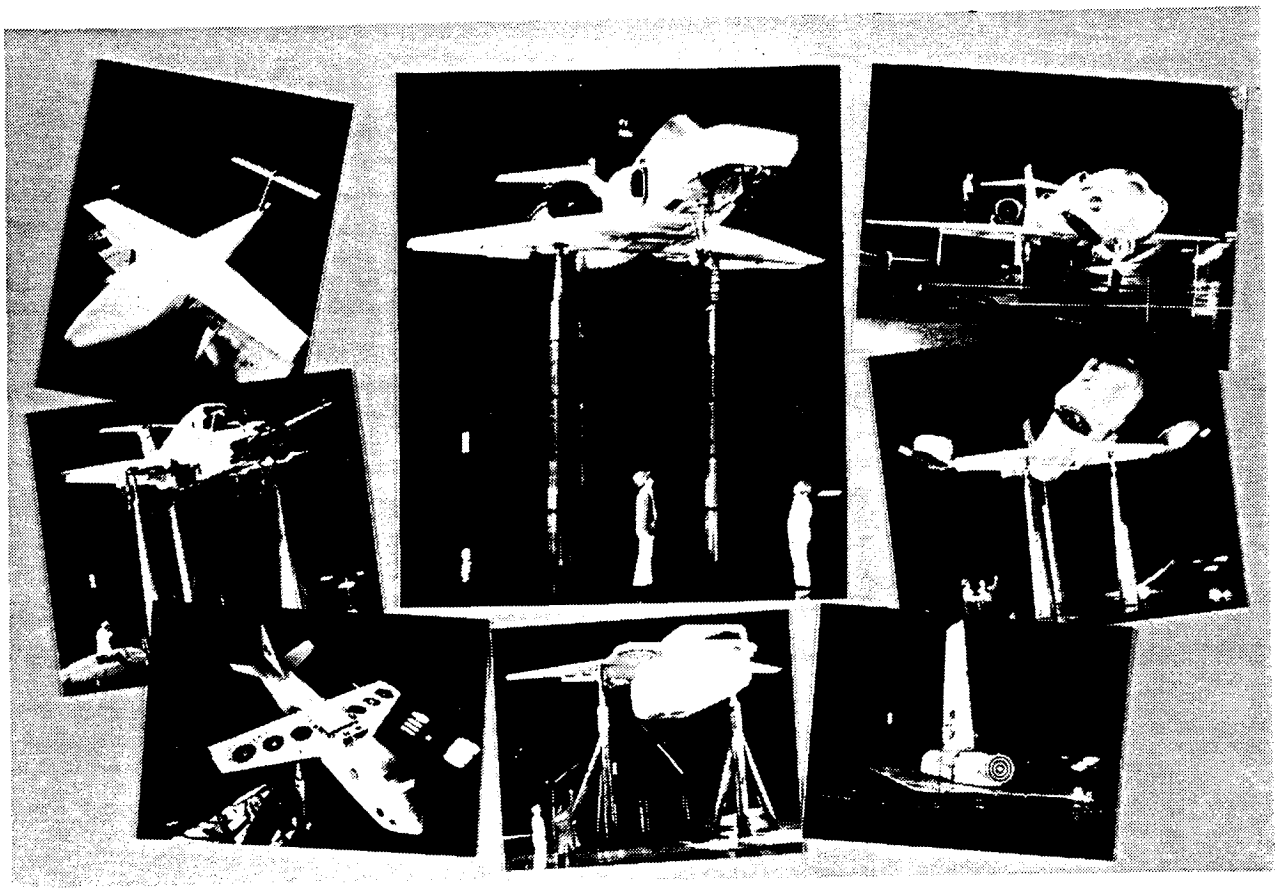

Figure 48. Examples of large-scale lift fan models tested in the 40x80-foot wind tunnel

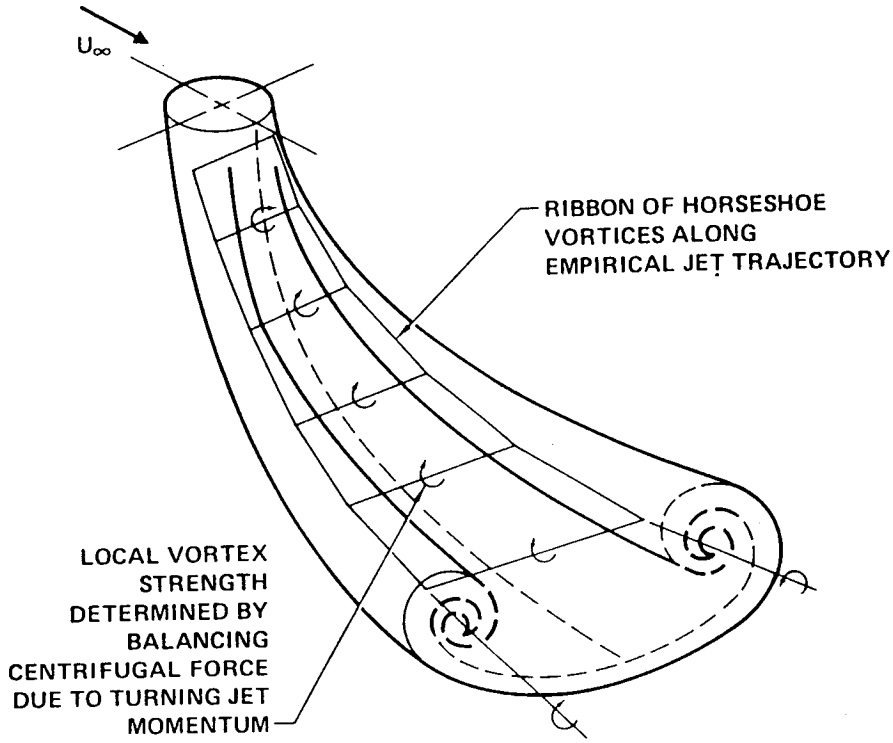

Figure 49. Typical model of a jet-in-crossflow

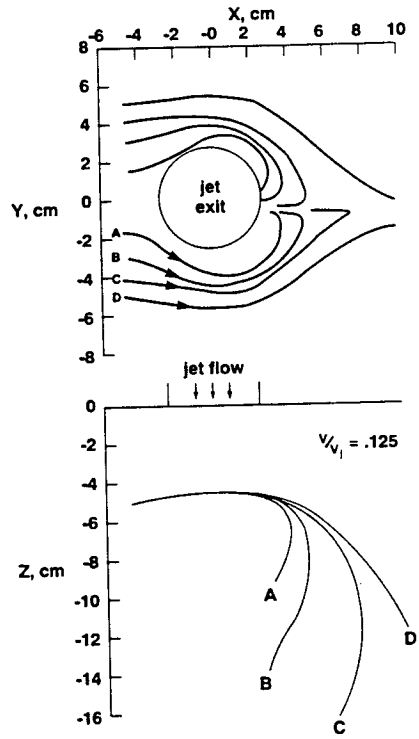

Figure 50. Streamlines of a jet-in-crossflow from a laser velocimeter, V/Vj = 0.125

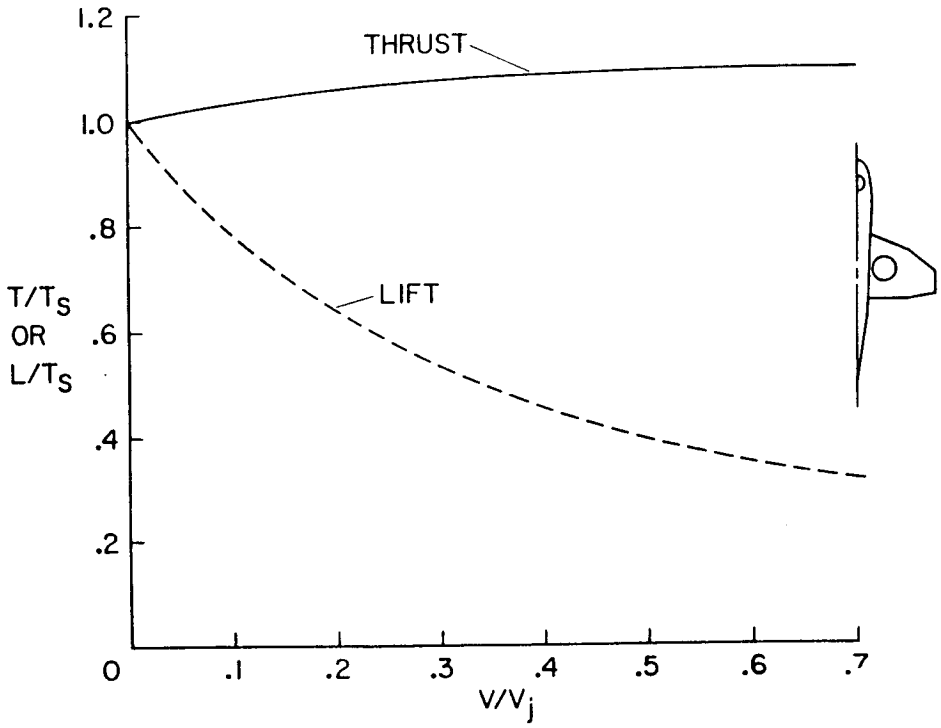

Figure 51. Loss of lift from a nose-mounted lift fan

MODEL	TYPE		WING ASPECT RATIO	SWEEP OF QUARTER CHORD LINE	TAPER	$\frac{A_f}{S}$	$\frac{D}{C}$	$\frac{D}{b}$	$\frac{X}{C}$	REFERENCE
1	Fan-in-fuselage		5	0°	.5	.084	.552	.147	.25	3
2	Fan-in-wing		3.5	16°	.5	.099	.428	.269	.392	14
3	Fan-in-wing		3.11	16°/25°	.32	.147	.48	.349	.43	9
4	Fan-in-wing, 6 fans AFT Fan-in-wing, 4 fans AFT Fan-in-wing, 2 fans AFT Fan-in-wing, 6 fans forward		3.43	20°	.47	.115 .076 .038 .115	.292 .268 .245 .292	.505 .336 .168 .505	.42 .43 .44 .322	NASA TN D-4233
5	Fan-in-wing		2.2	52.4°	0	.12	.335	.363	.63	16
6	Tandem lift fan Fan-in-wing, 2 fans AFT Fan-in-wing, 2 fans forward		5.8 (basic) 3.44 (gross)	35°	.3	.073 .036 .036	.796 .398 .398	.164 .164 .164	.286 1.24 −.657	29
7	Folding lift fan Rotating cruise fan		5.8	35°	.3	.123	—	—	—	29
8	Tandem podded lift fan 2 fans forward 2 fans AFT		5.8 (basic) 4.04 (gross)	35°	.3	.086 .043 .043	.946 .473 .473	.164 .164 .164	— −.80 1.16	NASA TN D-6234
9	Lift-cruise fan 2 fans forward (podded) 2 cruise fans AFT		5.8 (basic) 4.4 (gross)	35°	.3	.094 .047 .047	— .473 —	.164 .164 .164	— −.80 —	NASA TM X-62151
10	Low wing tandem lift fan 2 fans forward (podded) Fan-in-wing, 2 fans AFT		5.6 (basic) 3.7 (gross)	35°	.3	.080 .040 .040	— .473 .370	.165 .165 .165	— −.80 1.19	NASA TM X-62102
11	Low wing, 2 lift Fans forward 2 lift/cruise fans AFT		8.14	23.5°	.23	.115 .057 .057	— .48 .48	.134 .134 .134	— −2.56 2.61	NASA TM X-62231
12	1 fan forward 2 lift/cruise/'D' deflector		4.5	25°	.3	.101	—	—	—	NASA CR-152181
13	2 tilting lift fans		7.6	0/10	.47	.12	—	.101	—	20

Figure 52. Geometry of large-scale lift-fan-powered models tested in the 40x80-foot wind tunnel

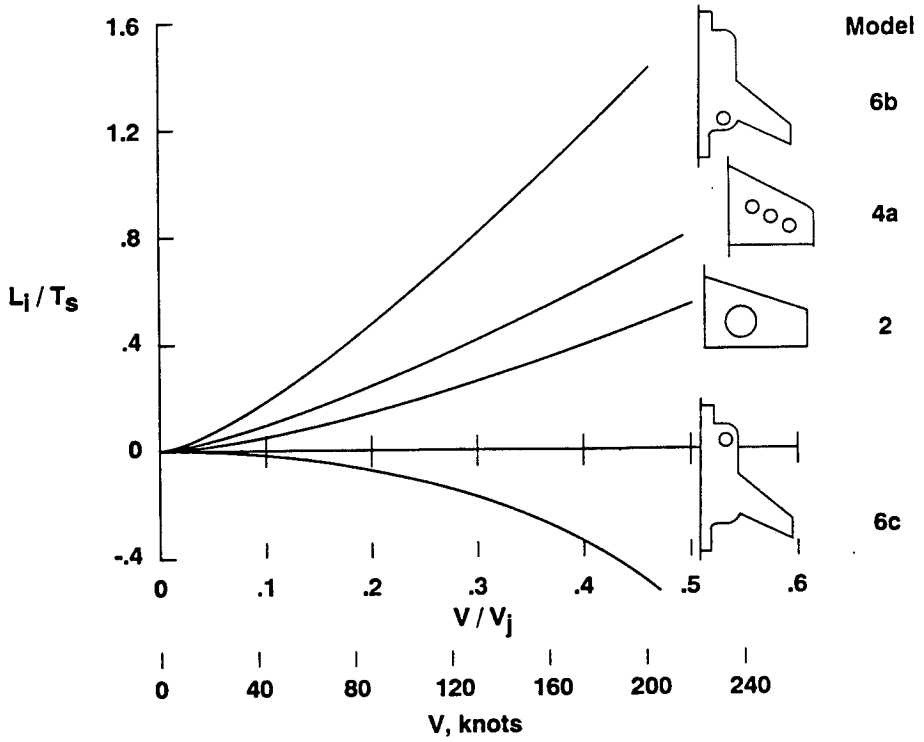

Figure 53. Induced lift variation with airspeed for several fan-in-wing configurations

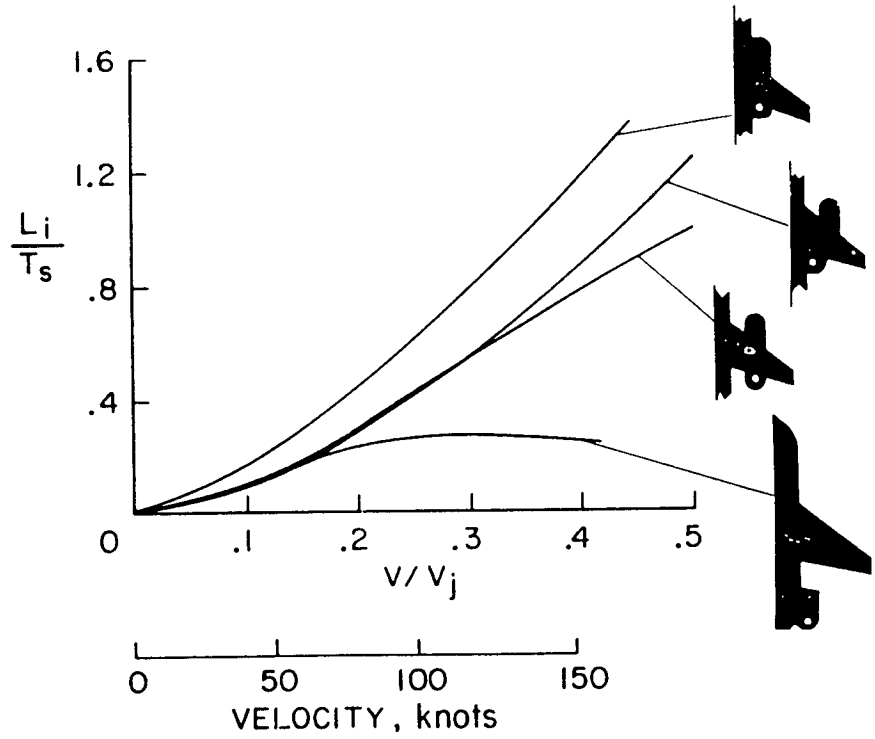

Figure 54. Induced lift variation with airspeed for several aft-mounted lift fan installations

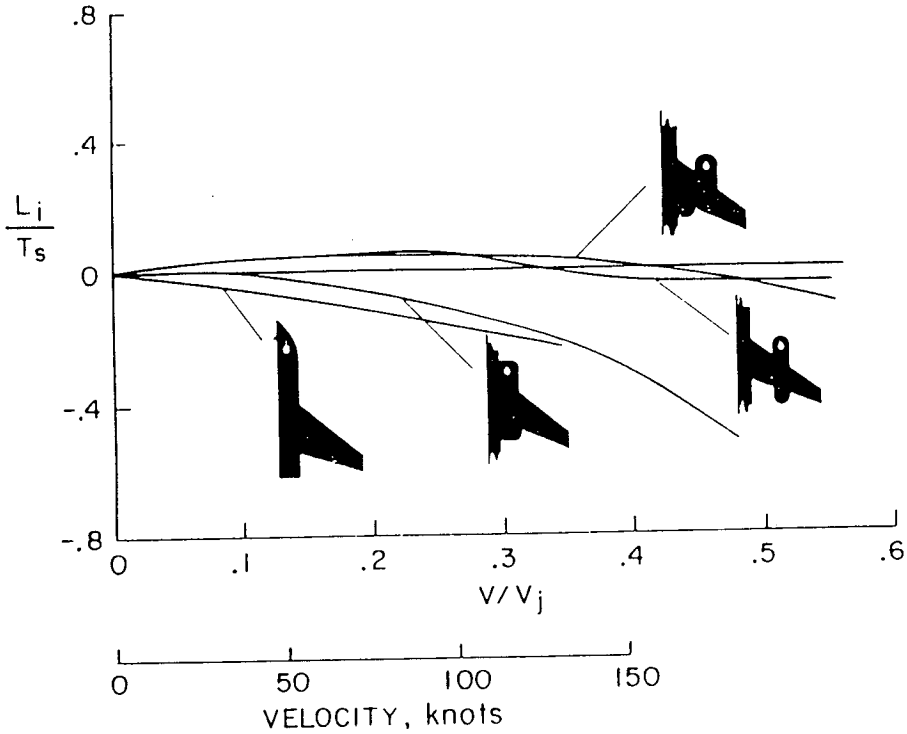

Figure 55. Induced lift variation with forward speed for several forward mounted lift fan installations

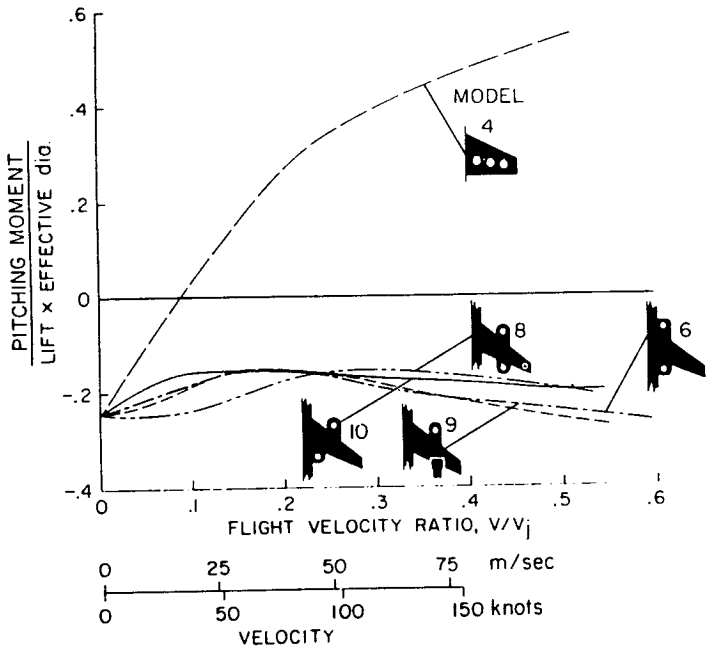

Figure 56. Pitching moment variation with airspeed for several fan installations

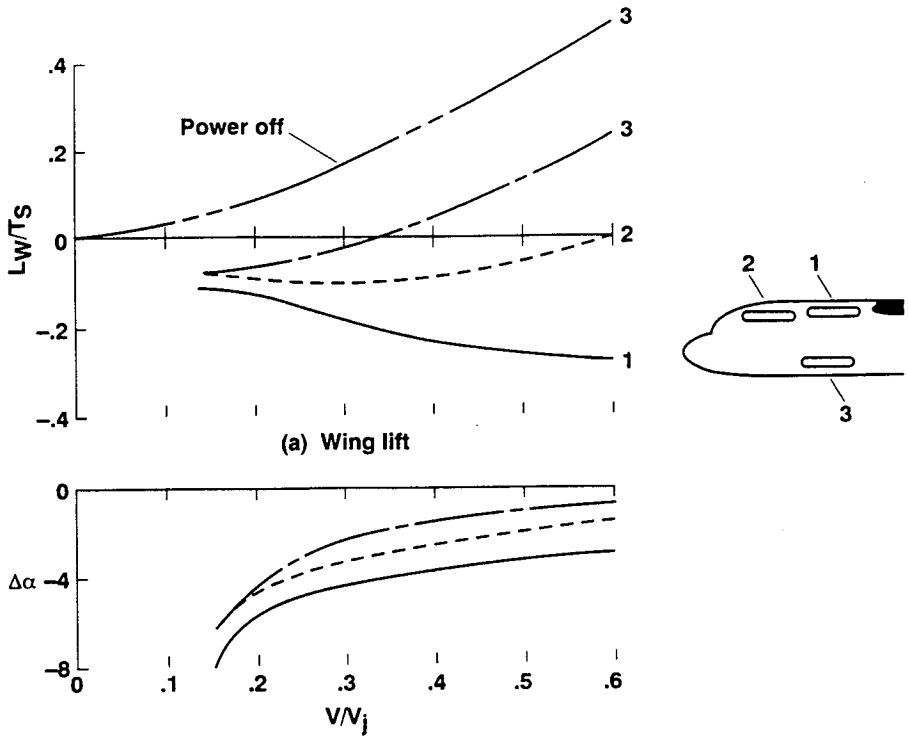

Figure 57. Effect of fan downwash on the wing

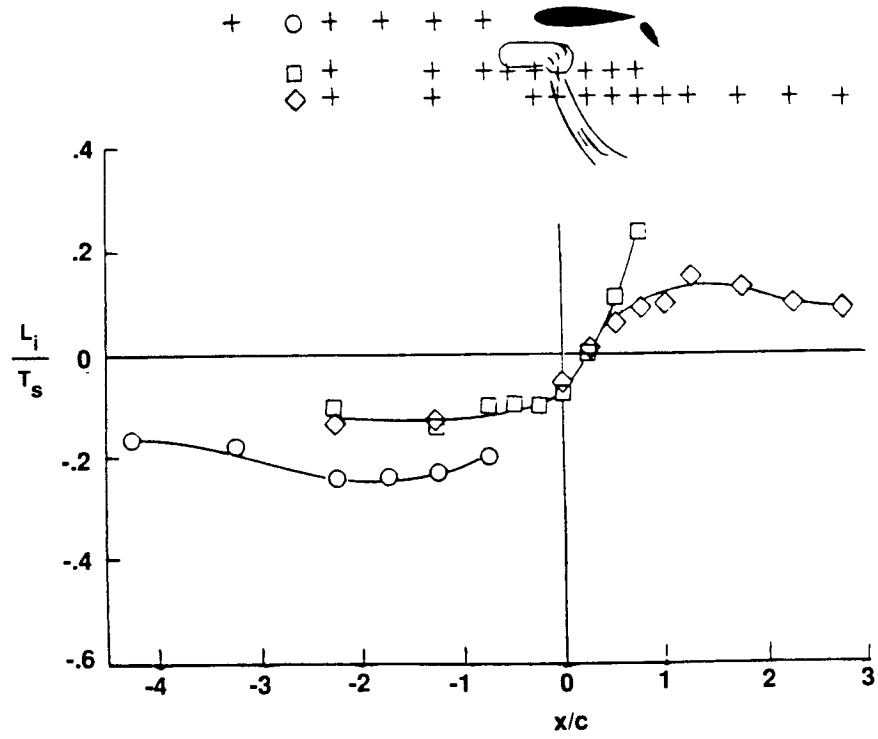

Figure 58. Lift induced on a wing by a vertically-oriented jet in several locations

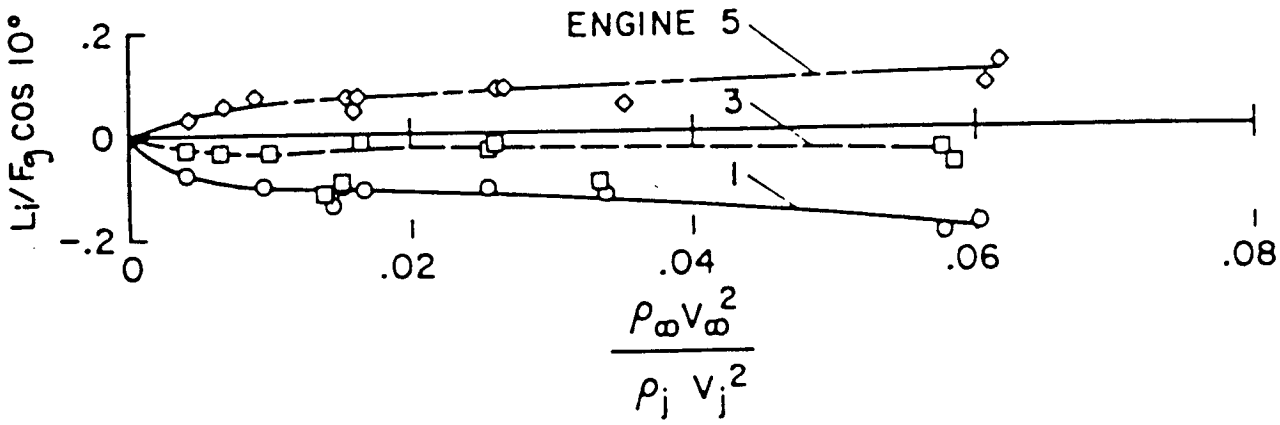

Figure 59. Induced lift from operation of the engines in the test rig

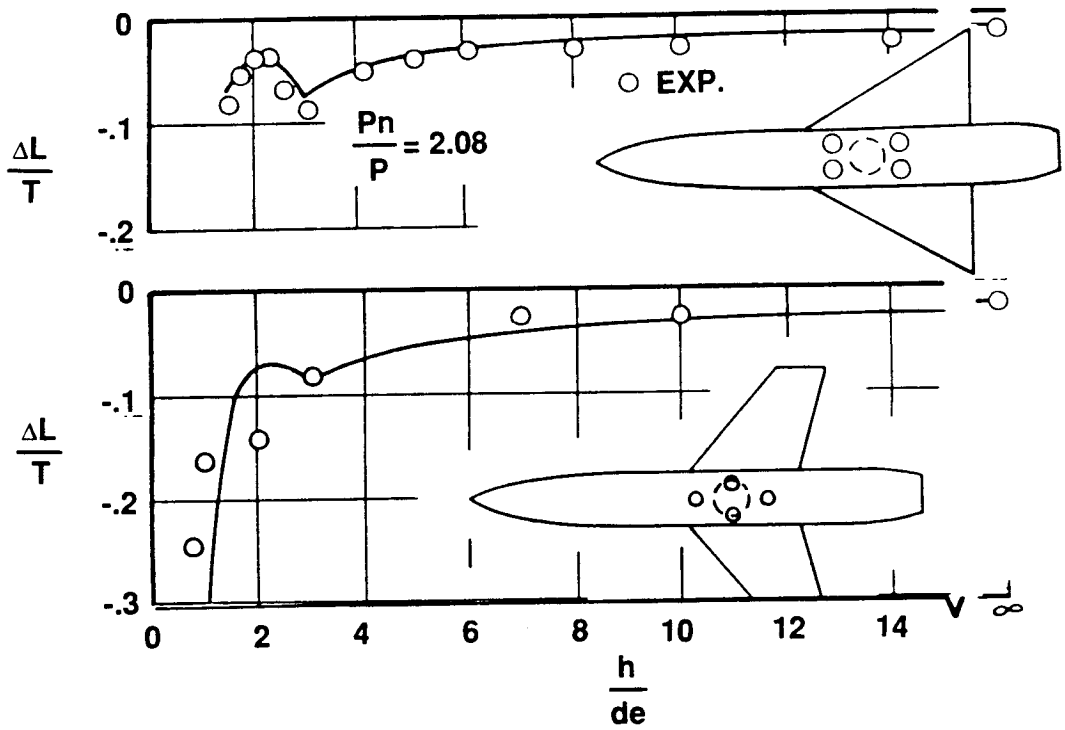

Figure 60. Comparison of predicted and measured lift in ground effect

SCHEMATIC FOR INDUCED LIFT CALCULATION

THE FLOW FIELD WITH FAN OPERATING

$$\frac{L_i}{T_S} = \frac{V^2}{V_{j_s}^2} \frac{C_{L\delta_1}}{4\pi A_f / S} \left[\frac{C_\ell}{\delta_j} \cdot \delta_j \frac{S_1}{S_{2d}} - \left(\frac{V_j}{V}\right)^{3/2} \frac{S_3}{S_{2d}} \right]$$

$\delta_j = 90 - \beta$

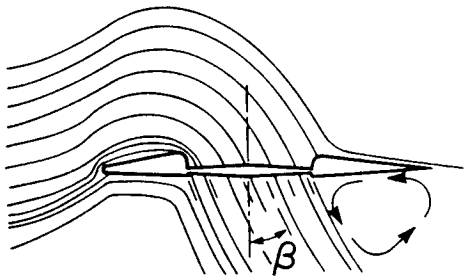

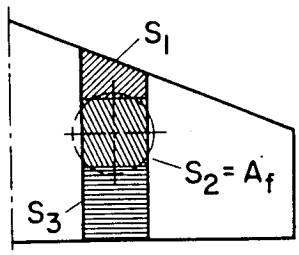

AREAS FOR INDUCED LIFT CALCULATION

Figure 61. Schematic for induced lift calculation

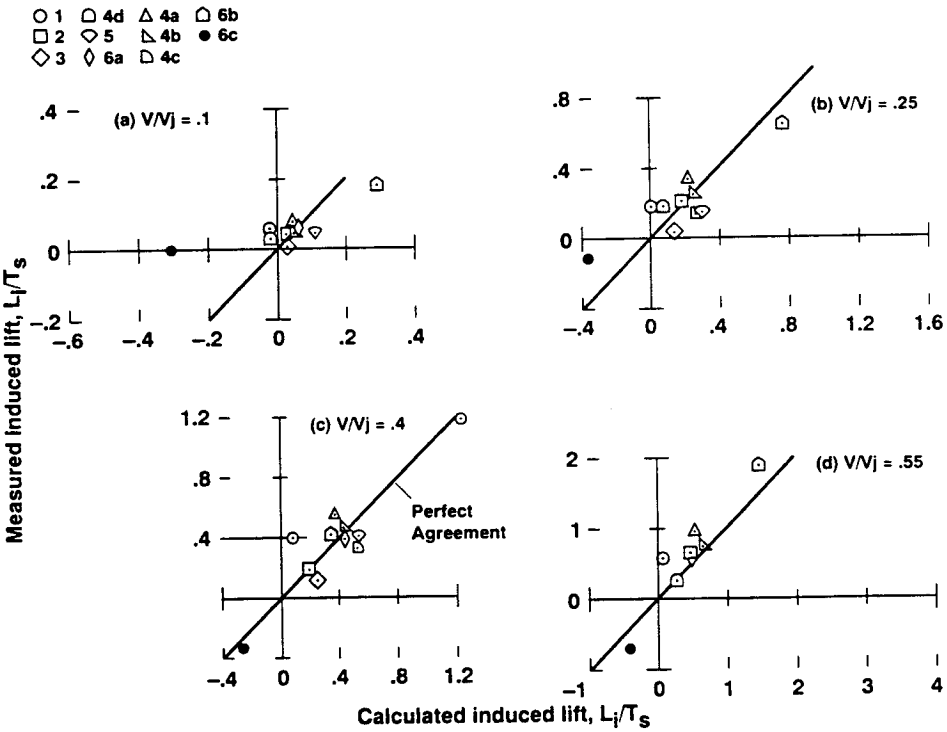

Figure 62. Comparison of measured and calculatedinduced lift with exit vanes vertical

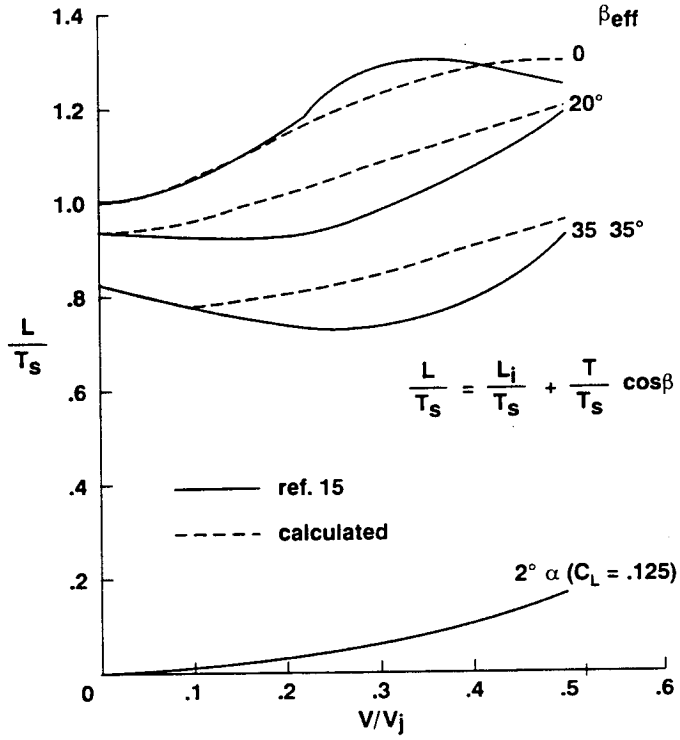

Figure 63. Calculated and measured variation with airspeed for 3 exit louver angles

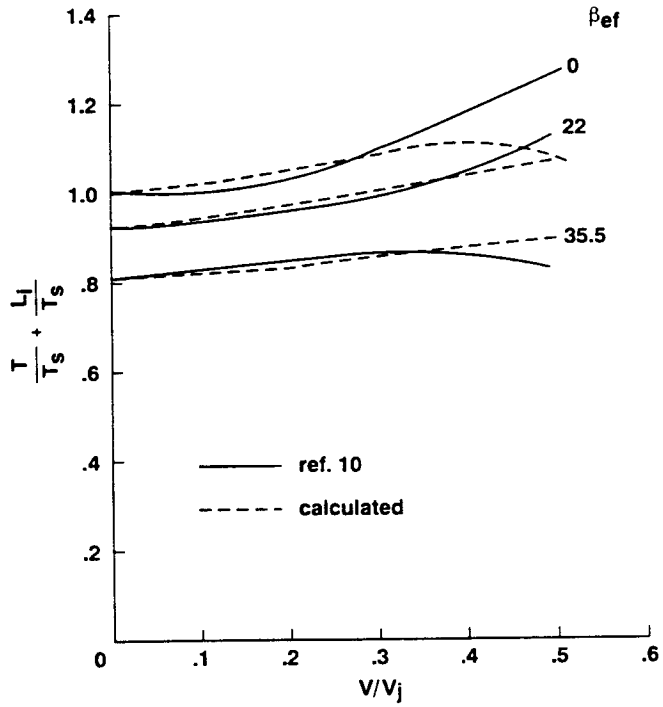

Figure 64. Calculated and measured variation with airspeed for 3 exit louver angles

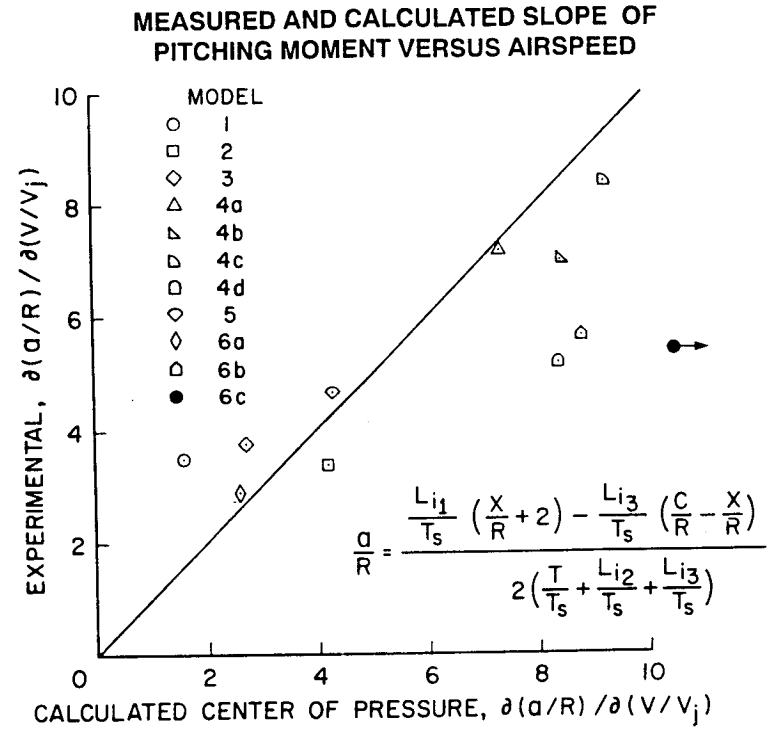

Figure 65. Measured and calculated slope of pitching moment versus airspeed

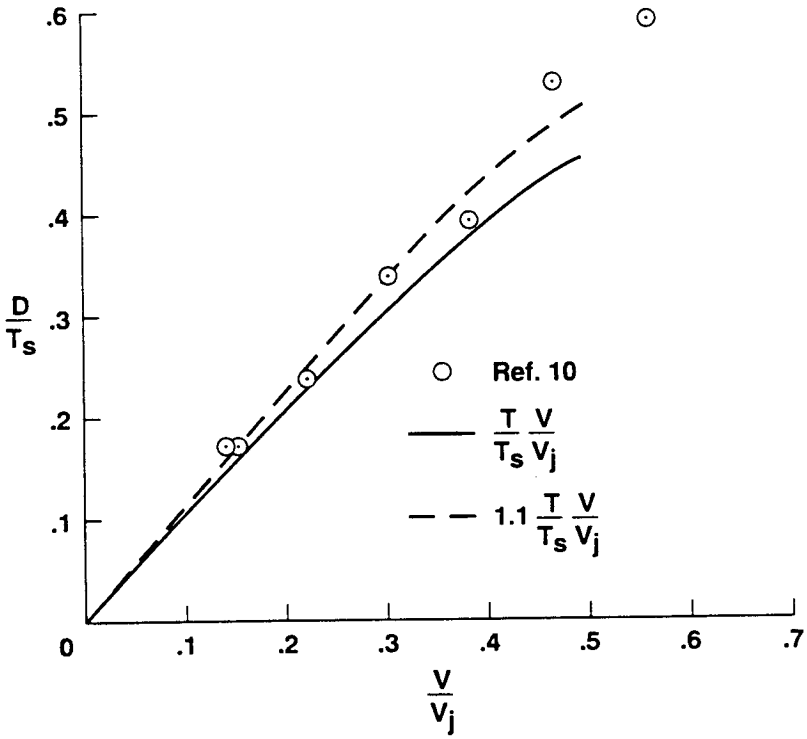

Figure 66. Calculated and measured variation of drag with airspeed

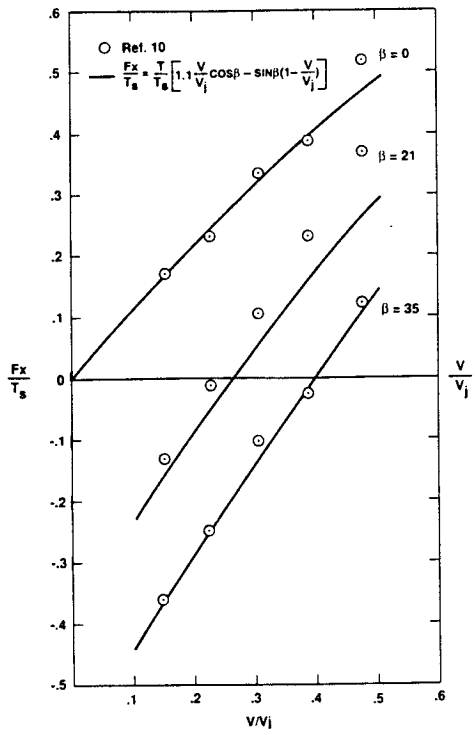

Figure 67. Calculated and measured horizontal force with a lift fan operating with 3 exit louver angles

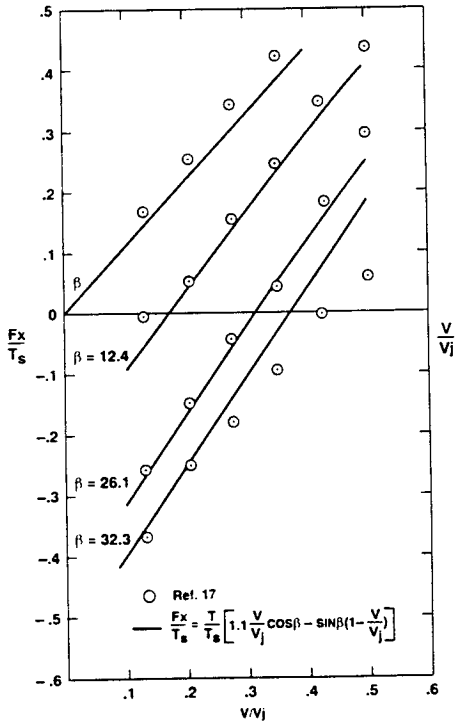

Figure 68. Calculated and measured horizontal force with a lift fan operating with 3 exit louver angles

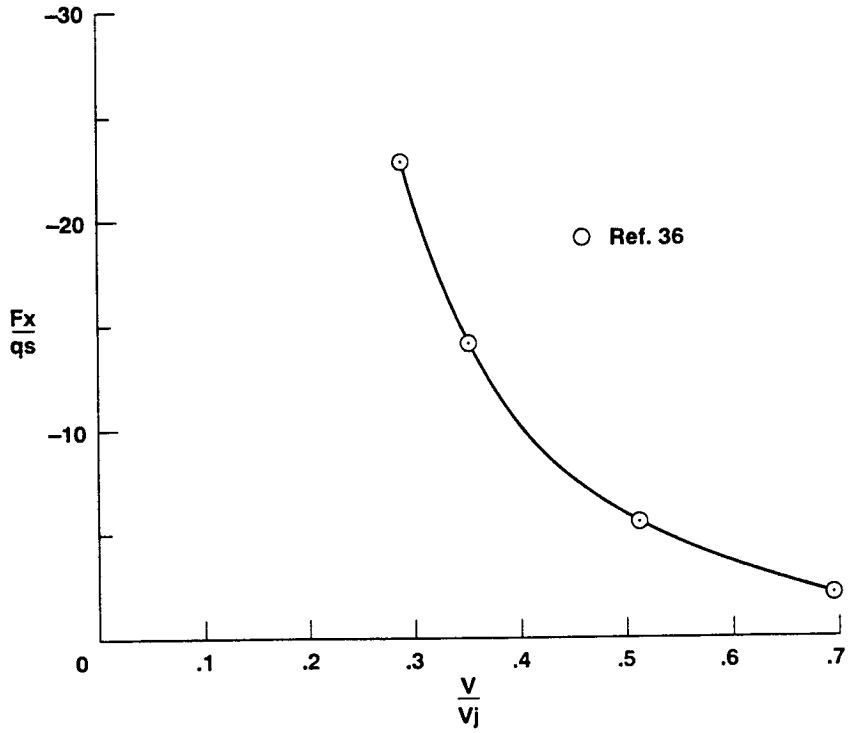

Figure 69. Variation of cruise fan horizontal force with airspeed at zero angle of attack

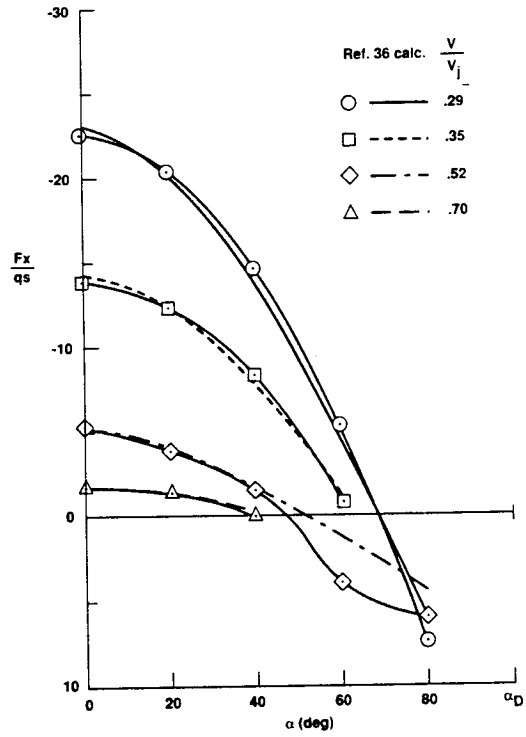

Figure 70. Variation of cruise fan horizontal force with angle of attack for several airspeeds

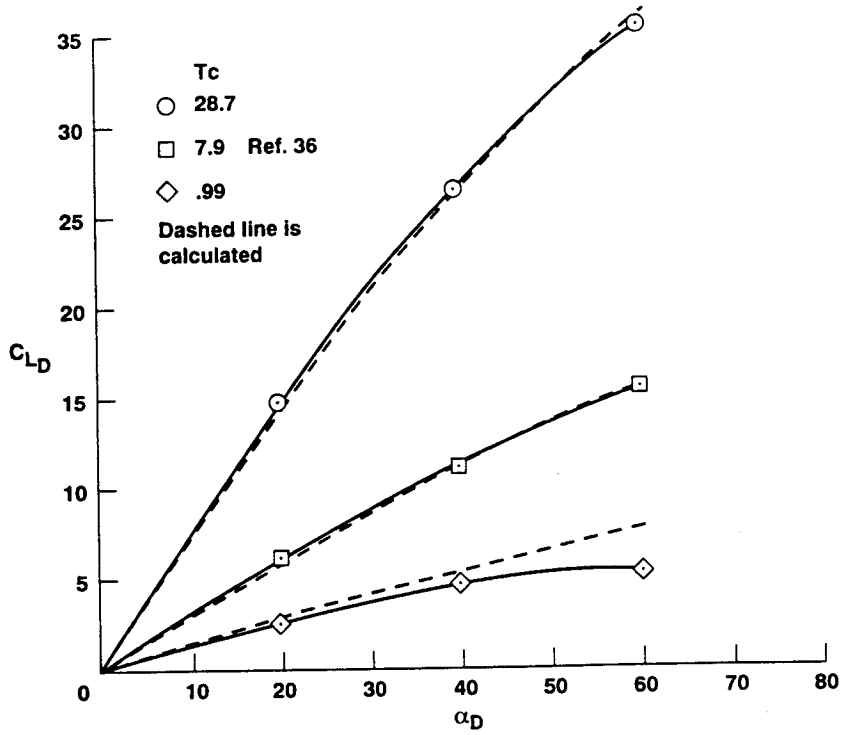

Figure 71. Variation of cruise fan lift coefficient with angle of attack for several airspeeds

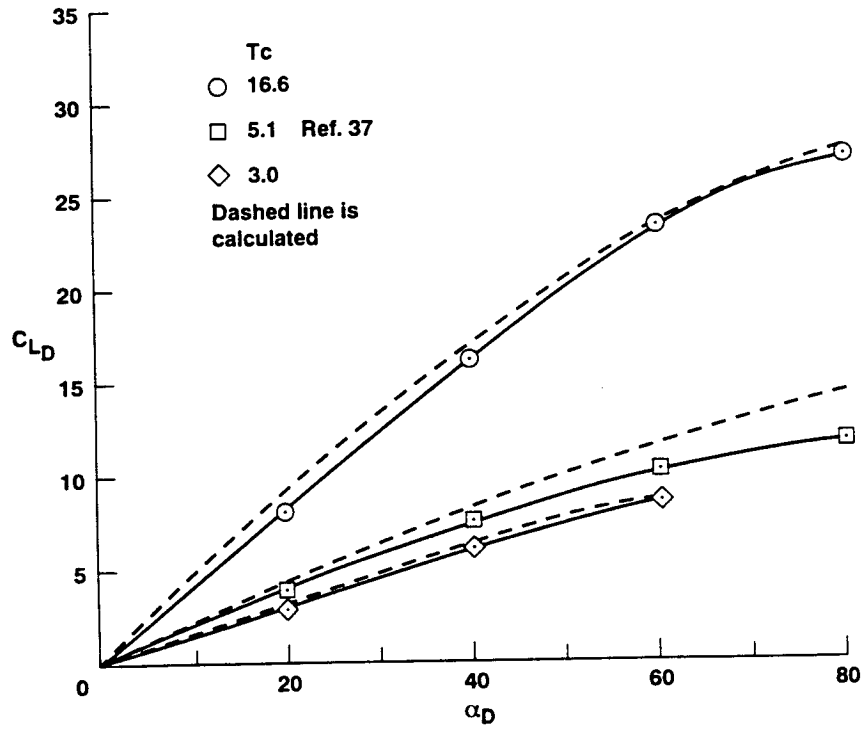

Figure 72. Variation of cruise fan lift coefficient with angle of attack for 2 airspeeds

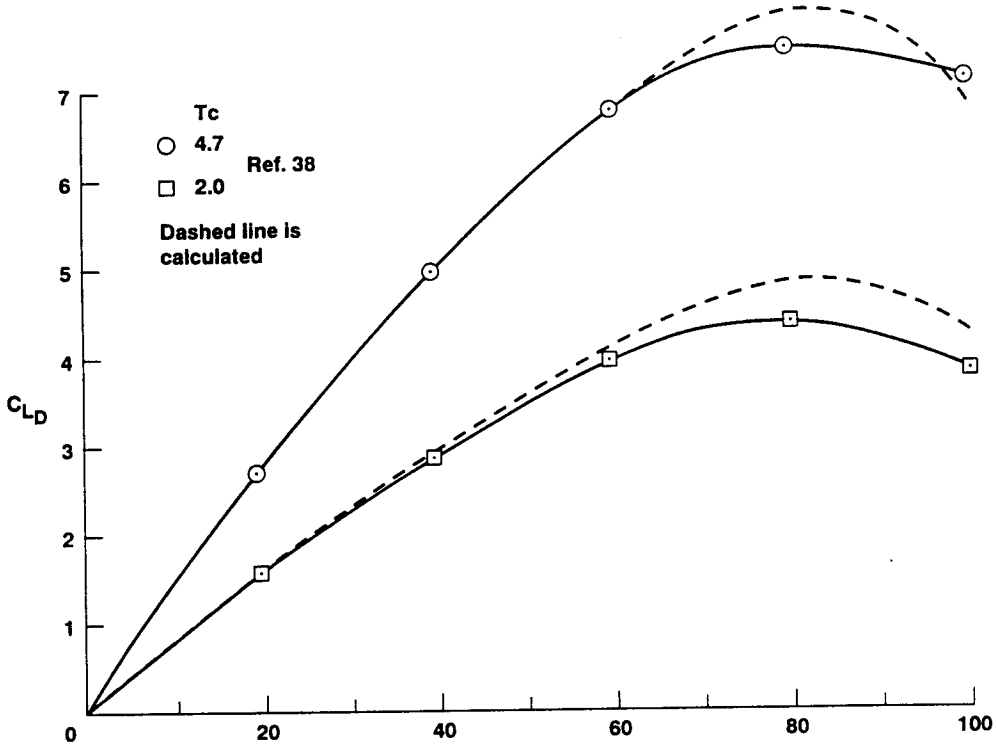

Figure 73. Variation of cruise fan lift coefficient with angle of attack for 2 airspeeds

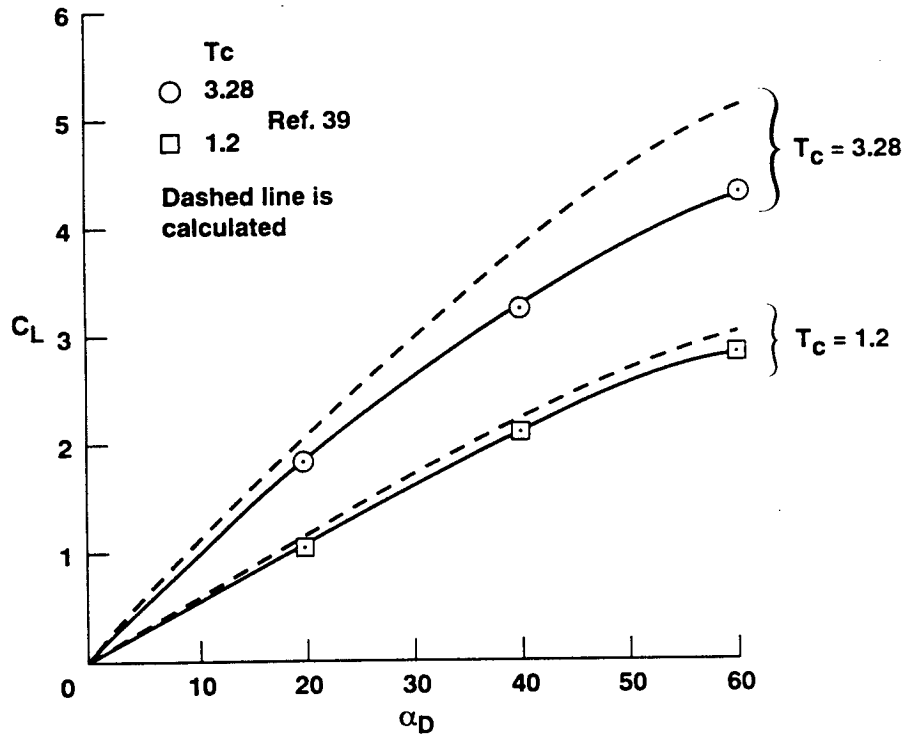

Figure 74. Variation of cruise fan lift coefficient with angle of attack for 2 airspeeds

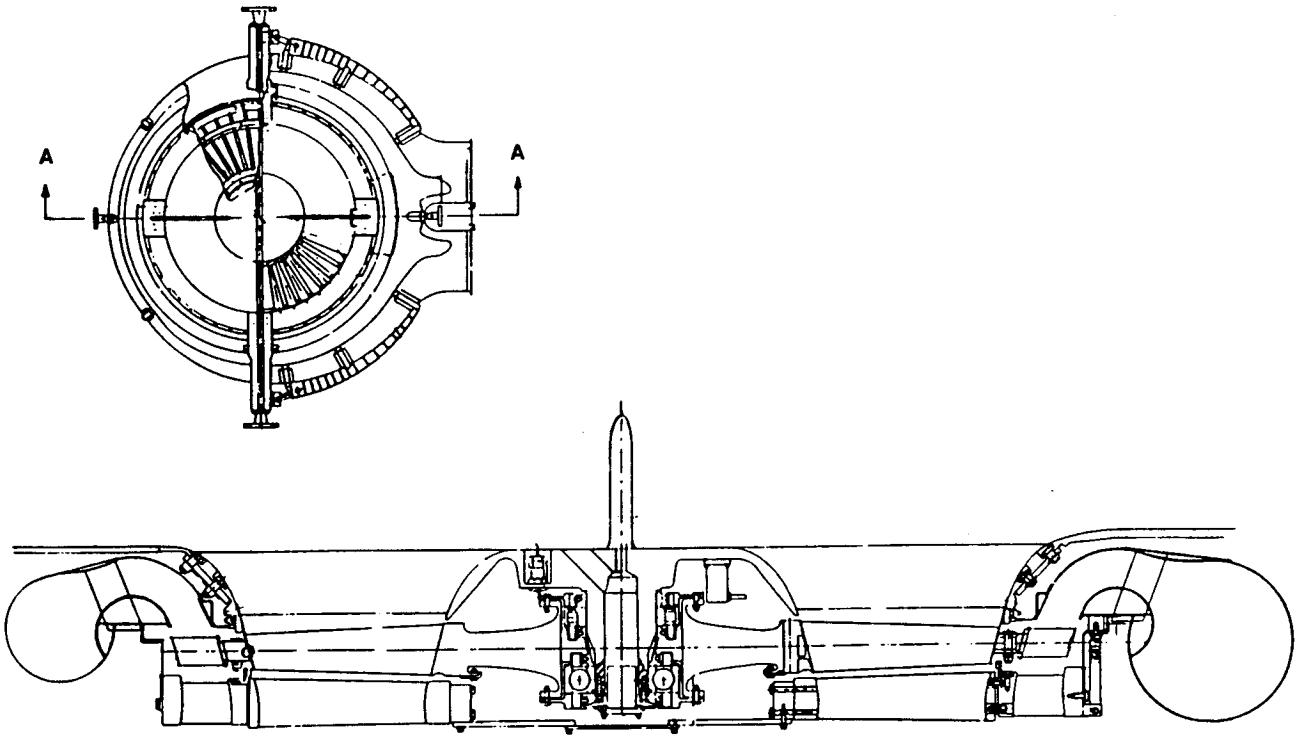

Figure 75. Cross section of LF-336 1.3 pressure ratio lift fan

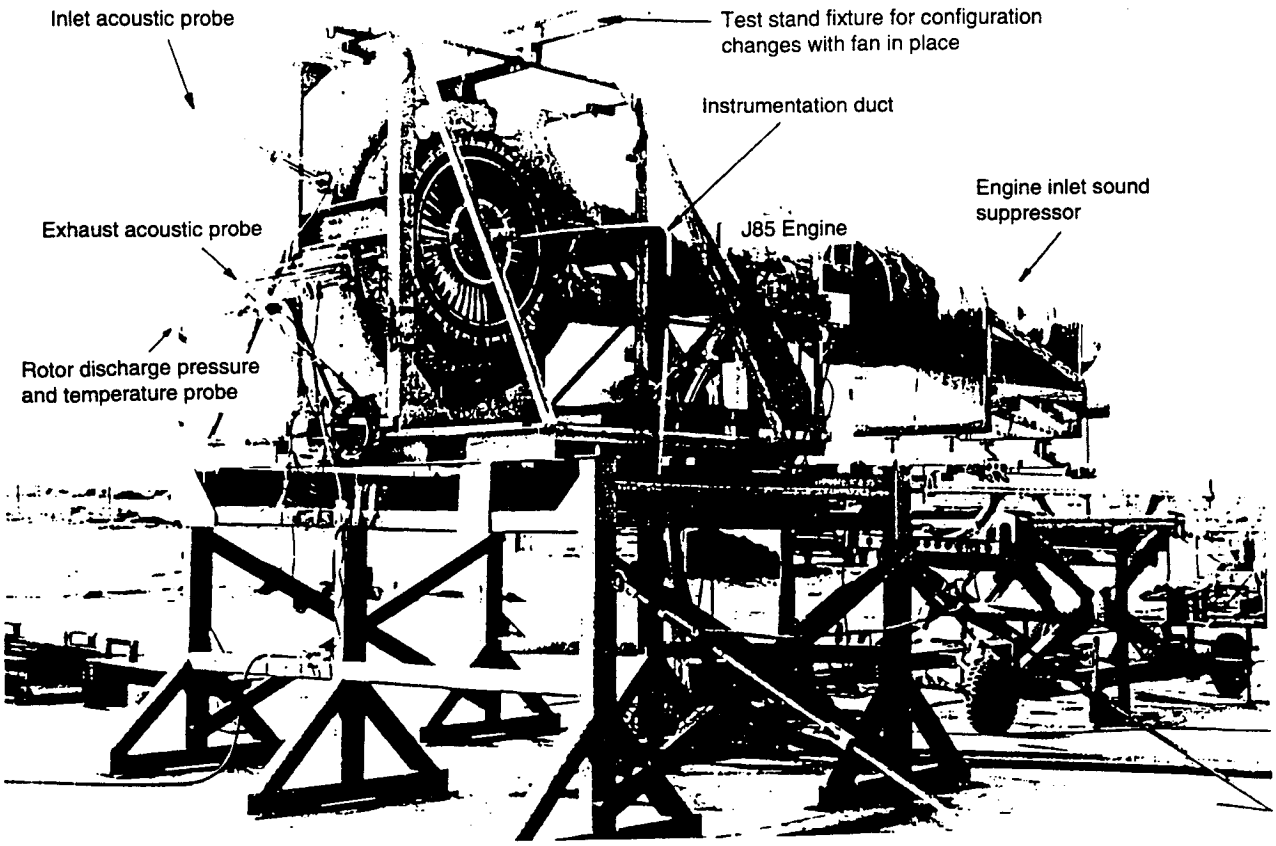

Figure 76. Set up acoustic measurements on the LF-336

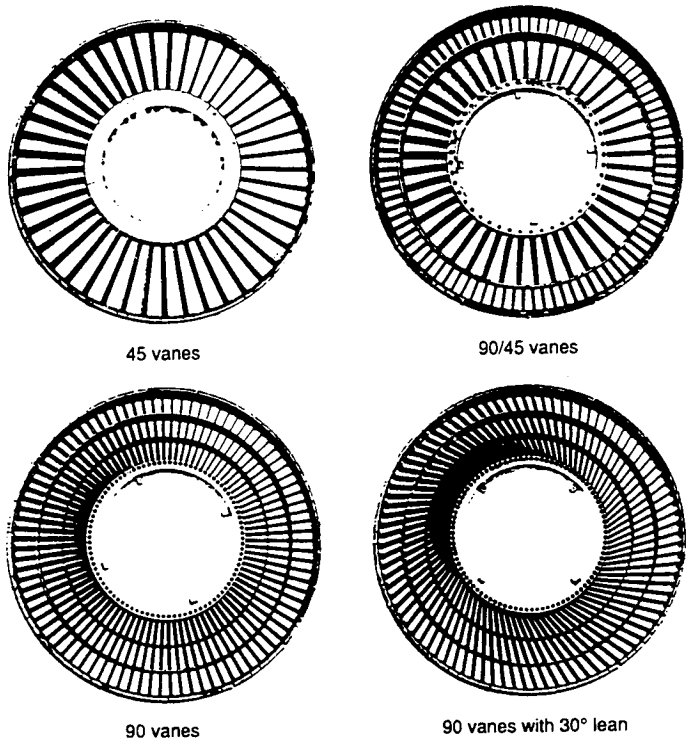

Figure 77. Stators for LF-336 acoustic tests

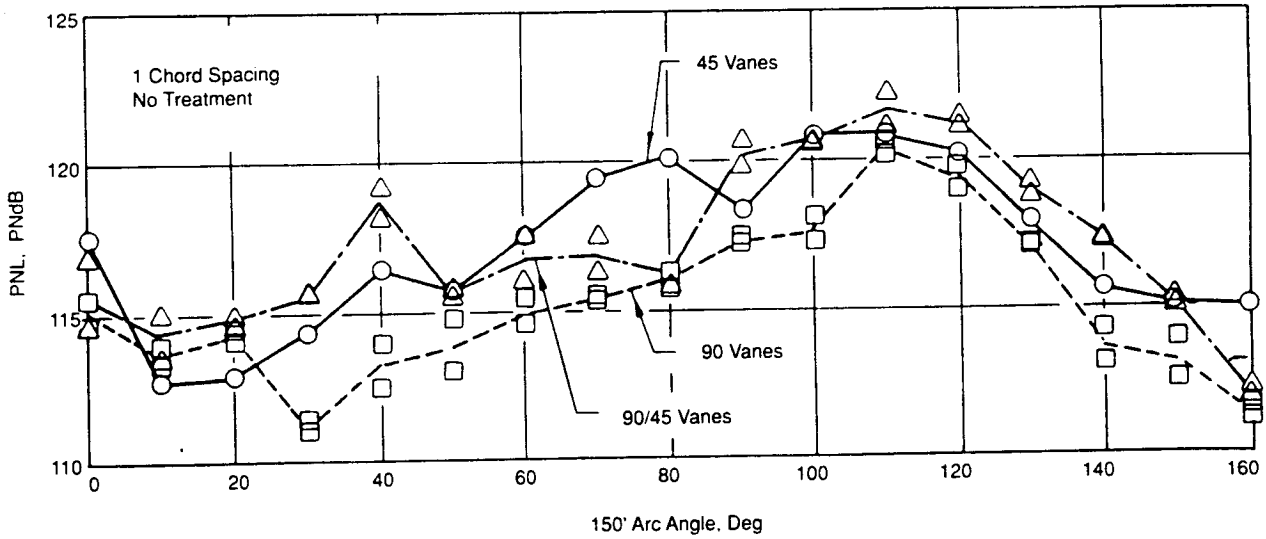

Figure 78. Perceived noise of the LF-336 with 3 different stators, 95% RPM

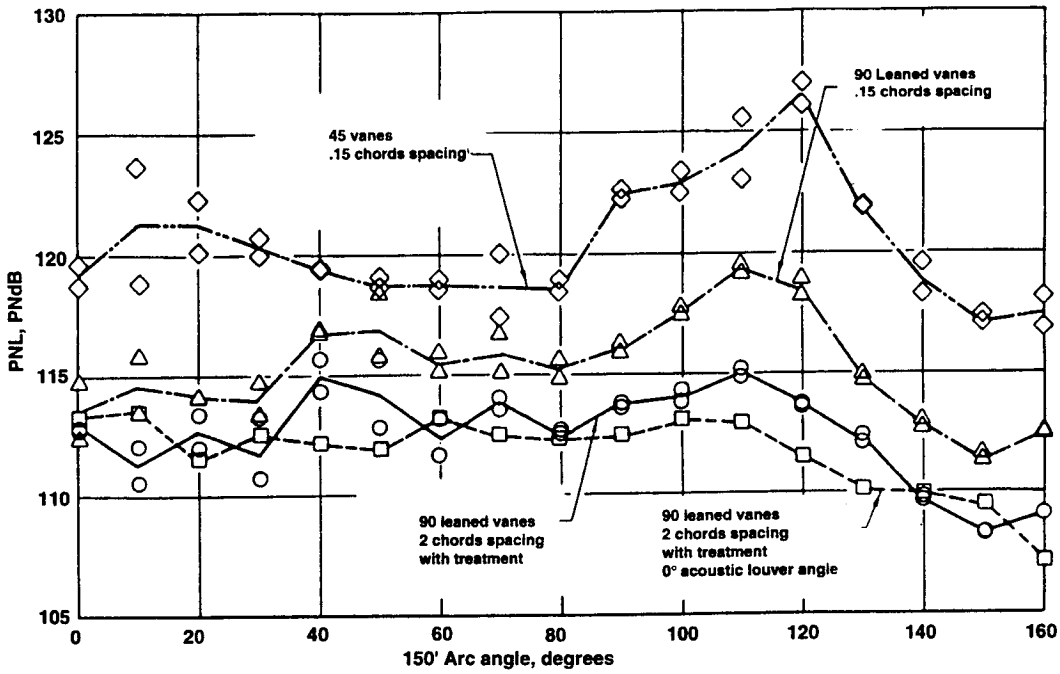

Figure 79. Effect of the rotor-stator spacing and stators on the LF-336 perceived noise level at 80% RPM

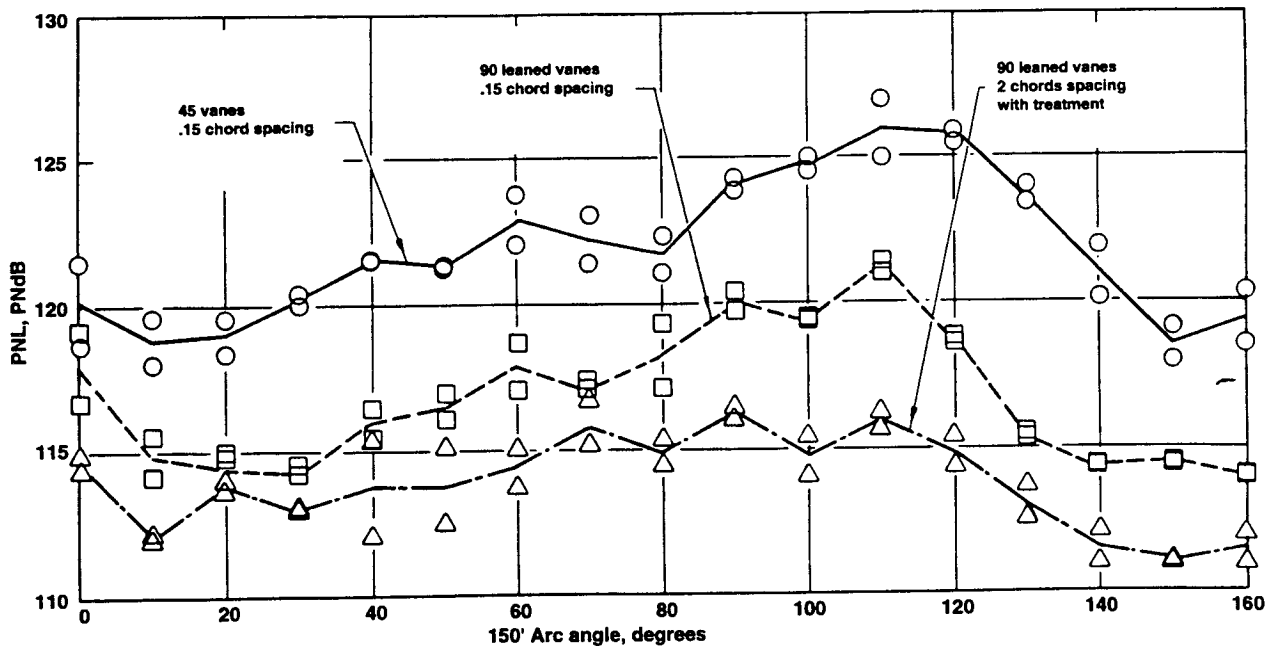

Figure 80. Effect of rotor-stator spacing, stator configuration, and acoustic treatment on perceived noise level at 95% RPM

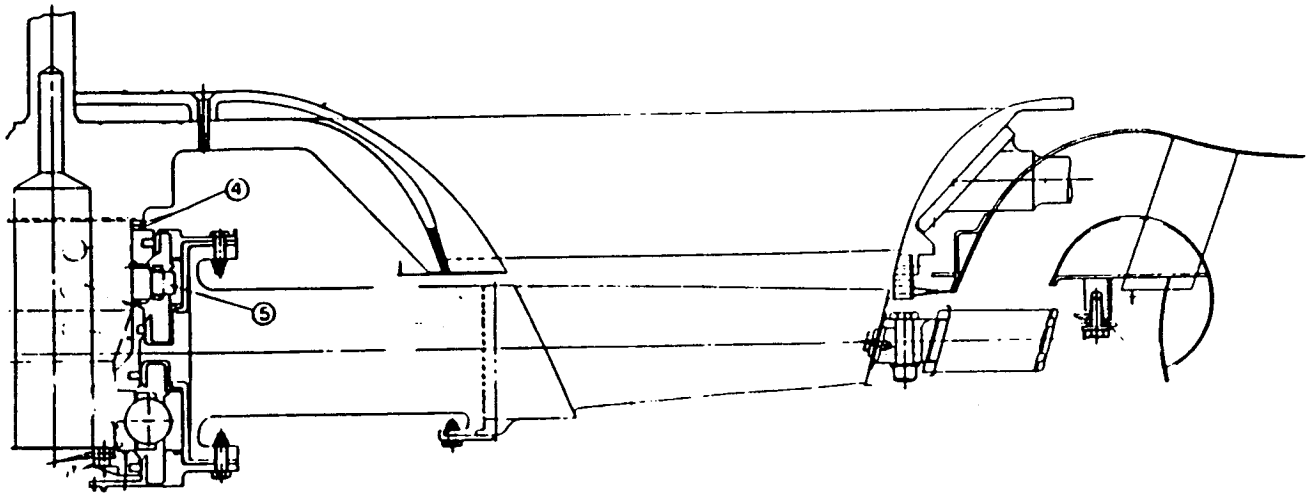

Figure 81. Cross section of statorless fan

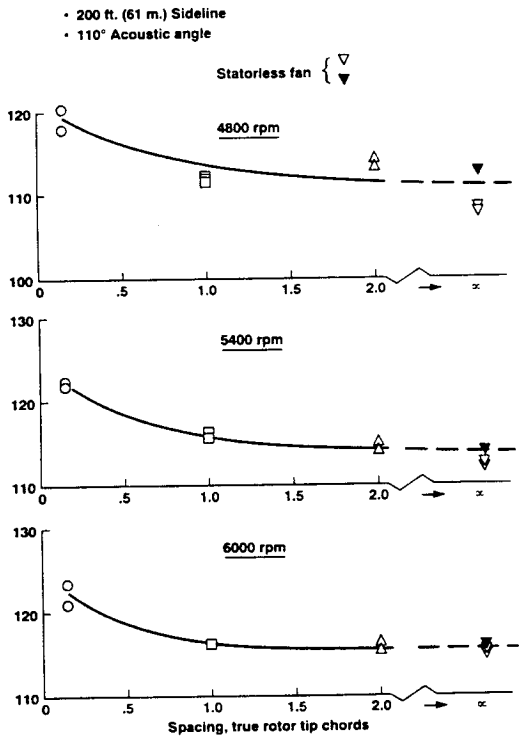

Figure 82. Comparison of the maximum perceived noise level of the statorless fan and the conventional fan

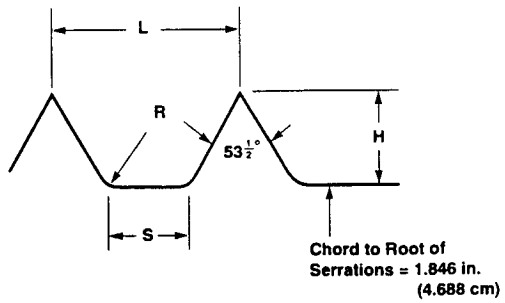

	Serration		H/C	S		L		R			
Serration	(in.)	(cm)	(in.)	(in.)	(cm)	(in.)	(cm)	(in.)	(cm)	(in.)	(cm)
BL1	0.116	0.295	–	–	–	–	–	–	–	–	–
SR1	0.116	0.295	0.063	0.036	0.091	0.153	0.389	0.024	0.061	3.2	1.32
SR2	0.077	0.196	0.042	0.024	0.061	0.102	0.259	0.016	0.041	3.2	1.32
SR3	0.116	0.295	0.063	0.076	0.193	0.193	0.490	0.024	0.061	1.5	1.66
SR4	0.152	0.386	0.083	0.100	0.254	0.253	0.643	0.031	0.079	1.5	1.66
SR5	0.077	0.196	0.042	0.072	0.183	0.150	0.381	0.016	0.041	1.1	1.95
SR6	0.116	0.295	0.063	0.076	0.193	0.193	0.490	0.061	0.155	1.5	1.66
BL2	0.000	0.000	–	–	–	–	–	–	–	–	–

Figure 83. Serrated leading-edge configurations tested in cascade facility

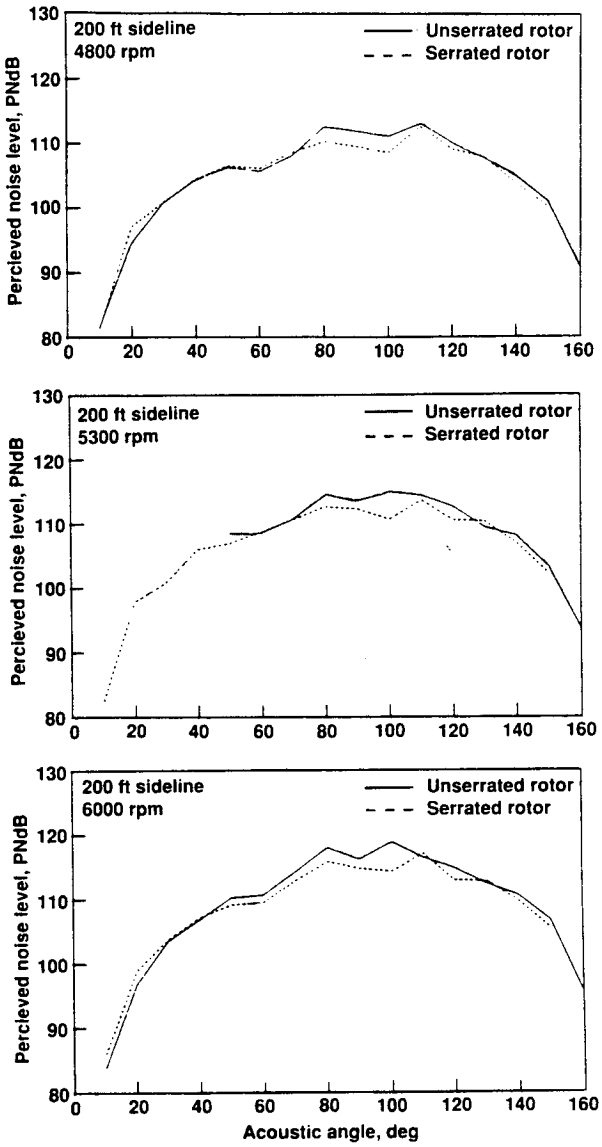

Figure 84. Effect of leading-edge configurations tested in cascade facility

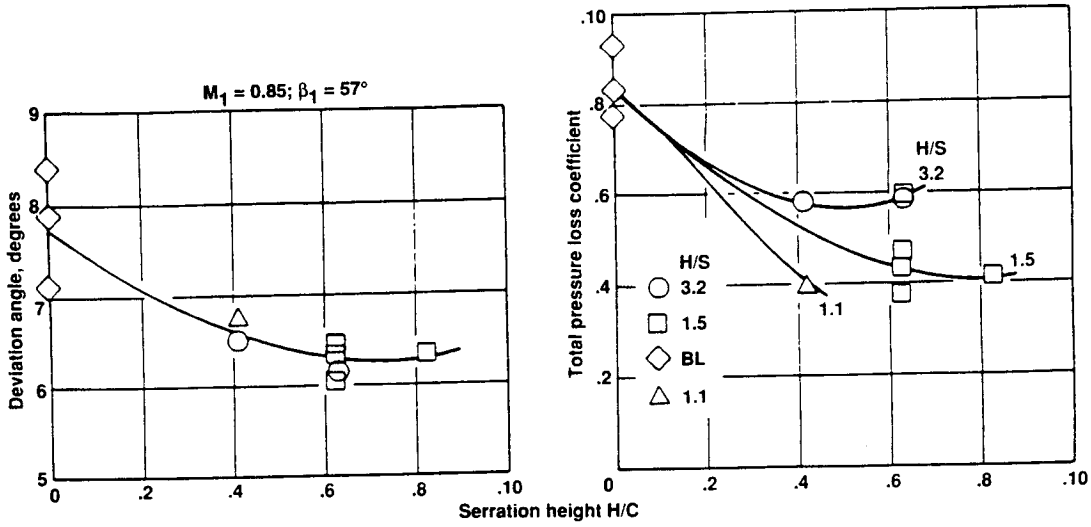

Figure 85. Effect of leading-edge serrations on cascade aerodynamic performance

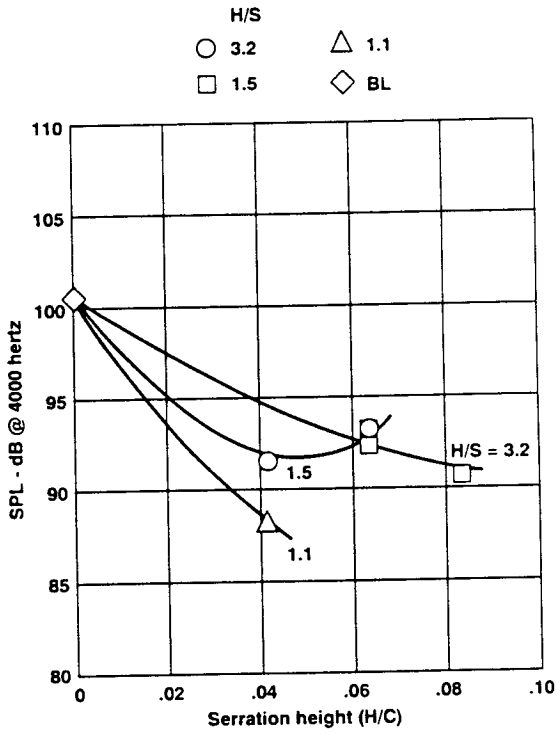

Figure 86. Effect of leading-edge serrations on cascade flow noise

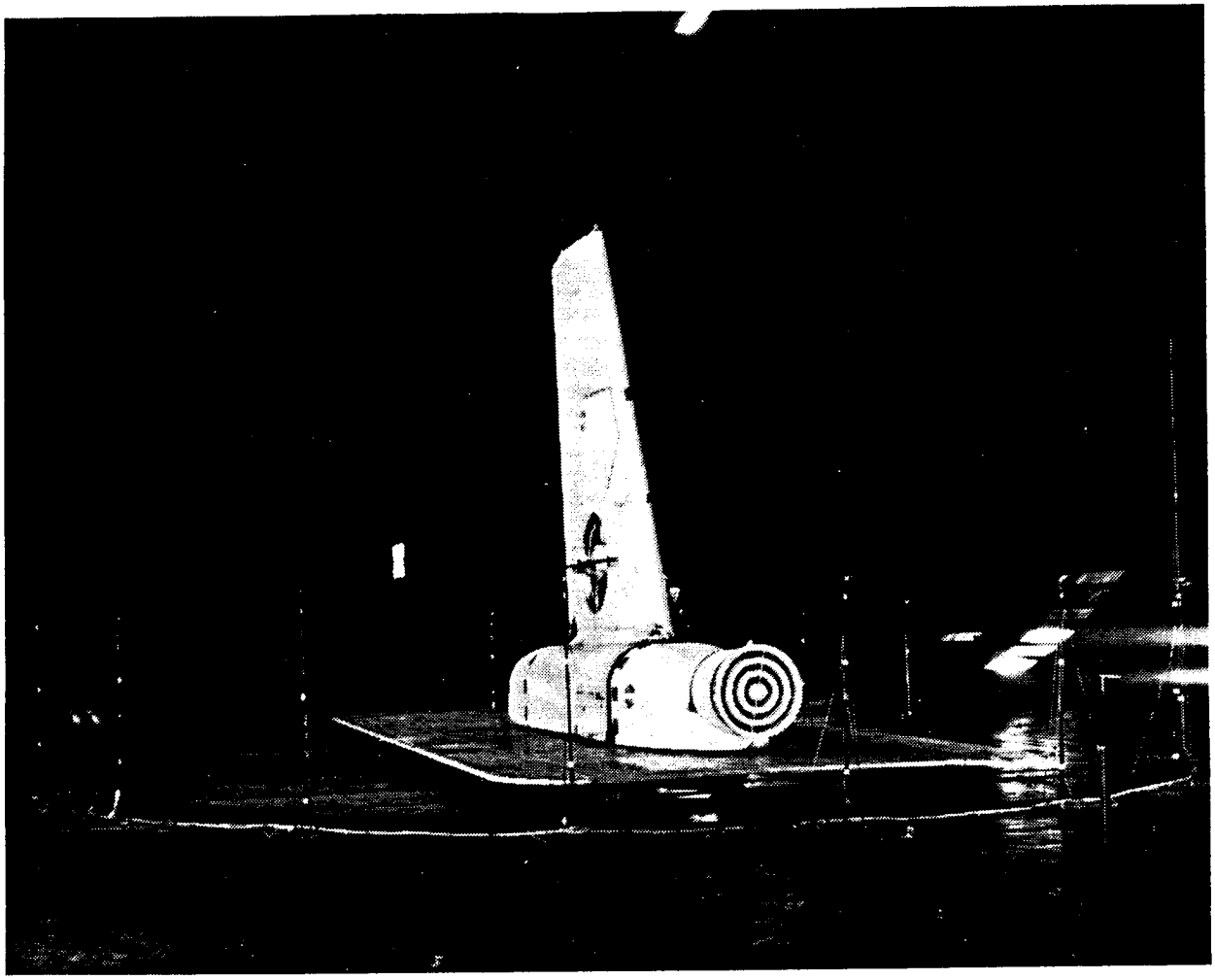

Figure 87. Semispan wing with a LF-336 in the 40x80-foot wind tunnel

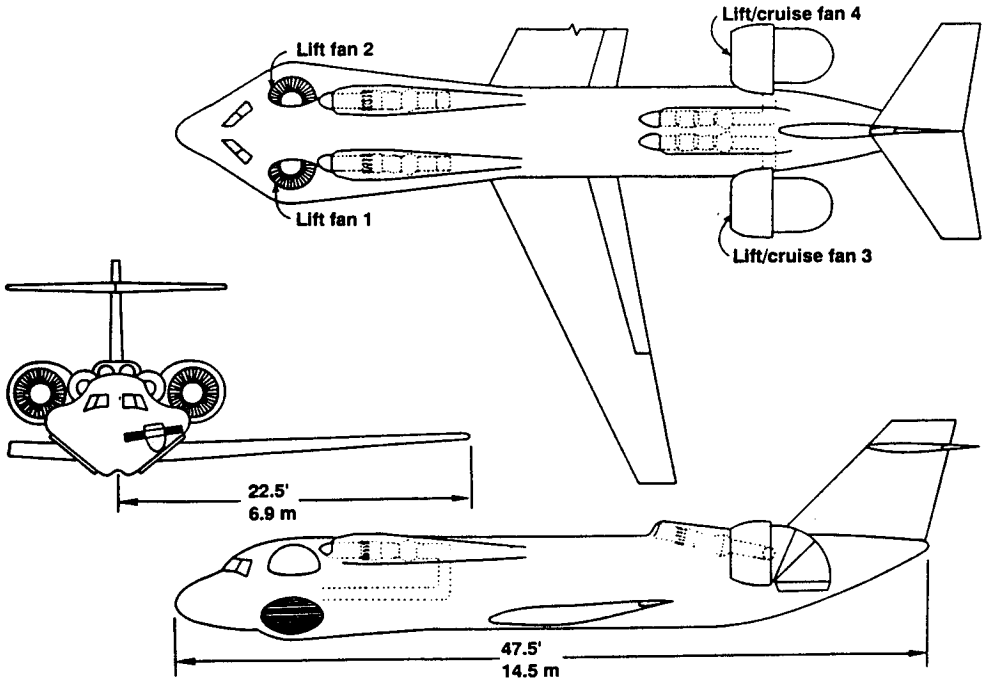

Figure 88. Lift fan model used for noise studies

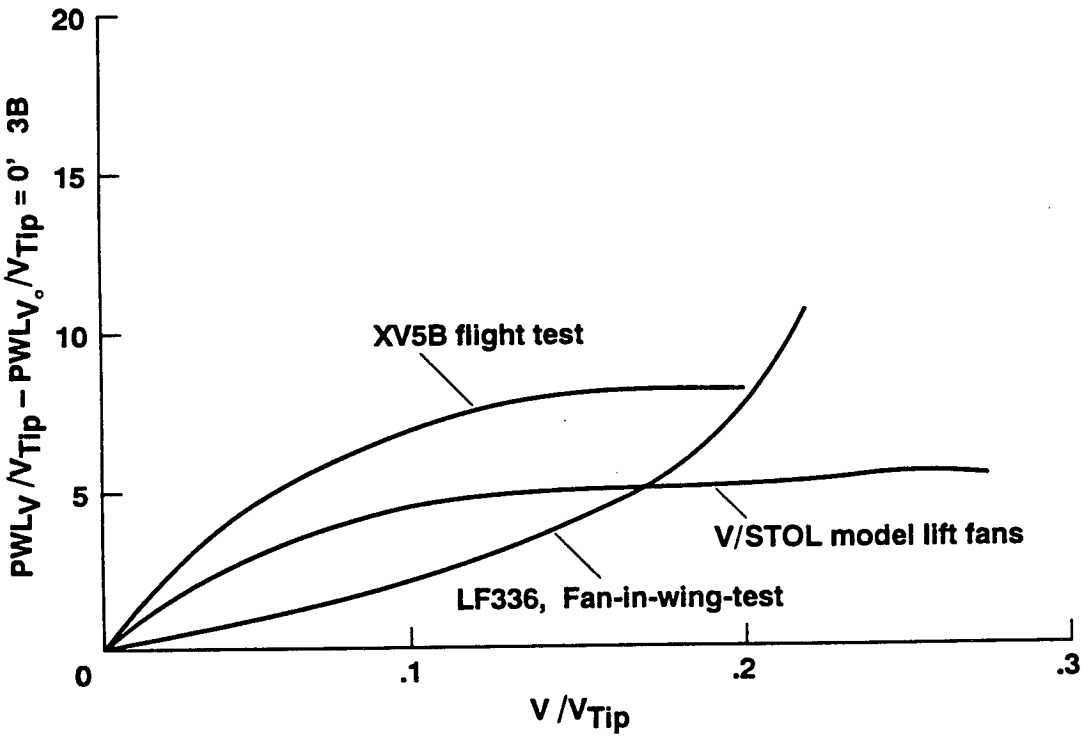

Figure 89. Variation of blade passing frequency noise with airspeed

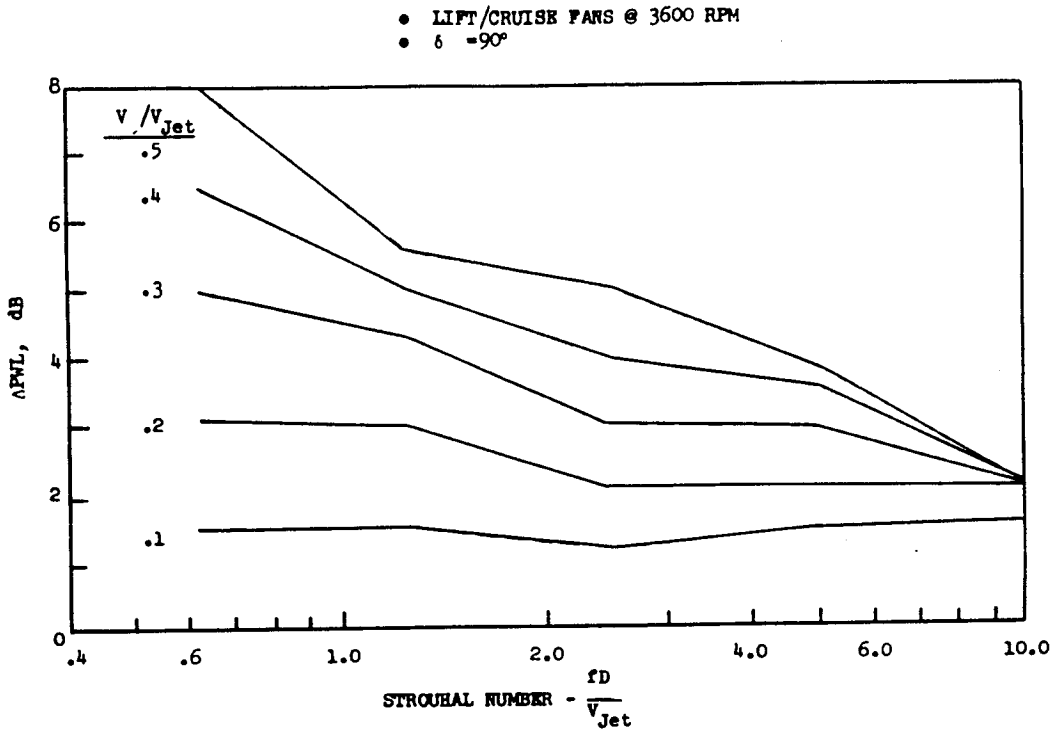

Figure 90. Variation of jet mixing noise with airspeed

REPORT DOCUMENTATION PAGE

Form Approved
OMB No. 0704-0188

1. AGENCY USE ONLY *(Leave blank)*	2. REPORT DATE	3. REPORT TYPE AND DATES COVERED
	September 1993	Contractor Report

4. TITLE AND SUBTITLE

Survey of Lift-Fan Aerodynamic Technology

5. FUNDING NUMBERS

A25364D

6. AUTHOR(S)

David H. Hickey and Jerry V. Kirk

7. PERFORMING ORGANIZATION NAME(S) AND ADDRESS(ES)

NASA Ames Research Center
STOVL/Powered-Lift Technology Branch
Moffett Field, CA 94035-1000

8. PERFORMING ORGANIZATION REPORT NUMBER

A-93106

9. SPONSORING/MONITORING AGENCY NAME(S) AND ADDRESS(ES)

National Aeronautics and Space Administration
Washington, DC 20546-0001

10. SPONSORING/MONITORING AGENCY REPORT NUMBER

NASA CR-177615

11. SUPPLEMENTARY NOTES

Point of Contact: K. Clark White, Ames Research Center, MS 237-3, Moffett Field, CA 94035-1000; (415) 604-5653

12a. DISTRIBUTION/AVAILABILITY STATEMENT

Unclassified — Unlimited
Subject Category 05

12b. DISTRIBUTION CODE

13. ABSTRACT ***(Maximum 200 words)***

Representatives of NASA Ames Research Center asked that a summary of technology appropriate for lift-fan powered short takeoff/vertical landing (STOVL) aircraft be prepared so that new programs could more easily benefit from past research efforts. This paper represents one of six prepared for that purpose. The authors have conducted or supervised the conduct of research on lift-fan powered STOVL designs and some of their important components for decades.

This paper will first address aerodynamic modeling requirements for experimental programs to assure realistic, trustworthy results. It will next summarize the results or efforts to develop satisfactory specialized STOVL components such as inlets and flow deflectors. It will also discuss problems with operation near the ground, aerodynamics while under lift-fan power, and aerodynamic prediction techniques. Finally, results of studies to reduce lift-fan noise will be presented. The paper will emphasize results from large scale experiments, where available, for reasons that will be brought out in the discussion. Some work with lift-engine powered STOVL aircraft is also applicable to lift-fan technology and will be presented herein. Small-scale data will be used where necessary to fill gaps.

14. SUBJECT TERMS	15. NUMBER OF PAGES
Lift-fan, Powered-lift, Short takeoff/vertical landing (STOVL)	76
	16. PRICE CODE: A05

17. SECURITY CLASSIFICATION OF REPORT	18. SECURITY CLASSIFICATION OF THIS PAGE	19. SECURITY CLASSIFICATION OF ABSTRACT	20. LIMITATION OF ABSTRACT
Unclassified	Unclassified		